Petrological and Geochemical Studies of an Abyssal Peridotite from the Atlantis II Fracture Zone

by

Kwok-Lin Lee

M.S. National Taiwan University
(1993)

Submitted in partial fulfillment of the
requirements for the degree of

Master of Science

at the

MASSACHUSETTS INSTITUTE OF TECHNOLOGY

and the

WOODS HOLE OCEANOGRAPHIC INSTITUTION

January 1997

Signature of Author.....
Joint Program in Marine Geology and Geophysics
Massachusetts Institute of Technology
Woods Hole Oceanographic Institution
January 17, 1997

Certified by.....
Stanly R. Hart
Senior Scientist
Thesis Supervisor

Accepted by.....
Deborah K. Smith
Chair, Joint Committee for Marine Geology and Geophysics
Massachusetts Institute of Technology
Woods Hole Oceanographic Institution

Petrological and Geochemical Studies of an Abyssal Peridotite from the Atlantis II Fracture Zone

by

Kwok-Lin Lee

Submitted in partial fulfillment of the requirements for the degree of Master of Science at the Massachusetts Institute of Technology and the Woods Hole Oceanographic Institution
January 19, 1997

ABSTRACT

This thesis investigates the petrology and geochemistry of an abyssal peridotite dredged from the Atlantis II Fracture Zone in the southwestern Indian Ocean Ridge. Texturally, this sample is a serpentinized peridotite with a crosscutting coarse-grained clinopyroxenite vein. One of the alteration veinlets contains rutile and ilmenite in association with plagioclase and amphibole. This veinlet is not related to the pyroxenite vein. In terms of mineralogy, the composition of the major silicate minerals indicates that this plagioclase lherzolite represents the depleted residue after mantle melting, similar to other abyssal peridotites from this region.

In addition to the presence of the unique pyroxenite vein, this sample was earlier shown to be a carrier of 'orphan Sr-87'. Unfortunately, I was unable to find such high Sr isotopic ratios in the magnetic separations of different fractions of the sample. The sulfide mineralogy, together with the whole rock chemistry, suggests that sea water alteration occurs mainly as a result of serpentinization at temperatures higher than 200°C. Since the sample is less than 1 Ma old, and the low temperature weathering occurred only after the sample was exposed at the sea floor, it is possible that the weathering process was restricted to major alteration veins. This suggests that the alteration process is highly fracture controlled and time dependent.

Trace element data from clinopyroxene grains in the peridotite shows large variations from grain to grain. The (Ce/Yb)n ranges from 0.17 to 0.54 in the pyroxenite vein, and from 0.75 to 2.35 away from the vein. The tendency for LREE enrichment with the increase of distance from the vein suggests the presence of highly reacted melts. An assimilation-fractional crystallization (AFC) model was derived which supports the idea that the source of the clinopyroxenite vein reacts with the depleted peridotite to form a central reaction zone. Some of the highly reacted melt, after melt-rock reaction, migrates out of the reaction zone, and precipitates some late magmatic phases while being trapped in the country rocks. Since the sulfide is a major Os reservoir in the abyssal peridotites, as shown in leaching experiments, and the melt is saturated in sulfur as a consequence of the reaction process, it is possible to model the heterogeneous distribution of the Os isotopic data by mixing the residual peridotite with 0.2 to 0.5 wt% of sulfides precipitated from the melt. This mixing process can explain most of the heterogeneity from 1.034 to 1.148 for $^{187}Os/^{186}Os$. The impact on the peridotite from the melt-rock reaction and impregnation of the late melt is obvious. As evident in Hess Deep gabbroic rocks, conductive heat loss in the transform fault fulfils the physical requirement to create and to preserve such geochemical signature.

Thesis Supervisor:
Dr. Stan R. Hart, Senior Scientist
Woods Hole Oceanographic Institution

TABLE OF CONTENTS

1. INTRODUCTION

Ever since the first introduction of porous flow models for the upper mantle from theoretical investigations and field observations (Frank, 1968; Sleep, 1974; Turcotte and Ahern, 1978; Boudinier and Nicolas, 1977; Dick, 1977), it has been an active subject of research for both geochemists and geophysicists. Most of the studies have focused on the ocean ridges because of their relatively simple tectonic and geochemical history. By combining both the geochemical and geophysical evidence, it was recently suggested that the melt from the deep mantle is capable of interacting with the surrounding peridotites to form dunite and orthopyroxene-rich peridotites during its migration through the mantle by porous flow (Dick, 1977; Kelemen, 1990; Kelemen et al., 1992; Kelemen et al., 1995). Although these studies are conducted mostly in ultramafic massifs on continents, which are not as depleted as the suboceanic upper mantle, and which reflect somewhat different tectonic emplacement, they still provide valuable insight with respect to the mantle flow mechanism.

In the oceanic environment, late-stage melt-wall rock interaction and the presence of trapped melt in the shallow East Pacific Rise mantle near the Hess Deep has recently been documented (Dick and Natland, 1996; Allan and Dick, 1996). These authors show that the melt-rock interaction is a consequence of chemical disequilibrium between the melt and the depleted suboceanic lithophere. In the present study, one dredged abyssal peridotite boulder from a slow spreading ocean ridge provides further compelling evidence for this process. A central melt-rock reaction zone which grades gradually outward into the trapped-melt region is observed both in rare earth element and mineralogical variations. The combination of a slow spreading rate and the deep, rapid cooling environment of a transform fault are probably sufficient to preserve the geochemical signature of the melt-rock interaction.

The second part of the present study focuses on the effects of alteration on the abyssal peridotite. Traditionally, researchers have used two methods to determine the degree of alteration. One is to reconstruct the original bulk rock composition by measuring the mobility of the elements relative to some known immobile elements. This method was established in mid-ocean-ridge basalts and was successfully applied to some ultramafic rocks. The second method is the direct analysis of the alteration products, and the counting of modal abundance of phases. Both these methods could be applied in the ultramafic rocks if the source is known to be homogeneous. Given the uncertainties of the depletion and refertilization histories of the peridotites, the present study simply looks for the correlation between the bulk rock compositional variations and the water content, which is supposed to

be the most effective index of a hydration process such as serpentinization. The results show that most of the data do not show correlation with the water content. In addition, mass balance calculation between the bulk rock and the mineral compositions suggests that the hydration process is mostly isochemical. Combined with the sulfide mineralogy study which shows little evidence of low temperature phases, it indicates that the dominant sea water alteration in this sample is during the serpentinization. Low temperature weathering is not as prevalent as the serpentinization in this sample.

A more concerned problem is the Os isotopic system in abyssal peridotites. The range of abyssal peridotites is from 1.00 to 1.09 in $^{187}Os/^{186}Os$ (Snow and Reisberg, 1995, fusion data). Several lines of evidence from ophiolites and abyssal peridotites suggest that the present day bulk silicate earth $^{187}Os/^{186}Os$ value should be between 1.05 to 1.10 (Luck and Allegre, 1991; Martin et al., 1992), while data from peridotite xenoliths ranges from 0.90 to 1.12 (Walker et al., 1989; Pearson et al., 1991; Carlson and Irving, 1994). MORB data range from 1.08 to 2.74 (Roy-Barman and Allegre, 1994) in $^{187}Os/^{186}Os$, while OIB data range from 1.11 to 1.30 (Pegram and Allegre, 1992; Hauri and Hart, 1993; Martin et al., 1994; all fusion data). In addition, the picked sulfides from MORB from the Famous region have $^{187}Os/^{186}Os$ around 1.08 (Roy-Barman et al., 1994). Although not well constrained, it seems that if the suboceanic lithosphere has been depleted by the extraction of continental crust, the abyssal peridotites, and possibly MORBs should fall in the lower range of the data bracket. While most of the abyssal peridotites have values less than 1.10, the high $^{187}Os/^{186}Os$ values from the present study need more thought on their origins. One strategy is to use leaching methods to extract Os from sulfides, while minimizing the alteration-derived Os to the lowest degree, if sulfides are the major Os reservoir in ultramafic and mafic rocks (Roy-Barman et al., 1994; Hart and Ravizza, 1996). The high concentration of Os in the sulfides implies that the isotopic composition should not be changed significantly under the conditions of alteration. The leaching experiments show optimal results, which indicates that sulfides are the major Os carrier in the abyssal peridotites. Data from combined leachates and residues suggest that part of the high Os isotopic composition is probably real, and that the clinopyroxenite vein represents an exotic source mixing with a residual peridotite. Given the effect of alteration, a $^{187}Os/^{186}Os$ value of 1.03 or lower for normal abyssal peridotites is probably closer to the true value.

2. SAMPLE DESCRIPTION

This sample was dredged from the Atlantis II fracture zone on the SW Indian Ocean Ridge. The geological background is summarized below, and the detailed sampling location, age and tectonic setting can be found in Dick et al. (1991) and the references cited there. The Southwest Indian Ocean Ridge extends from the Bouvet triple junction in the west to the Indian Ocean Triple Junction in the east and forms the boundary between the African and Antarctic plates. The Atlantis II Fracture Zone is located at a longitude of approximately 57°E on the Southwest Indian Ocean Ridge, and is the best studied fracture zone in this region (Dick et al., 1990; ODP Leg 118, von Herzen, Robinson, et al. 1991). It is far away from any of the hot spots, with the nearest one being the Marion-Prince Edward island chain some 2000 km away. The actively slipping portion of the Atlantis II Fracture Zone extends in a north-south direction from 31°51'S to 33°40'S, producing a maximum age offset of 22 million years (Snow, 1993). The great dredging density and peridotite recovery, combined with the long offset, provide the opportunity to map the variation in mantle compositions as a function of time along the lithosphere flow lines (Johnson, 1989). The dredging was carried out on the Robert Conrad cruise RC2709, and is located in the rift valley south of the northern margin of the northern nodal deep (Fig 1). This study will focus on one of the dredged samples from this cruise, namely RC2709-6-2.

This sample was analyzed by Snow (1995) for both major and trace elements as well as Sr-Nd-Os isotopes. A striking feature of this sample is that there is one coarse-grained clinopyroxene vein crosscutting the sample (Plate 1). Snow (1993) avoided the effect of this vein in his study. Unlike some orogenic peridotites, clinopyroxenite veins are very rare in abyssal peridotites. The vein in this sample does not seem to follow the physical texture of the sample in hand specimen scale, which indicates that the vein may not be the product of gravity or chemical segregation. The vein is about 1 cm thick through most of the sample, and probably spreads outward to the left. The boundary between the vein and the rest of the sample is clear. Mineralogically, the vein is mainly clinopyroxene, with trace amounts of spinel, sulfide, plagioclase, and rarely, orthopyroxene. A narrow band of olivine (dunite) separates both sides of the vein from the rest of the sample. Outside of the pyroxenite and dunite zone, the sample (host) grades into a plagioclase lherzolite, based on Streckeisen's (1976) classification of coarse grained igneous rocks.

Texturally, the primary mineral assemblages are overprinted by metamorphic and low temperature mineral assemblages. Olivine is mainly altered to serpentine and magnetite, and shows the greatest degree of alteration. Exsolution in the pyroxenes is common. Most of the pyroxenes have only undergone hydration process(es) along the grain boundaries and

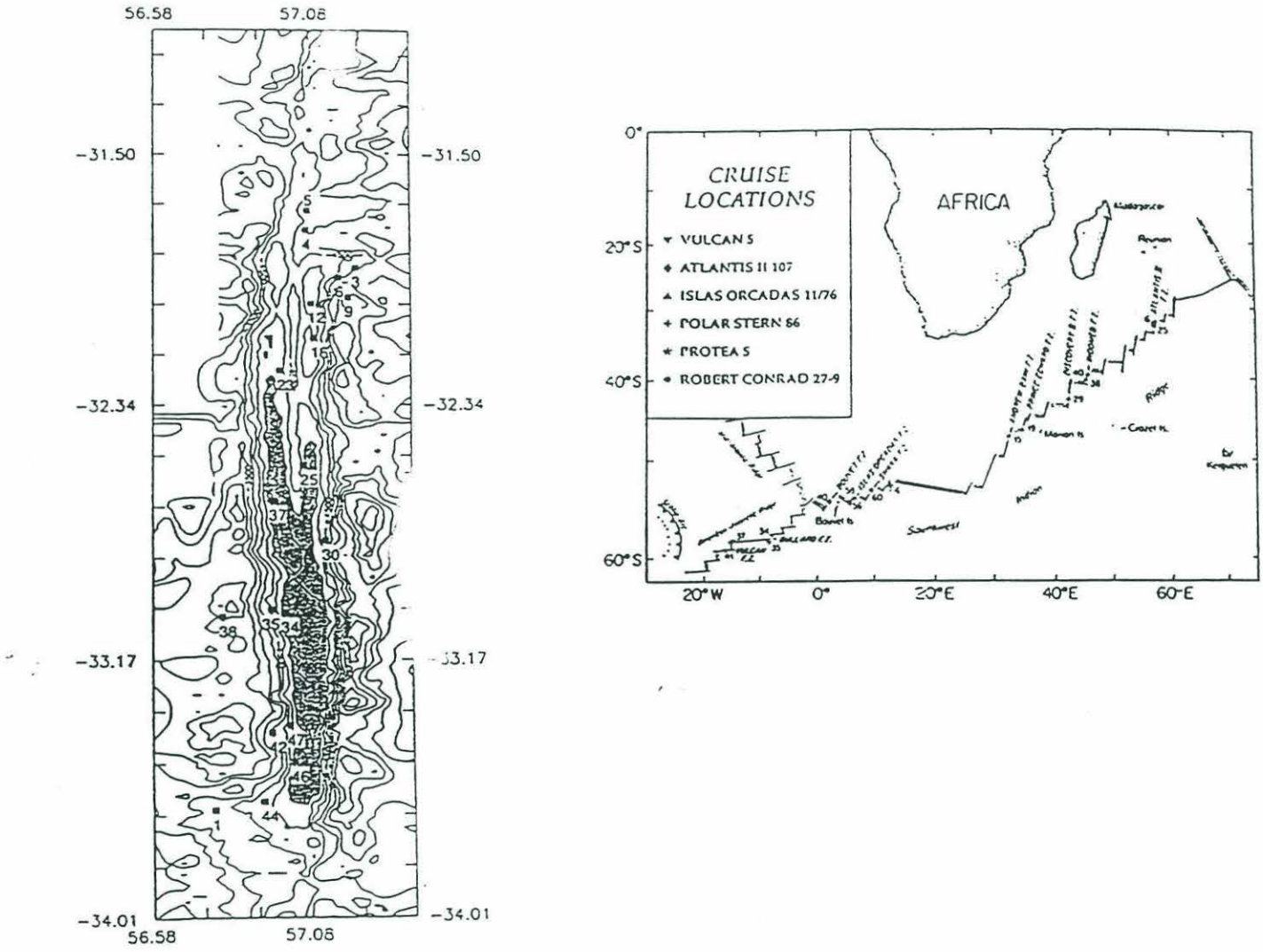

Fig.1: Bathymetric map and location map of the Atlantis II Fracture Zone, adopted from Johnson et al. (1990) and Johnson and Dick (1992).

Plate 1: Photograph of the sample slab RC 27-9-6-2 (between slab 1 (for Sr, Nd, Os isotopic analysis and part of the major and trace element of bulk rocks) and slab 2 (for the thin sections)). The clinopyroxenite vein is highlighted.

cleavage planes. Some of the clinopyroxene exsolution in the orthopyroxene has been altered to amphibole, indicating an event of high temperature metamorphism. There is a thin veinlet crossing the upper part of the sample, which contains intergrown chlorite, amphibole, rutile, ilmenite after rutile and possibly apatite. Otherwise, few low-temperature alteration mineral assemblages have been found in the sample. This veinlet is very small so that it is difficult to follow its trace in three dimensions, and its Ti-rich characteristics do not show up in the bulk rock composition. There is no evidence that the veinlet and the pyroxenite vein are physically related, although they both may represent brittle fracturing in the conductive cooling regime. One of the objectives of the present work is to study the origin of the clinopyroxene vein, and its relationship to the rest of the sample.

3. ANALYTICAL PROCEDURES

3.1 Major and Trace Elements

Diopsides were analyzed in thin sections of the abyssal peridotite. Major element data were collected on a JEOL 733 Superprobe at the Massachusetts Institute of Technology, using mineral standards. For clinopyroxene and orthopyroxene, a broad beam of 10 μm was used to obtain bulk analysis of grains incorporating possible exsolution lamellae.

REE and the trace elements Sr, Zr, Ti, Y, V and Cr were analyzed in situ by Dr. Henry Dick, using the Cameca IMS 3f ion microprobe at the Woods Hole Oceanographic Institution, employing energy filtering to exclude molecular ion interferences (Shimizu et al., 1978). Analytical techniques can be found in Johnson et al. (1990). Overall accuracy and precision of the data is generally believed to be: 5%-10% for Ti ,Cr and V, 10%-15% for Sr and Zr, 10%-20% for the light rare earth elements and 10%-15% for the heavy rare earth elements (Johnson et al., 1990).

3.2 Water, Carbon and Sulfur Analysis

H_2O, CO_2 and S bulk rock analysis was performed by gas chromatography on a FISONS EA 1108 Elemental Analyzer at the Woods Hole Oceanographic Institution.

3.3 Sr-Nd Isotopic Analysis

Samples were prepared for Nd-Sr analysis by standard methods (Zindler et al., 1979). Nd and Sr isotopes were run on the WHOI VG-354 mass spectrometer using dynamic multicollection. $^{87}Sr/^{86}Sr$ data are relative to 0.710240 for the NBS 987 standard and are normalized to 0.1194. Nd isotopes are normalized to $^{146}Nd/^{144}Nd=0.7219$ and are relative to 0.51264 for the USGS BCR-1 standard.

For the Sr and Nd isotopic analysis of hand-picked clinopyroxene, the leaching and dissolving procedures followed those of Snow (1993) and Snow et al. (1994).

3.4 Magnetic Fraction Separation

The conditions for the magnetic separations are given in Table 1. All samples were leached in 2.5N HCl for 15 mins at room temperature for Sr isotopic analysis.

3.5 Os Isotopic Analysis and Leaching Procedures

F (μm)/Sample	D(g)	E(g)	DM(g)	EM(g)	Current(a)
start	90.48	87.22			
437-760 (μm)	11.80	11.94	3.82 (48%)	4.07 (52%)	0.0135
			2 [illegible]%)	2.06 (102%)	0.0085
<437 (μm°	3.38	3.10			
start	105.8	103.9			
157-286 (μm)	5.94	7.10	0.76 (15%)	1.00 (18%)	0.0085
<157 (μm)	8.37	9.00			
start					
111-157 (mm)	25.27	24.70	[illegible]%)	0.13 (14%)	0.0075
<111 (μm)	24.36	23.57			

Table 1. Magnetic separation data. Numbers in the parenthesis in the fourth and the fifth columns are the ratios of the magnetic fractions to the non-magnetic fractions at certain magnet currents. e.g., (the weight of magnetic fraction)*100%/(the weight of non-magnetic fraction) at current of 0.0085a.

For bulk rocks and leached residues, standard Os isotopic analysis techniques were used (Hauri and Hart, 1993, and ref. within) involving NiS fire assay. Nickel fire assay with sodium tetraborate flux was used for all the solid samples to ensure complete dissolution and sample-spike equilibration. Fusion and Os separation were based on the techniques of Luck (1982), Ravizza (1993), Reisberg et al. (1991), and Hoffman et al. (1978). Os isotope analysis was conducted on the NIMA-B mass spectrometer. Os isotopic compositions are corrected to both ^{192}Os and ^{188}Os.

3.5.1 Sequential leaching

Two splits of fine-grained powders (less than 256 μm) were carried through sequential leaching tests at the same time. After each step, the samples were magnetically separated at a current of 0.18a to test how much magnetite was being dissolved during the leaching. Leachate concentrations are reported both relative to the weight lost after each step and by the absolute Os present in the leachates.

First step: Sample was leached in 5 ml Vycor 80% HF+20% HCl in a 15 ml Teflon beaker. The beaker with threaded lid was placed on a hot plate at 75°C for 4.5 hrs. At the end, the residue powder and leachate were separated by centrifuge. The residue powder was rinsed several times with Vycor water and dried down with ethyl alcohol in an oven at 100°C. I collected the leachate and the first water rinse together.

Second step: To the residue from the first leaching, 5 ml 6.2N Vycor HCl was added in a 15 ml Teflon beaker with threaded lid, placed on a hot plate between 50°C to 70°C for 2.5 hrs. This was followed by sonicating for 30 mins. The residue and leachate were separated by centrifuge. The residue was treated as in the first step. The leachate and the first water rinse were combined.

Third step: A Cr (VI) oxide solution was made by dissolving about 1 g of CrO_3 powder in about 10 ml 36N Seastar H_2SO_4. The solution was over saturated. To the second residue from one of the splits, 2 ml of this solution was quickly added in a 15 ml Teflon beaker and capped immediately. The mixture was sonicated for 20 mins and left overnight at room temperature, and was then put onto a hot plate at 50°C for 15 mins the next day. The residue was centrifuged and dried down in an oven with a large amount of ethyl alcohol, at less than 100°C. The leachate and all the water rinses were combined.

Leachate: All of the leachates were transferred to 30 ml Teflon bombs. Enough ethyl alcohol was added to total 30 ml, and heated on a hot plate at less than 100°C, with lids, overnight. This was to reduce Os to $OsCl^{2-}$ form. The leachates were dried down to about 1/3-1/2 of the volume, on a hot plate the next day. 4N Seastar H_2SO_4 was added to total 30

ml, in order to equilibrate the sample with sulfate. Evaporation was continued to dry down to the last few drops (before sample became gravy) and prepared for distillation.

Spike: All the residues and leachates were spiked using a 24 ppb spike. The leachates were spiked directly in the distillation flask.

3.5.2 Single step leaching

For all of the single step leachings, the samples were distilled right from the distillation flask with a mixture of Vycor acid and water. The spike was added in the HBr collector tube to ensure sample-spike equilibration. The term 'first leachate' refers to the Os collected at this stage. The acid mixtures and residues then were centrifuged and separated. The acid mixture is referred to as the 'real leachate' or the 'second leachate' for this particular method.

The leachate concentrations are reported both as total Os present in the solutions, and relative to the weight loss for each step (less precise).

H_2O_2 leaching: 10 ml of Vycor water and sample powder were added into the distillation flask. The unit was sealed, and 30% H_2O_2 was fed in from the carrier gas arm to make 5% H_2O_2. The carrier gas arm was sealed immediately. Distillation was done at room temperature without running cooling water in the condenser. Bubbling in the HBr collector tube was strong and constant for the first 30 mins even without gas feeding, then the bubbling decreased. I collected the 'first leachate' in the HBr tube for about 2 hrs.

The residue and the acid mixture in the flask were centrifuged and separated. The residue was rinsed with Vycor water and air-dried. To the real leachate, enough CrO_3 solution was added to oxidize the H_2O_2 leachate until the solution became brownish, collecting Os in the HBr tube as usual.

HCl leaching: 10 ml of Vycor water and sample powder were added into distillation flask. The unit was sealed, 10 ml 6.2N Vycor HCl was fed in from the carrier gas arm. The carrier gas arm was sealed immediately. The solution was distilled at room temperature for about 10 mins, then the temperature was increased to variac@70 for another 30 mins with cooling water running in the condenser. Bubbling in the HBr collector tube increased with increasing temperature at first, then decreased dramatically. The 'first leachate' was collected in the HBr tube for about 2 hrs.

The residue was treated following the procedures as in the H_2O_2 leaching. The 'real leachate' was saved in a Teflon jar.

HNO_3 leaching: 10 ml of Vycor water and the sample powder were added into distillation flask. The unit was sealed, then 10 ml 8N 2B HNO_3 was fed in from the carrier gas arm. The carrier gas arm was sealed immediately. The solution was distilled at room

temperature for about 30 mins, then increased temperature to variac@80 for another 30 mins with cooling water running. The reaction became very strong at the final 30 mins. The 'first leachate' was collected in the HBr tube for about 3 hrs.

The residue was treated following the procedures as in the H_2O_2 leaching. The 'real leachate' was saved in a Teflon jar.

3.6 Sulfide Analysis

The data are in-situ analysis of sulfides in thin sections. Major elements (S, Fe, Ni, Cu and Co) were collected on a JEOL 733 Superprobe at the Massachusetts Institute of Technology using an accelerating voltage of 15 KeV and a beam current of 10 nA. A beam spot size of 1 μm was used for all the sulfides. Double correction on sulfide standards was necessary to improve the results.

4. RESULTS

4.1 Results of Clinopyroxene Compositions From The Pyroxenite Vein

Clinopyroxene from the pyroxenite vein was picked and leached for Sr and Nd isotopic analysis. The results show that the Cpx has a slightly elevated Sr isotopic ratio (0.704067±0.0027%) and a Nd isotopic ratio close to N-MORB (0.513091±0.0009%). The data is close to those of the previous study (Snow et al., 1994) which has $^{87}Sr/^{86}Sr$=0.704870±0.0013% and $^{143}Nd/^{144}Nd$=0.512994±0.0015%. The concentrations of the Sr and the Nd are 19.33 and 1.013 ppm, respectively. For Nd, the concentration data are close to that from Snow et al. (1994) of 1.056 ppm.

4.2 Results of Magnetic Fraction Separation---the Fate of the 'Orphan ^{87}Sr'

The results are given in Table 2.

Snow et al. (1994) suggested a hypothesis for the anomalously high $^{87}Sr/^{86}Sr$ in magnetic separations from several abyssal peridotites. He proposed that the fine-grained detrital fraction of oceanic sediments was somehow infiltrated into abyssal peridotites on the sea floor as a result of very large water/rock ratios. In order to understand this hidden alteration mechanism, I took one of Snow's most radiogenic samples in an attempt to reconstruct the alteration history. The first step was to locate where this anomalous radiogenic Sr was concentrated in the peridotite. The strategy was to conduct an analysis of different parts of the sample, and then through different sieve sizes of magnetic separations. In the sampling, the dredged boulder was first cut into different segments, in terms of outer, more altered rims and inner, fresher cores (see Plate (2,3,4)). The clinopyroxenite vein, which cross-cuts the sample, was also separated to avoid any confusion from different origins. The idea of testing different sieve sizes of the magnetic separations was the belief that the smaller grains should contain more radiogenic isotopic ratios than the coarser grains. Rock powders and thin sections were made for each part of the sample, and all locations were carefully mapped in order to reconstruct later on. Crushed rock powder was carefully picked and alcohol washed in order to avoid unnecessary contamination during the processing. The crushed powder then was separated using the same magnetic separator used by Snow (1993). The magnet current was adjusted for the best conditions for bimodal separation of magnetic and non-magnetic parts of the individual samples.

As shown in Table 2, there are no samples with $^{87}Sr/^{86}Sr$ higher than the seawater, even the unleached whole rock. All of the data have $^{87}Sr/^{86}Sr$ between 0.705 and 0.708. The

Sample No.	$^{87}Sr/^{86}Sr$	err	Sr (ppm)
Whole rock			
A	0.707257	81	7.38
B	0.706019	90	4.68
D	0.706150		3.50
E	0.705978	21	3.14
RC27-9-6-2 (Snow, 1993)	0.706222	23	4.13
Leached whole rock			
LA	0.707145	110	5.34
LB	0.704782		4.35
LD	0.706118	68	2.03
LE	0.705582	14	2.49
Leached magnetic separations			
DLM11	0.705252		0.67
ELM11	0.707265		0.87
DLM12	0.707435	275	0.65
ELM12	0.707755	25	0.60
FLM12	0.708173	181	1.19
DLM47	0.707102	23	1.16
ELM47	n.d.		n.d.

Table 2: Sr isotopic ratios and concentrations for the whole rock powder and the leached magnetic separates. The samples are leached in 2.5 N HCl at room temperature. Numbers after the magnetic separations represent the seive sizes of magnetic separations, e.g., 11 indicates the size fraction between 111to 157 μm. For the size legend in the first column, see Table 1. The errors of Sr isotopic analysis are relative to the last reported digid based on in-run statistics.
n.d. = not detetable

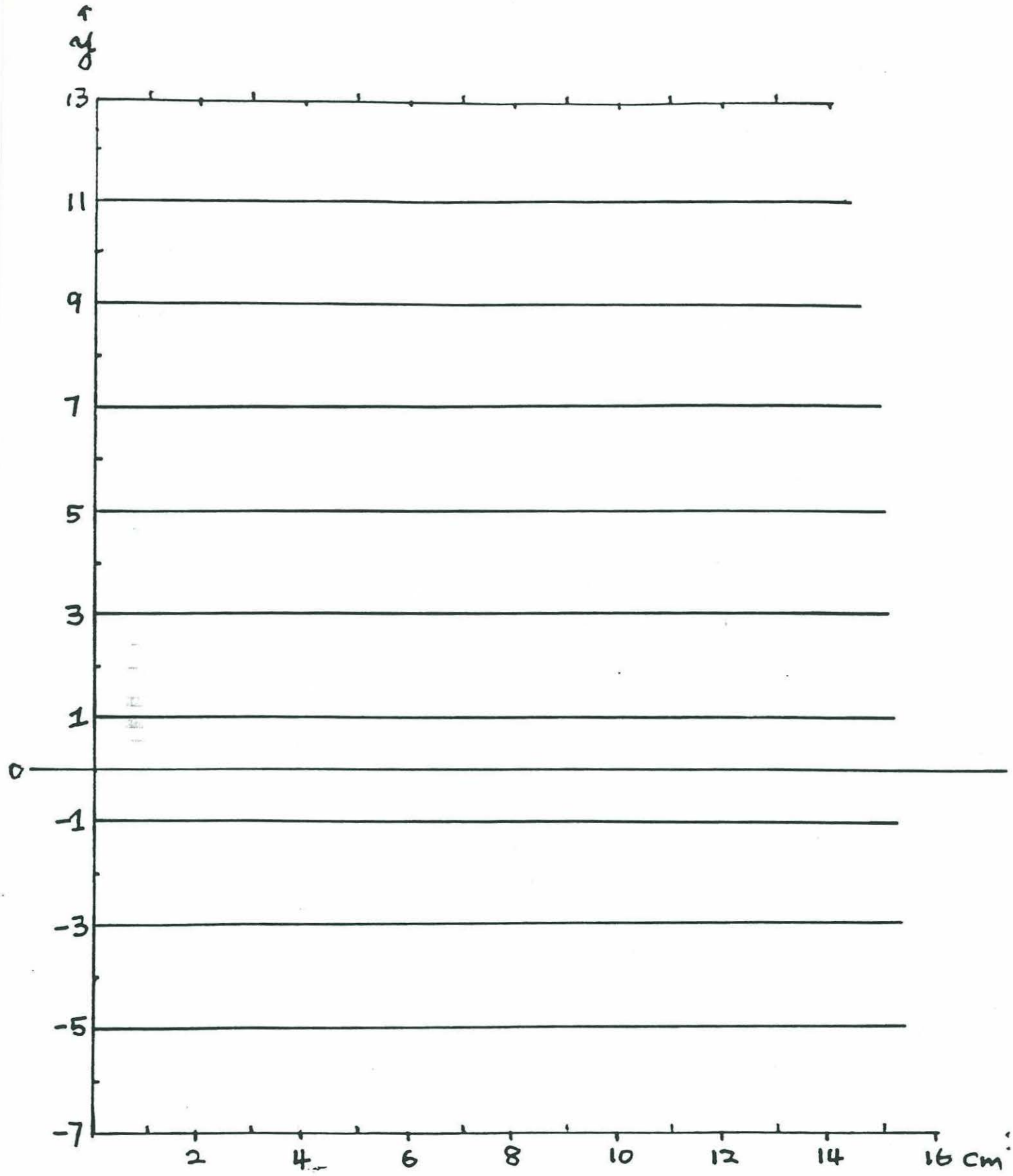

Plate 2: The reference coordinates for the sample slab relative to the clinopyroxenite vein. The coordinates are mainly based on the position of the vein in slab 2 (the thin section slab).

Plate 3: Outline of sample slab1 relative to the reference coordinates. Different fractions for isotopic and bulk rock analyses are also shown.

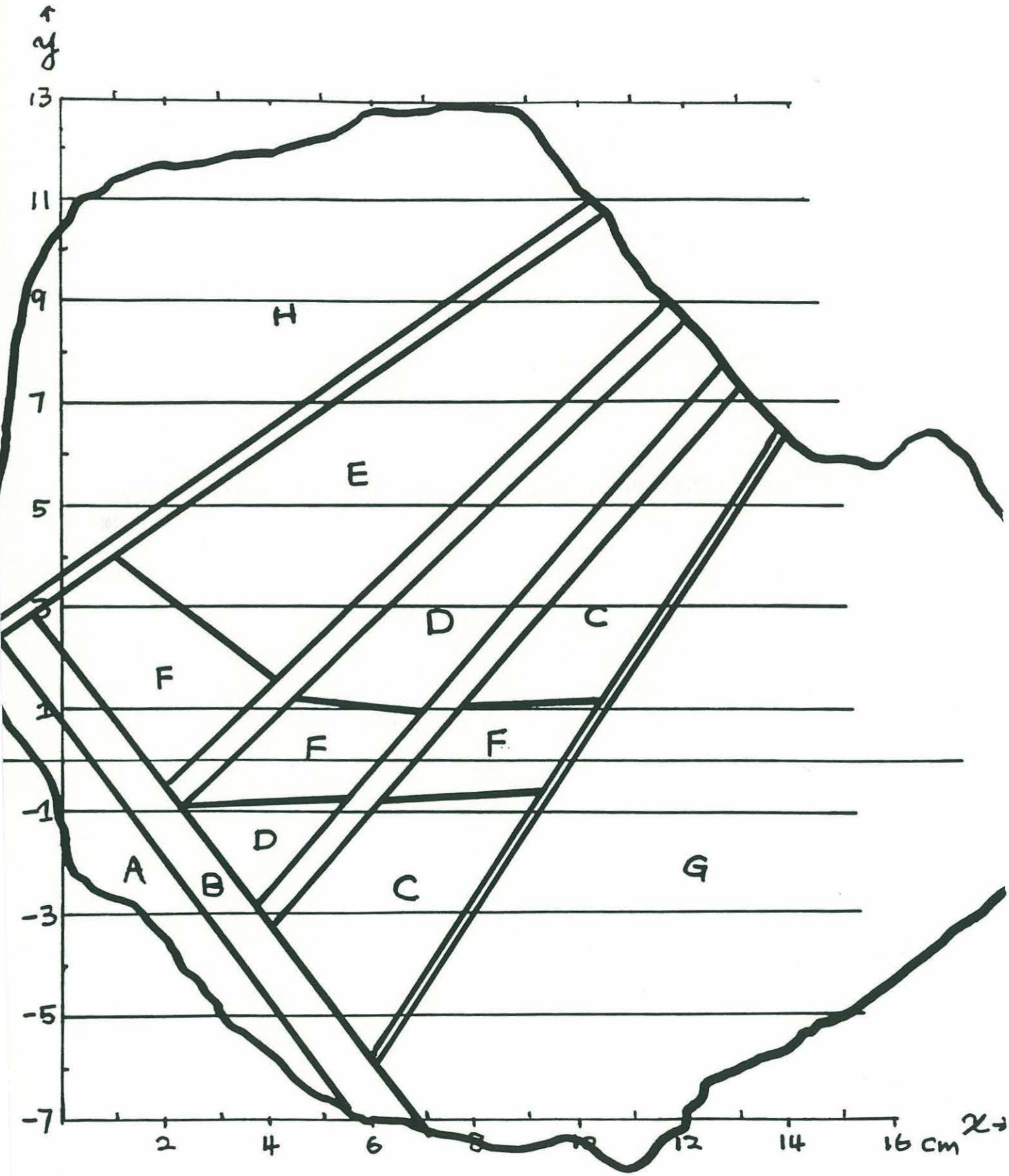
y
13
11
9
7
5
1
-1
-3
-5
-7
H
E
D
C
F
F
F
D
A
B
C
G
2
4
6
8
12
14
16 cm
x

Plate4: Xerox of sample slab 1. Data in parenthesis are Os isotopic ratios for each fraction.

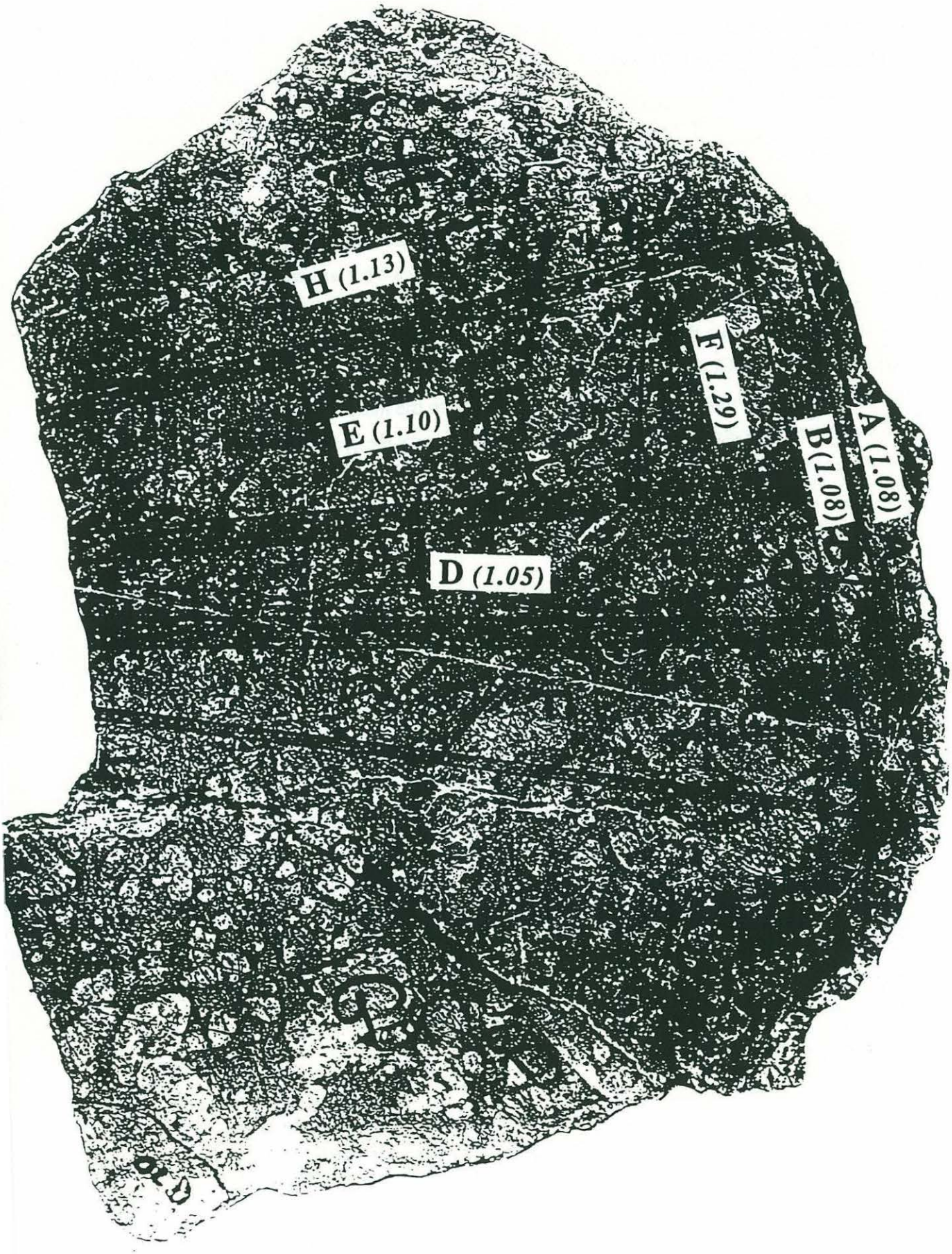
H (1.13)
F (1.29)
E (1.10)
B (1.08)
A (1.08)
D (1.05)

highest value is from the 157-286 μm fraction from sample F. It is probably premature to conclude that there is any relationship between different grain sizes, though for sample D and E, there is a tendency for the 157-256 μm size fractions to have higher $^{87}Sr/^{86}Sr$ than the 111-157 μm fraction. This is contrary to what is expected for the infiltration mechanism. For sample D, the 157-256 μm fraction is more radiogenic than the 437-760 μm fraction. Taking the whole data set into consideration, the magnetic separations of sample E have higher $^{87}Sr/^{86}Sr$ than the leached and unleached whole rock, suggesting a normal seawater alteration effect, while sample D shows a heterogeneous distribution of $^{87}Sr/^{86}Sr$. For the leached and unleached whole rock data, sample D has higher $^{87}Sr/^{86}Sr$ than sample E, while the magnetic fractions for both show the reverse. The leaching reagent is 2.5N HCl acid, which removes only contaminating carbonate. In general, the magnetic separations have higher $^{87}Sr/^{86}Sr$ than both the leached and unleached whole rock, which indicates that the magnetic separations carry the sea water signature. While the differences between each fraction are not dramatic, the heterogeneous distribution of Sr isotopic ratios is probably real, and this points either to a different source generation related to the clinopyroxenite vein, or to the complex mechanism of this infiltration process.

4.3 Results of Os Leaching Experiments

No clear core-altered rim relationship has been found (Fig. 2) in the present study. We take sample H, the outer part of the boulder right next to parts E and F (see Plate 4), as a proxy to address both the alteration and magmatic effects in the leaching study. We started with a powder size less than 256 μm. The results are given in Table 3 and Fig. 3.

We conducted both single and sequential leaching tests in order to look for the efficiency of different acids on target minerals. In the single leaching studies, we used conventional acids that have been used previously in leaching studies for isotopic analysis: hydrogen peroxide (H_2O_2) has been reported to remove the contamination of radiogenic Fe-Mn oxyhydroxides (Palmer et al., 1988; Martin, 1991; Roy-Barman and Allegre, 1994); hydrochloric acid (HCl) is traditionally used in Sr and Nd isotopic analysis to remove contaminating carbonate and some Fe-oxides. Nitric acid (HNO_3) (and even hydrofluoric) are more active on silicate minerals. These minerals often decompose and show frosted surfaces after the nitric treatment. The nitric acid also dissolves and oxidizes most of the sulfide minerals (Hart and Ravizza, 1996) such as pyrrhotite and chalcopyrite. Pentlandite, on the other hand, may rather be dissolved in concentrated hydrochloric instead of nitric acid, but the effect was not clear when tested on hand-picked sulfides.

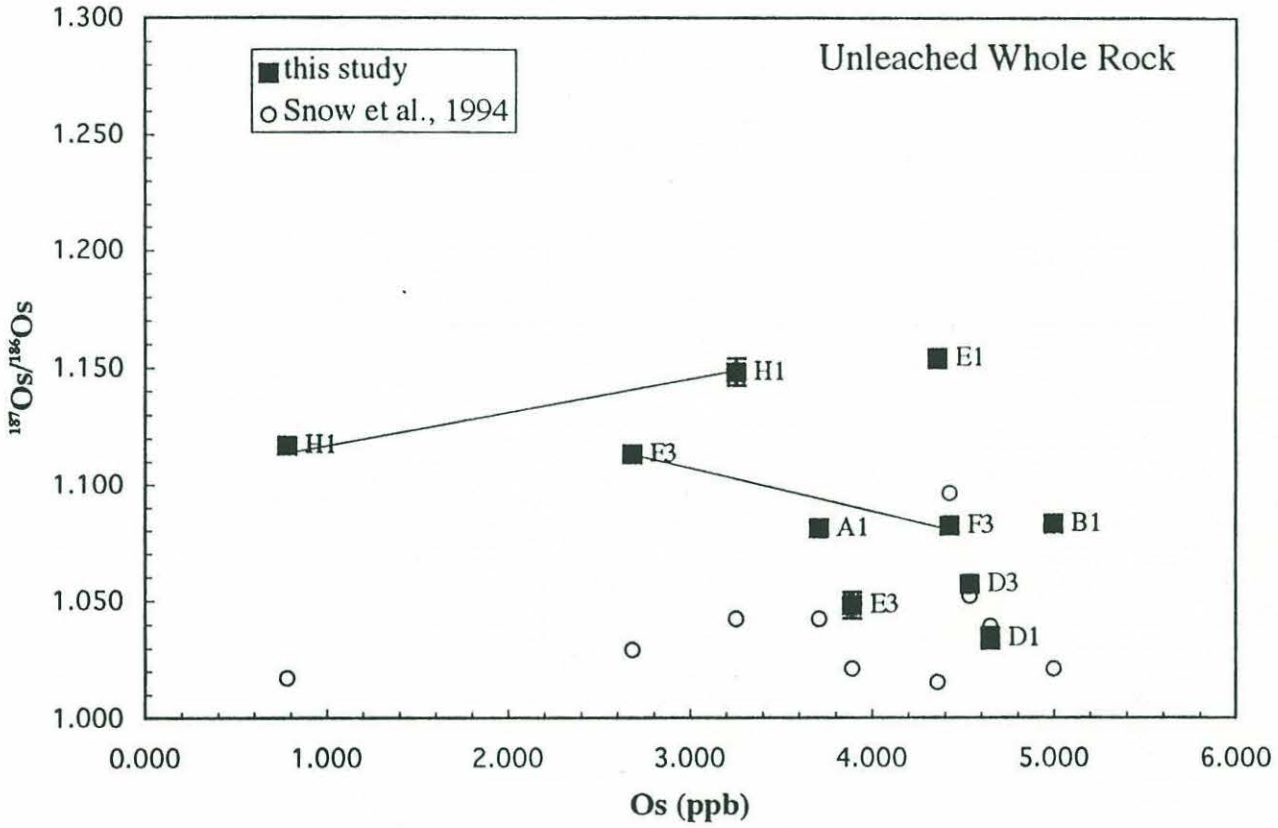

Fig.2: $^{187}Os/^{186}Os$ vs. Os concentration in bulk abyssal peridotites. Tie lines connect the duplicate analysis data from the same slab. The abyssal peridotites from Snow et al. (1995) are also shown for comparison.

Table 3: Os isotopic and trace element data for the whole rock fractions, the magnetic separations and the Os leaching experiments.												
	Slice No	Split	Sample Type	wt(g)	$^{187}Os/^{188}Os$	2S.E. (%)	$^{190}Os/^{192}Os$ ($^{190}Os/^{188}Os$)*	2S.E. (%)	Conc.'(ng)	Conc.²(ppb)	2S.E. (%)
Unleached bulk rock											
UA	1	1	whole rock	0.5066	1.081	0.37	2.558	0.11		3.713	0.19
UB	1	1	whole rock	0.5032	1.083					5.000	
UD1	1	1	whole rock	1.9874	1.057	0.24	1.133	0.07		4.541	0.19
UD3	3	1	whole rock	0.5036	1.034+	0.45	1.183	0.22		4.652	0.54
UE1	1	1	whole rock	0.5081	1.154	0.40	1.595	0.13		4.362	0.27
UE3	3	1	whole rock	0.5027	1.048	0.56	1.199	0.18		3.894	0.48
UF3-1	3	1	whole rock	0.4935	1.113	0.25	1.514	0.09		2.683	0.30
UF3-2	3	2	whole rock	0.5207	1.082	0.23	4.797*	0.06		4.428	0.20
UH1-1	1	1	whole rock	0.5123	1.117	0.28	3.779	0.10		0.782	0.26
UH1-2	1	2	whole rock	0.5067	1.148	0.58	1.308	0.20		3.256	0.48
RC27-9-6-2 (Snow, 1993)			whole rock		1.042					4.480	
Magnetic seperation											
LEM	1	1	111-157μ, 2.5N HCl leached	0.0372	1.063	1.41	6.642*	0.25		10.333	0.24
Single step leaching											
LHA-1-1	1	3	H2O2 ' first leachate'	1(0.0643)	0.480	7.82	38.787	1.53	0.007	0.103	6.51
LHA-1-2	1	3	H2O2 'real leachate'	1	1.173+	0.90	10.572	0.25	0.093	1.445	0.44
LH-1-3	1	3	residue after H2O2	0.5113(1.9979)	1.138	0.54	1.295	0.15		3.377	0.39
LHA-2-1	1	4	HCl 'first leachate'	1(0.733)	0.188	6.74	43.666	1.68	0.004	0.005	11.94
LH-2-3	1	4	residue after HCl	0.5082(1.9987)	1.139	0.34	1.228	0.11		3.977	0.34
LHA-3-1	1	5	8N HNO3 'first leachate'	1(0.7778)	1.147	0.24	0.933	0.08	3.836	4.932	0.36
LH-3-3	1	5	residue after HNO3	0.5222(1.9938)	1.117	0.34	3.446	0.11		0.825	0.27
LDA-1-1	3	2	8N HNO3 'first leachate'	1(0.9211)	1.028	0.55	1.280	0.16	2.337	2.537	0.39
LD-1-3	3	2	residue after HNO3	0.5101(2.0647)	0.858	2.26	13.550*	0.37		0.601	0.17
LFA-1-1	1	1	Conc. HNO3 'first leachate'	1(2.0390-1.4866)	1.110	0.15	3.187	0.07	4.052	7.336	1.04
LFA-2-1	3	3	Conc. HNO3 'first leachate'	1(2.0216-1.2491)	1.075	0.23	3.245	0.06	3.974	5.144	1.03
Standard(40.6ppb)		1	8N HNO3 leaching	0.0841	1.445	0.21	1.202	0.07		23.031	0.34
Standard(40.6ppb)		2	8N HNO3 leaching~	0.0864	1.375	1.16	4.330*	2.37		35.199	0.61
Standard(40.6ppb)		3	Conc. HNO3 leaching	0.0835	1.453	0.33	3.978*	0.07		27.454	0.08
Sequential leaching											
Experiment I											
LHA-1-1	1	6	(HF+HCl) leachate	1(1.58)	1.307	0.41	1.124	0.13	2.072	1.311	0.42
LHA-1-2	1	6	HCl leachate	1(0.54)	1.224	2.09	1.377	0.15	1.332	2.466	0.42
LHA-1-3	1	6	Cr (III) sol'n leachate	1(0.04)	1.199	0.62	1.513	0.21	1.203	30.085	0.52
LH-1	1	6	residue	0.496(3)	1.116	0.64	3.305	0.21		0.837	0.37
Experiment II											
LHA-2-1	1	7	(HF+HCl) leachate	1(1.71)	1.156	0.34	1.979	0.12	1.031	0.603	0.28
LHA-2-2	1	7	HCl leachate	1(0.4)	1.150	0.26	1.813	0.10	1.002	2.505	0.29
LH-2	1	7	residue	0.5001(2.97)	1.186	0.36	1.242	0.12		3.986	0.36
~: Sample was mixed with spike in distillation flask during leaching, otherwise was spiked seperately in HBr collection tube.											
+: dats are corrected based on ^{188}Os because of the ^{186}Os interference.											
(): The number in parenthesis in the fifth column are either the starting weight for residues, or the amount of the sample being leached in the leachates.											
': For the definition of the leachates, see the 'Os isotopic analysis and leaching procedures' in the 'Analytical Procedures'											
conc.'(ppb), Absolute amount of Os (ng) presents in this part of the sample.											
conc.²(ppb), Amount of Os (ng) divided by the amount of sample (g) being used.											

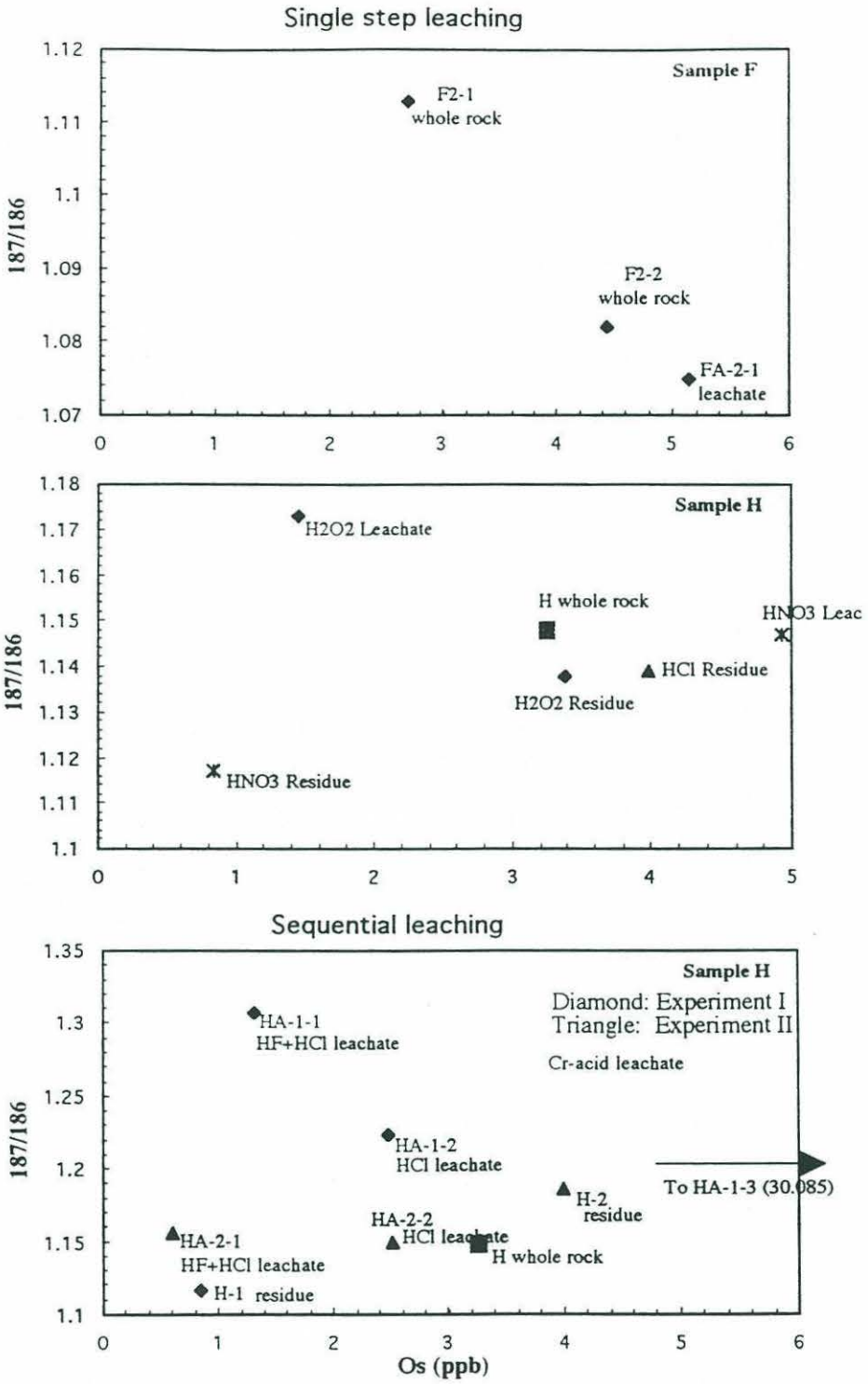

Fig.3: $^{187}Os/^{186}Os$ vs. Os concentration in the leached abyssal peridotite RC27-9-6-2 and its leachates. Leaching experiments were conducted on samples H and F only. For procedures for single and sequential leaching, see the 'Analytical Procedures' in text.

In the sequential leaching studies, we focus on both removing alteration and extracting primary Os from the whole rock powder. The first two steps in the sequential leaching were intended to decompose the silicates and get rid of alteration. The final step using the chromic acid was to oxidize the sample and remove Os from the sulfides, assuming that the sulfides are the major Os reservoir in this sample. Following each leaching step, magnetic separation was also conducted to keep track of the amount of iron oxides and iron sulfides relative to chromite and silicates (which are non-magnetic at roughly 0.18a) (Hart and Ravizza, 1996). The result shows that after the first HF+HCl leaching, the magnetic fraction at 0.18a decreases from 86% to 8.5% of the total. The second step decreases the magnetic fraction to less than 1.2%. The weight lost during leaching are 53% and 38% for the first two steps, indicating that there was a lot of magnetic minerals dissolved. The residue after the first two steps of leaching is a very fine-grained, clean powder composed of almost 100% silicates.

The leachate from the hydrogen peroxide acid leaching has a slightly higher isotopic composition than the residue. Fe-Mn oxyhydroxides do not seem to be the major contamination in this rock based on the leachate composition. The leachate contains a much lower Os concentration than the residue, though it is still significant when compared to other type of oceanic rocks. Although a weak oxidizer, H_2O_2 is still able to oxidize some reduced phases in the rocks such as sulfides, causing the concentration in the leachate to be higher than in the contaminants. Following the same rationale, H_2O_2 must be a weak oxidizer at room temperature (though the reaction was slightly heated up during the experiment) as the residue still contains 99% of the Os budget. Mass balance shows that 98% of the total Os was recovered.

The 'first leachate' of the hot HCl leaching experiment contains, as expected, a negligible amount of Os (Fig. 3). Because this fraction was over-spiked, the isotopic ratio is not meaningful. The residue is slightly more unradiogenic than the bulk rock. Mass balance shows that the residue contains 77% of the total Os budget. We expect that the Os concentration in the 'real leachate' should be higher, as it may contain Os from both the serpentinization products and some soluble sulfides.

Unlike the previous leachings, the hot nitric leaching has a reverse relationship between the 'first leachate' and the residue. The 'first leaching' contains a large amount of Os with almost the same isotopic ratio as the bulk sample. The residue, on the other hand, has a lower Os concentration and a lower $^{187}Os/^{186}Os$ than the bulk rock. Nitric acid is a very strong oxidizer, and it oxidizes reduced phases efficiently. The high concentration and the constant isotopic ratio in the 'first leaching' indicates that most of the Os budget is contained in these phases and is preferentially removed. The most probable identity for

these phases is sulfide. Other possible candidates are those being reduced during serpentinization, such as magnetite. Recovery was poor in this experiment, since the nitric acid interferes with the distillation and thus oxidizes the HBr and the spike in the collector tube, which in turn causes loss of spike and lack of spike-sample equilibrium. The recovery for this procedure is only about 70% as judged using standards.

Both leachates from the two sequential leachings have more radiogenic isotopic compositions than the bulk rock. Leachate 2 has a higher concentration due to the smaller weight loss in this step, in which fewer Fe-oxides were dissolved. A big difference between these two experiments is the nature of the residues. Cr (VI) oxide is a stronger oxidizer than nitric acid. The residue after this Cr-oxide leaching has a lower $^{187}Os/^{186}Os$ and much lower Os concentration than the bulk rock, which is consistent with the result from the nitric acid leaching. The leaching test without the Cr-oxide is more radiogenic, but similar to the result of the third leachate from experiment I. Mass balance in these two experiments was very poor; only about 55% of the Os was recovered. One possible cause is in the analytical technique, and the uncertainties in the phases actually dissolved in certain acids. However, this study does show a nice leachate-bulk rock trend with a decreasing $^{187}Os/^{186}Os$ and an increasing Os concentration. This indicates that some of the radiogenic Os was leached out, and it is unlikely to be from the primary phases. The residue from experiment 1 has the lowest isotopic composition of all the data (the residue from the nitric leaching is only slightly higher), indicating that this leaching procedure is promising to recover a primary Os signature from serpentinized rocks.

Another result obtained by fusing the weakly leached magnetic separation (111-157 μm) from part E shows that it also has a large amount of Os with very low $^{187}Os/^{186}Os$, compared to the bulk rock. This magnetic separation at a current of 0.0075a contains magnetite and possibly some pentlandite. It is obvious that the sulfides contained in this matrix contribute to the high Os concentration. Because of the presence of magnetite, the low isotopic composition suggests that the extent of seawater alteration is probably low. It is also possible that the low isotopic composition is a dilution effect from the pentlandite.

5. MINERALOGY

Major element analyses are summarized in Tables 4 through 8. Positions for most of the clinopyroxenes, orthopyroxenes, spinels and plagioclase analyzed are indicated (Plate 6) relative to the positions of the thin sections (Plate 5). Olivine shows little variation in Mg number ([Mg]), with an average value of 90.2. This is close to the average value of 90.1 for dredged peridotites away from hot spot regions (Dick, 1989, 1996). Diopside and enstatite compositions are plotted in the pyroxene quadrilateral in Fig. 4. Also shown for comparison are harzburgites from Hess Deep. The variations of Wo component between diopside and enstatite are larger than for normal abyssal peridotites, which may indicate that the two pyroxenes are reequilibrated over a larger temperature range. Spinel mainly lies on the mantle-melting array defined by abyssal peridotites from the Atlantic and Indian Oceans (Dick and Bullen 1984) (Fig. 5), with the exception of the part of the sample furthest away from the clinopyroxenite vein, in which the spinels are slightly off toward lower Mg and Cr contents relative to the array. Enstatite has a calcium content ranging from 0.81 to 2.65 wt%, with an average value of 1.56 wt%. This is lower than average abyssal peridotites. The alumina content in enstatite ranges from 1.94 to 4.03 wt%, which is low compared to average abyssal peridotites. Given the fact that the Mg number is buffered by olivine and two pyroxenes during melting, and that the coexistence of diopside and enstatite during melting buffers the minimum alumina content of enstatite, and therefore the upper limit of Cr number ([Cr]) in coexisting spinel (Dick 1996), this sample should melt in the four-phase field (Ol-Opx-Cpx-Sp) as do other abyssal peridotites. The low calcium content of the enstatite may indicate other processes such as a low closure temperature rather than a high degree of melting as in alpine peridotites (Dick and Fisher 1984).

Figs. 6 through 11 are plotted as element concentrations versus distance. There is a slight tendency for increasing Cr_2O_3 and TiO_2 contents and a decreasing MgO content from (-36) mm to 0 mm (the position of the pyroxenite vein). The Mg number for orthopyroxene near the vein also tends to be lower. The orthopyroxene adjacent to plagioclase has anomalously low Al_2O_3, Cr_2O_3 and CaO contents. Spinel has uniform composition throughout the sample except in the very upper part. These spinels are the ones that are off the mantle-melting array. In general, there is no strong correlation between the vein and the rest of the sample; the variation for both sides of the sample relative to the pyroxenite vein is not symmetric either.

A few unusual vein areas in the upper part of the sample were found to include minerals such as plagioclase and amphibole. The plagioclase composition in the pyroxenite vein is An74, while the anorthite content in the upper part of the sample could be as sodic as

Plate 5: Outline of the positions of the thin sections relative to the reference coordinates. Cpx grains in the clinopyroxenite vein are emphasized. Also shown on the right top is the thin plagioclase-rutile veinlet. This thin veinlet is basically limited to thin section 2B.

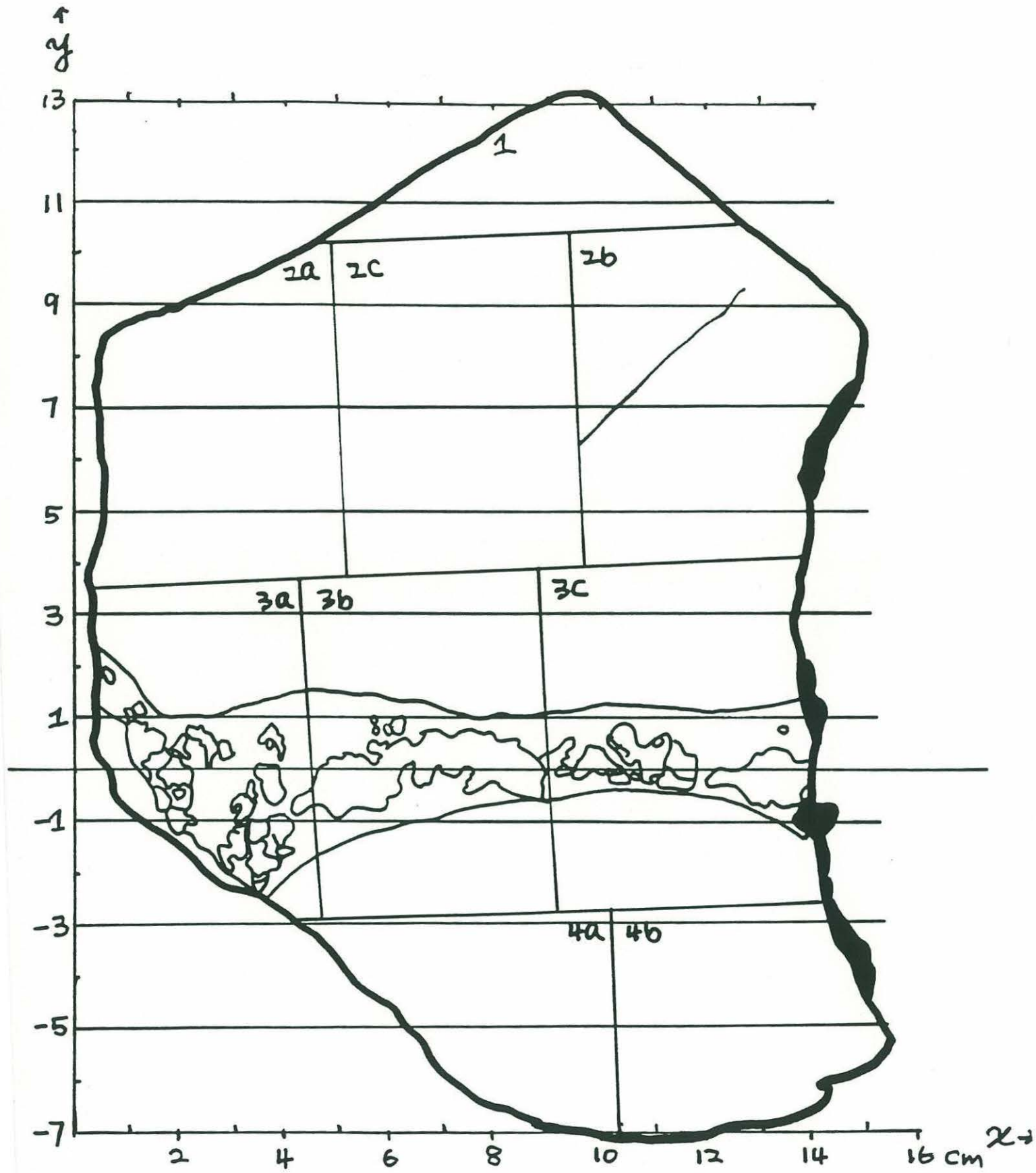
y
13
11
9
7
5
3
1
-1
-3
-5
-7
1
2a
2c
2b
3a
3b
3c
4a
4b
2
4
6
8
10
12
14
16 cm
x

Plate 6: Positions of onprobed clinopyroxene grains relative to the reference coordinates. The orthopyroxenes coexisting with clinopyxene grains are also shown. Positions of the plagioclase in thin sections 2B and 3A, and most of the spinel grains are also plotted for reference.

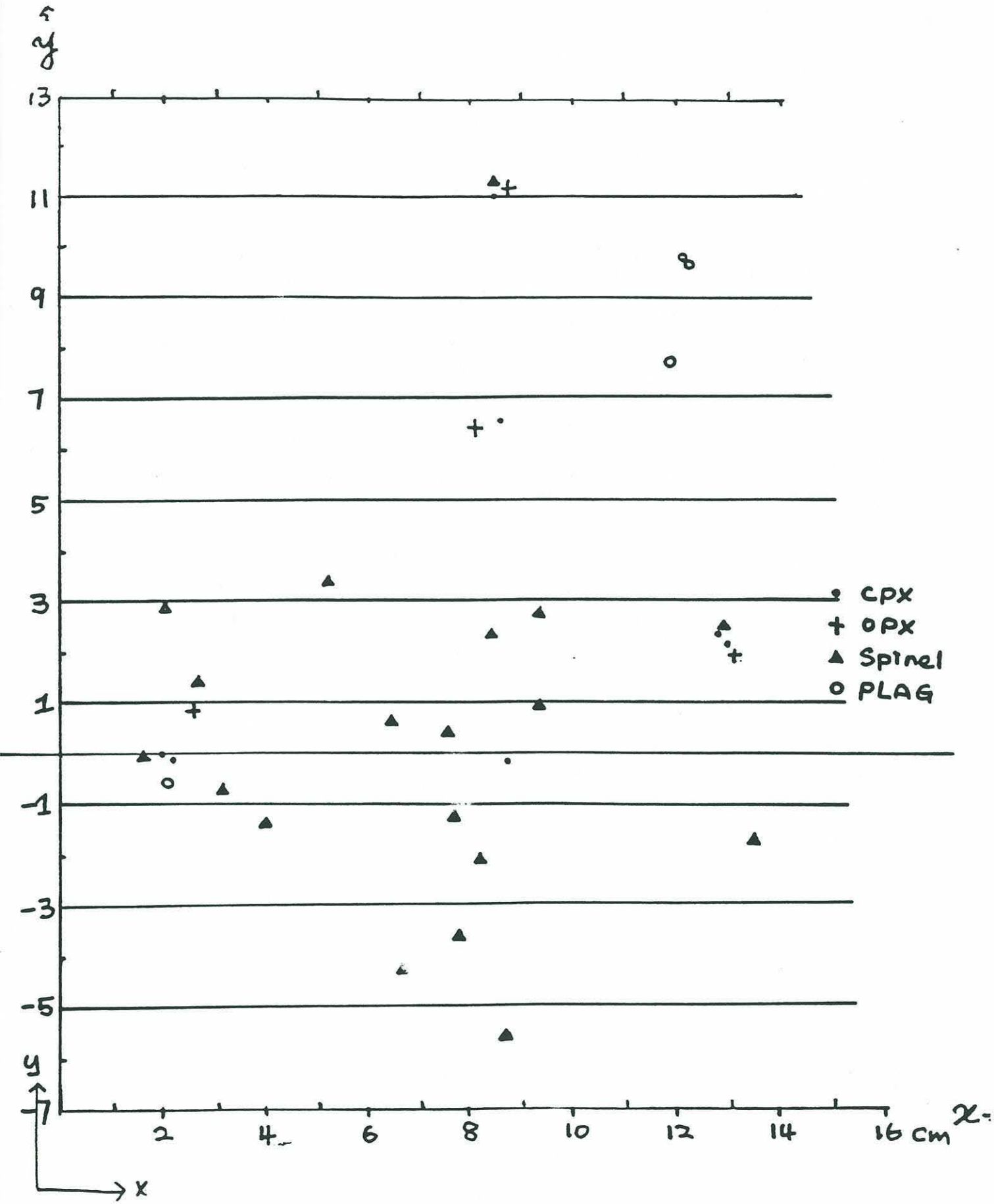
y
13
11
9
7
5
3
1
-1
-3
-5
y
x
2
4
6
8
10
12
14
16 cm
x
cpx
opx
Spinel
PLAG

An54. A plagioclase precipitated directly from MORB liquid has an anorthite content from An60 to An 85 (Dick, 1996), although plagioclase found in trapped melt in the Hess Deep has anothite content as calcic as An94, depending on the melt/rock ratio (Dick, 1996). The plagioclase in the pyroxenite vein could be explained as precipitating from liquid with MORB composition, while the others could be either magmatic in origin, or caused by hydrothermally Ca exchanged with seawater. There is no Eu anomaly observed in clinopyroxene coexisting with plagioclase in the vein, which may indicate that either the plagioclase was crystallized after the Cpx recrystallized, or the oxygen fugacity is much higher than the normal MORB mantle condition at the time Cpx and plagioclase coprecipitated (Irving, 1978; Green, 1994). In the upper part of the sample, no Cpx adjacent to plagioclase has been found, and the appearance of ilmenite after rutile suggests a high oxygen fugacity event. In general, no analyzed Cpx shows any Eu anomaly (see Fig. 12). The lack of a Eu anomaly in Cpx and the origin of plagioclase in the upper part of the sample still needs further detailed studies.

Table 4: Major element abundances for CPX from RC 27-9.																								
Thin Sect.	Piece	Cord X	Cord Y	Ref X	Ref Y	Gr.	Pts.	Loc	Gr.size(mm)		SiO2	TiO2	Al2O3	Cr2O3	FeO	MnO	MgO	CaO	Na2O	Total	[Mg]	Wo	En	Fs
RC27-9-6-2 CPX Composition																								
1A		41.60	13.06	83	111	1	10	R	2	1.2	51.8	0.23	4.18	1.59	2.62	0.11	16.82	22.02	0.60	99.9	92.0	46.4	49.3	4.3
1A		42.05	12.79	83	111	1	20	C	2	1.2	52.3	0.13	4.76	1.62	3.41	0.12	19.18	18.43	0.51	100.4	91.1	39.0	55.5	5.5
2B		30.72	22.85	134	65	1	6	R	2	2	52.1	0.17	4.41	1.49	2.59	0.09	16.4	23.3	0.65	101.1	91.9	48.4	47.4	4.2
2B		30.15	24.20	134	65	1	11	C	2	2	52.3	0.14	4.81	1.59	3.24	0.10	18.6	19.6	0.50	100.9	91.2	41.1	53.7	5.2
2B		42.64	37.82	122	64	2	1				54.8	0.24	2.20	0.71	2.30	0.11	17.53	23.93	0.40	102.3	93.1	47.7	48.7	3.6
2C	2	40.07	44.09	86	66	1	10	C	3	2	52.1	0.15	4.85	1.59	2.92	0.10	17.77	19.85	0.84	100.2	91.6	42.5	52.6	4.9
2C	2	40.72	43.34	86	66	1	10	R	3	2	51.9	0.17	4.99	1.49	2.72	0.08	17.55	20.12	1.11	100.1	92.1	43.1	52.3	4.6
3A	3	39.05	71.80	19	-1	1A	10	C	1.75	1	52.1	0.27	5.34	1.69	3.62	0.13	19.32	17.46	0.46	100.4	90.7	37.7	56.4	5.9
3A	3	39.45	71.07	19	-1	1A	10	R	1.75	1	52.5	0.30	4.04	1.62	2.93	0.12	17.79	20.74	0.50	100.5	91.6	43.6	51.7	4.8
3A	3	40.96	70.57	22	-2	3	20	B	6	3	52.0	0.46	4.96	1.61	3.35	0.11	18.67	22.69	0.51	104.4	90.9	41.8	52.9	5.3
3A	3	40.87	70.26	22	-2	4	10	lam	?	?	51.5	0.25	4.99	1.59	2.72	0.11	15.70	22.55	0.57	100.0	91.1	48.5	47.0	4.6
3A	3	40.49	64.86			1B	10	R	?	?	52.0	0.23	4.78	1.52	3.08	0.12	18.11	20.02	0.51	100.4	91.3	42.1	52.9	5.0
3B		16.15	38.19	65	28	12	1	I	2	5	52.0	0.15	5.37	1.86	2.75	0.10	16.5	21.2	0.65	100.5	91.5	49.6	45.8	4.6
3B		20.73	34.21	62	23	11	5	C	2	3	52.5	0.14	5.21	1.67	3.75	0.09	19.9	17.3	0.56	101.2	90.7	36.8	57.2	6.0
3B		21.43	33.72	62	23	11	5	R	2	3	52.4	0.18	5.16	1.73	2.83	0.07	16.7	22.5	0.76	102.3	91.4	47.1	48.3	4.6
3B		37.10	31.95	63	7	10	5	C	2.5	3	52.1	0.22	5.40	1.71	3.17	0.10	17.5	20.3	0.70	101.2	90.9	43.2	51.5	5.2
3B		36.97	32.64	63	7	10	5	R	2.5	3	51.9	0.25	5.55	1.80	2.49	0.06	16.3	23.0	0.77	102.1	92.1	48.4	47.6	4.1
3B		49.47	79.62	87	2	13	10	C	8	6	52.2	0.20	5.23	1.51	4.17	0.14	20.71	15.92	0.50	100.6	89.9	33.3	59.9	6.8
3B		51.55	77.41	87	2	13	10	R	8	6	52.5	0.18	5.05	1.50	3.81	0.13	20.04	16.94	[illegible]	100.7	90.4	35.6	58.2	6.2
3B		45.58	23.75	55	-13	9	5	R	7	5	52.0	0.25	5.32	1.62	3.46	0.09	17.9	19.8	[illegible]	101.1	90.4	42.0	52.4	5.7
3B		46.57	57.70	55	-13	8	5	I	7	5	51.7	0.27	5.48	1.72	2.89	0.10	16.1	22.2	0.69	101.1	90.9	47.4	47.8	4.8
3B		53.25	52.17	83	-18	6	5	C	3.5	1.5	52.6	0.17	4.94	1.57	3.48	0.09	19.9	18.0	0.56	101.3	91.2	37.8	56.7	5.6
3B		53.23	53.37	83	-18	6	5	R	3.5	1.5	52.2	0.24	4.95	1.52	2.57	0.07	16.3	22.9	0.67	101.4	91.9	48.1	47.7	4.2
3B		55.31	55.40	85	-20	7	5	C	3	2	52.8	0.15	5.00	1.54	3.66	0.10	20.1	18.1	0.58	102.1	91.0	37.8	56.5	5.7
3B		55.42	54.66	85	-20	7	5	R	3	2	52.0	0.19	5.04	1.60	3.29	0.09	18.6	20.1	0.66	101.5	91.1	41.4	53.3	5.3
3B		55.22	23.41	54	-21	9	2	B	3	2	52.0	0.25	4.66	1.35	2.58	0.06	16.4	23.3	0.59	101.2	91.9	48.5	[illegible]	4.2
3B		47.03	24.32	54	-21	9	5	I	3	2	52.4	0.23	5.07	1.50	3.36	0.10	18.6	19.5	0.43	101.3	90.9	40.8	[illegible]	5.5
3B		58.99	45.70	77	-25	3	3	R	2.5	2	50.7	0.33	6.49	1.38	2.71	0.08	17.0	20.8	1.16	100.7	91.8	44.4	51.0	4.6
3B		58.95	46.16	77	-25	3	4	C	2.5	3	52.4	0.18	4.94	1.64	2.69	0.08	16.7	22.2	0.65	101.5	91.7	46.6	49.0	4.4
3B		58.90	31.41	61	-25	5	5	C	4	3	52.3	0.14	4.88	1.57	3.71	0.11	20.3	15.5	0.49	98.9	90.9	33.8	60.1	6.1
3B		59.62	29.92	61	-25	5	5	R	4	3	52.3	0.19	4.89	1.57	3.19	0.09	18.9	19.0	0.56	100.6	91.5	40.1	54.7	5.2
3B		59.33	37.26	68	-26	4	5	C	2.5	2	53.3	0.14	4.75	1.35	4.22	0.09	22.9	14.2	0.43	101.4	90.9	30.0	63.5	6.6
3B		59.47	36.67	68	-26	4	5	R	2.5	2	52.2	0.23	5.03	1.53	2.78	0.07	16.6	22.0	0.64	101.1	91.5	46.5	48.9	4.6
3B		61.[illegible]	[illegible]7.48	79	-26	2	1	I	2	3	52.2	0.24	4.12	1.24	2.25	0.05	16.5	24.1	0.41	101.1	92.9	49.5	46.9	3.6
3B		68.19	21.14	54	-36	1	5	R	4	2.5	51.6	0.23	5.28	1.42	3.12	0.09	17.6	20.5	0.70	100.5	91.1	43.3	51.6	5.1
3B		69.26	22.14	54	-36	1	10	C	4	2.5	53.0	0.10	4.91	1.46	4.26	0.11	[illegible]2.5	14.4	0.48	101.3	90.7	30.3	63.0	6.7
3C	1	63.27	30.57	129	24	2 T1	10	B	1	0.25	52.2	0.20	4.25	1.21	2.77	0.1[illegible]	[illegible]3	21.09	0.60	100.0	92.0	44.2	51.3	4.5
3C	1	63.07	29.66	129	24	2 T2	10	B	1	0.25	52.1	0.19	4.35	1.28	2.67	0.11	[illegible].12	21.58	0.63	100.0	92.0	45.5	50.1	4.4
3C	1	61.60	31.03	131	22	1	10	C	1.3	1	51.9	0.16	4.82	1.49	3.18	0.10	18.57	18.89	0.66	99.8	91.4	40.4	54.4	5.2
CordX and CordY: the eletronprobe coordinate for thin sections																								
RefX and RefY: the reference coordinate relative to the position of the clinopyroxenite vein (see Plate 2 and Plate 5)																								
sd.': standard deviation of point averages.																								
sd.*': Counting statistics of electroprobe for single point.																								

Table 4: Continued																									
Thin Sect.	Piece	Cord X	Cord Y	Ref X	Ref Y	Gr.	Pts.	Loc	Gr.size(mm)		SiO2	TiO2	Al2O3	Cr2O3	FeO	MnO	MgO	CaO	Na2O	Total	[Mg]	Wo	En	Fs
RC27-9-6-5 CPX Composition																									
						1a	10	C	1.75	1.2	51.3	0.24	6.23	1.13	3.11	0.09	16.30	22.06	0.39	100.9		46.7	48.1	5.2
						1a	10	R	1.75	1.2	51.8	0.25	5.55	0.88	2.82	0.07	16.46	22.64	0.35	100.8		47.4	48.0	4.6
RC 27-9-6-3 and RC 27-9-6-8 CPX Composition (from Johnson, thesis 1990)																									
											51.2	0.22	5.51	0.86	2.38	0.00	16.17	22.89	0.41	99.6	92.3	48.5	47.6	3.9
											52.0	0.18	4.41	0.79	2.41	0.10	16.38	22.96	0.26	99.5	92.3	48.2	47.9	4.0
											50.3	0.24	6.95	1.11	2.67	0.08	14.97	23.20	0.46	100.0	90.9	50.3	45.2	4.5
											51.0	0.27	6.33	1.04	2.57	0.08	15.39	23.02	0.40	100.1	91.4	49.6	46.1	4.3
RC 27-9-6-2 CPX Composition (from Snow, thesis 1993)																									
											52.3	0.13	4.94	1.63	2.58	0.08	15.85	22.81	0.78	101.1	91.6	48.7		
RC27-9-6-2 CPX Composition																									
1A		41.60	13.06	83	111	1	sd	R			1.0	0.04	0.16	0.17	1.12	0.03	4.63	5.85	0.16	0.5	0.2	12.9	11.3	1.6
1A		42.05	12.79	83	111	1	sd	C			0.4	0.02	0.10	0.04	0.16	0.02	0.70	0.77	0.04	0.4	0.6	1.9	1.7	0.2
2B		30.72	22.85	134	65	1	sd	R			0.2	0.02	0.20	0.02	0.06	0.02	0.1	0.2	0.04	0.3	0.2	0.3	0.4	0.1
2B		30.15	24.20	134	65	1	sd	C			1.0	0.03	0.27	0.19	0.99	0.03	4.5	5.9	0.19	1.2	0.5	12.5	11.1	1.4
2B		42.64	37.82	122	64	2	sd.*				0.0	0.09	0.01	0.04	0.03	0.22	0.01	0.01	0.11					
2C	2	40.07	44.09	86	66	1	sd	C			0.5	0.03	0.19	0.11	0.67	0.02	3.17	3.92	0.14	0.3	0.5	9.0	8.1	1.0
2C	2	40.72	43.34	86	66	1	sd	R			1.9	0.09	2.05	0.24	0.70	0.03	2.43	3.81	0.55	0.8	0.8	8.0	6.8	1.2
3A	3	39.05	71.80	19	-1	1A	sd	C			1.0	0.13	0.30	0.46	1.56	0.03	6.13	7.63	0.21	0.9	0.8	16.9	14.7	2.2
3A	3	39.45	71.07	19	-1	1A	sd	R			0.9	0.09	0.34	0.17	0.78	0.03	3.33	4.29	0.13	0.9	0.5	9.4	8.3	1.1
3A	3	40.96	70.57	22	-2	3	sd	B			1.0	0.42	0.33	0.38	0.85	0.03	3.57	17.90	0.15	17.1	0.5	13.3	11.9	1.5
3A	3	40.87	70.26	22	-2	4	sd	lam.			0.2	0.02	0.09	0.04	0.17	0.02	0.42	0.60	0.04	0.3	0.3	1.4	1.1	0.3
3A	3	40.49	64.86			1B	sd	R			0.4	0.04	0.16	0.09	0.36	0.03	1.62	1.98	0.08	0.5	0.3	4.6	4.1	0.5
3B		16.15	38.19	65	28	12	sd.*	I			0.0	0.14	0.01	0.02	0.02	0.24	0.0	0.0	0.07					
3B		20.73	34.21	62	23	11	sd.	C			1.3	0.06	0.19	0.27	1.70	0.02	7.1	9.2	0.32	1.5	0.7	19.5	17.2	2.4
3B		21.43	33.72	62	23	11	sd.	R			0.6	0.02	0.08	0.07	0.49	0.02	2.4	2.2	0.08	1.1	0.3	5.7	5.1	0.6
3B		37.10	31.95	63	7	10	sd.	C			1.0	0.06	0.13	0.15	1.20	0.02	4.6	6.2	0.23	0.4	0.8	13.8	12.0	1.8
3B		36.97	32.64	63	7	10	sd.	R			0.7	0.06	0.75	0.31	0.17	0.02	0.4	1.2	0.30	0.8	0.3	2.1	1.8	0.3
3B		49.47	79.62	87	2	13	sd.	C			0.6	0.04	0.18	0.11	0.73	0.02	2.94	3.76	0.14	0.2	0.3	8.4	7.4	1.0
3B		51.55	77.41	87	2	13	sd.	R			0.6	0.03	0.18	0.14	0.67	0.02	3.07	3.74	0.13	0.3	0.3	8.5	7.6	0.9
3B		45.58	23.75	55	-13	8	sd.	R			0.9	0.05	0.22	0.12	1.05	0.03	3.4	4.4	0.17	0.7	0.9	10.3	8.7	1.6
3B		46.57	57.70	55	-13	9	sd.	I			0.3	0.06	0.18	0.06	0.12	0.02	0.6	0.9	0.07	0.4	0.1	1.9	1.7	0.2
3B		53.25	52.17	83	-18	7	sd.	C			1.2	0.07	0.32	0.27	1.58	0.03	6.9	8.8	0.28	0.3	0.7	19.0	16.7	2.2
3B		53.23	53.37	83	-18	7	sd.	R			0.3	0.01	0.20	0.04	0.20	0.01	0.7	1.2	0.03	0.2	0.3	2.4	2.1	0.3
3B		55.31	55.40	85	-20	6	sd.	C			1.6	0.07	0.37	0.30	1.82	0.04	7.7	9.9	0.33	1.0	0.7	20.9	18.4	2.5
3B		55.42	54.66	85	-20	6	sd.	R			2.5	0.04	0.17	0.13	1.04	0.02	3.7	6.0	0.18	1.1	0.9	12.3	10.7	1.7
3B		55.22	23.41	54	-21	8	sd.	B			0.3	0.00	0.29	0.05	0.12	0.00	0.0	0.1	0.04	0.1	0.4	0.1	0.1	0.2
3B		47.03	24.32	54	-21	8	sd.	I			0.7	0.06	0.38	0.20	0.90	0.02	3.5	4.4	0.27	0.2	0.7	10.0	8.7	1.3
CordX and CordY: the eletronprobe coordinate for thin sections																									
RefX and RefY: the reference coordinate relative to the position of the clinopyroxenite vein (see Plate 2 and Plate 5)																									
sd.': standard deviation of point averages.																									
sd.*': Counting statistics of electroprobe for single point.																									

Table 4: Continued

Thin Sect.	Piece	Cord X	Cord Y	Ref X	Ref Y	Gr.	Pts.	Loc	Gr.size(mm)		SiO2	TiO2	Al2O3	Cr2O3	FeO	MnO	MgO	CaO	Na2O	Total	[Mg]	Wo	En	Fs
RC27-9-6-2 CPX Composition																								
3B		58.99	45.70	77	-25	4	sd.	R			3.4	0.16	3.85	0.35	0.40	0.04	1.0	5.1	1.19	1.6	0.6	8.1	7.1	1.0
3B		58.95	46.16	77	-25	4	sd.	C			0.5	0.01	0.03	0.06	0.30	0.02	1.1	1.4	0.09	0.5	0.4	3.2	2.8	0.5
3B		58.90	31.41	61	-25	5	sd.	C			0.4	0.07	0.43	0.33	1.75	0.04	7.1	9.3	0.36	2.4	0.9	20.0	17.5	2.5
3B		59.62	29.92	61	-25	5	sd.	R			0.5	0.07	0.51	0.15	1.17	0.04	4.7	5.8	0.25	1.0	0.9	13.0	11.3	1.7
3B		59.33	37.26	68	-26	3	sd.	C			1.9	0.09	0.32	0.33	2.23	0.04	9.6	12.3	0.39	0.5	0.9	26.1	23.0	3.1
3B		59.43	36.67	68	-26	3	sd.	R			0.4	0.01	0.05	0.04	0.45	0.02	1.4	2.6	0.11	0.5	0.6	5.2	4.5	0.8
3B		61.43	47.48	79	-26	2	sd.*	I			0.0	0.10	0.01	0.03	0.03	0.26	0.0	0.0	0.11					
3B		68.19	21.14	54	-36	1	sd	R			1.5	0.07	0.43	0.30	1.90	0.03	7.5	9.6	0.33	0.4	1.0	20.6	18.0	2.7
3B		69.26	22.14	54	-36	1	sd	C			0.9	0.12	0.26	0.08	1.07	0.03	0.5	0.1	0.01	0.9	0.2	0.2	0.3	0.2
3C	1	63.27	30.57	129	24	2 T1	sd.	B			0.4	0.02	0.12	0.05	0.52	0.03	1.98	2.56	0.08	0.3	0.5	5.8	5.0	0.8
3C	1	63.07	29.66	129	24	2 T2	sd.	B			0.4	0.03	0.19	0.04	0.36	0.02	1.31	1.69	0.06	0.4	0.4	3.9	3.4	0.5
3C	1	61.60	31.03	131	22	1	sd.	C			1.2	0.05	0.31	0.18	1.11	0.02	4.37	5.46	0.16	0.7	0.8	12.4	10.8	1.6
RC27-9-6-5 CPX Composition																								
						1a	sd	C			0.6	0.03	1.06	0.08	0.29	0.02	0.87	1.67	0.23	0.3		3.2	2.7	0.5
						1a	sd	R			0.6	0.03	0.89	0.08	0.44	0.02	1.10	1.73	0.10	0.4		3.6	3.0	0.7

CordX and CordY: the eletronprobe coordinate for thin sections

RefX and RefY: the reference coordinate relative to the position of the clinopyroxenite vein (see Plate 2 and Plate 5)

sd.': standard deviation of point averages.

sd.*': Counti[illegible] of electroprobe for single point.

Table 5: Major element abundances for OPX from the RC 27-9.

Thin Sect.	Piece	Cord X	Cord Y	Ref X	Ref Y	Gr.	Pts.	Loc	Gr.size(mm)		SiO2	TiO2	Al2O3	Cr2O3	FeO	MnO	MgO	CaO	Na2O	Total	[Mg]	Wo	En	Fs
RC27-9-6-2 OPX Composition																								
1A		44.21	13.97	86	112	1	10	C	2	0.8	56.2	0.07	2.06	0.67	6.23	0.08	33.07	1.46	0.00	99.9	90.4	2.8	87.9	9.3
2B		43.39	57.79			1	10	C			55.7	0.07	3.67	1.98	6.26	0.16	33.0	1.74	0.04	101.6	90.4	3.3	87.4	9.3
2B		62.55	34.23	125	111	8	1	C			58.0	0.02	0.76	0.11	6.46	0.16	35.05	0.45	0.00	101.0	90.6	0.8	89.9	9.3
2B		62.54	34.20	125	111	9	1	C			58.2	0.05	1.17	0.11	6.50	0.17	35.31	0.53	0.00	102.0	90.6	1.0	89.8	9.3
2B		62.82	34.50	125	111	10	1	C			57.7	0.25	1.46	0.32	6.34	0.13	34.94	0.65	0.00	101.8	90.8	1.2	89.7	9.1
2B		62.49	34.72	125	110	11	1	C			57.8	0.16	1.29	0.23	6.32	0.10	35.12	0.60	0.00	101.6	90.8	1.1	89.8	9.1
2B		62.43	34.21	125	110	12	3	C			57.9	0.21	1.34	0.32	5.82	0.15	35.02	0.48	0.01	101.7	90.8	0.9	90.0	9.1
2B		62.12	34.55	125	110	13	1	C			57.4	0.31	1.61	0.31	6.21	0.11	34.59	0.78	0.00	101.3	90.9	1.5	89.8	9.0
2B		54.02	45.66	111	90	2	10	C	3.5	3	55.3	0.07	3.61	1.87	6.23	0.15	33.2	1.24	0.02	100.8	90.5	2.4	88.3	9.3
2B		54.76	43.23	111	90	2	10	R	3.5	3	56.4	0.20	1.94	0.62	6.22	0.17	34.0	1.15	0.01	100.7	90.7	2.2	88.8	9.1
2B		22.85	21.97	134	60	3	9	I	12	11	55.4	0.07	3.96	1.00	6.13	0.15	32.5	1.92	0.02	101.1	90.4	3.7	87.1	9.2
2C	2	44.28	46.43	82	64	1	10	C	2.5	1.5	55.2	0.08	3.57	0.81	6.07	0.07	32.21	1.88	0.04	100.0	90.5	3.7	87.1	9.2
2C	2	44.50	45.78	82	64	1	10	R	2.5	1.5	55.9	0.05	2.58	0.46	6.32	0.08	33.24	0.69	0.05	99.4	90.4	1.3	89.2	9.5
2B		42.72	37.86	122	64	4	1	C			56.7	0.02	1.12	0.08	6.77	0.15	34.74	0.45	0.00	100.0	90.1	0.8	89.4	9.8
2B		42.66	38.10	122	64	5	1	C			57.9	0.04	0.90	0.13	6.93	0.15	36.47	0.34	0.00	102.8	90.3	0.6	89.8	9.6
2B		43.03	38.25	121	64	6	5	C			57.5	0.10	1.81	0.57	6.22	0.15	33.99	1.29	0.13	101.6	90.7	2.4	88.5	9.1
2B		42.77	38.12	122	64	7	1	C			58.1	0.02	0.97	0.07	6.28	0.19	35.00	0.38	0.00	101.0	90.8	0.7	90.2	9.1
3A	3	65.84	66.05	26	7	1	10	B	?		56.1	0.09	2.29	0.62	6.54	0.18	33.38	0.81	0.02	100.0	90.1	1.6	88.7	9.7
3B		25.74	34.12	64	21	4	5	I	8	5	55.8	0.06	3.91	0.93	6.10	0.14	32.5	2.12	0.02	101.6	90.5	4.1	86.8	9.1
3B		62.90	46.95	77	-18	2	5	C	7	5.5	56.2	0.04	3.70	0.90	6.16	0.12	33.6	1.02	0.01	101.7	90.7	1.9	88.9	9.1
3B		63.60	46.60	77	-18	2	5	R	7	5.5	56.9	0.04	2.98	0.61	6.14	0.13	34.0	1.04	0.00	101.9	90.8	2.0	89.0	9.0
3B		64.18	38.63	65	-21	3	5	C	7	7	55.9	0.06	4.03	0.97	5.89	0.15	32.2	2.65	0.07	101.9	90.7	5.1	86.0	8.8
3B		64.90	39.63	65	-21	3	5	R	7	7	56.2	0.06	3.69	0.76	6.18	0.15	33.4	1.53	0.02	102.0	90.6	2.9	88.0	9.1
3B		69.48	30.02	59	-25	1	5	C	6	6	56.0	0.06	3.90	0.92	6.06	0.14	33.0	1.61	0.00	101.6	90.6	3.1	87.9	9.1
3C	1	60.20	32.48	131	20	1	10	C	2	1.25	54.9	0.09	3.87	0.92	6.18	0.08	32.41	1.63	0.00	100.1	90.3	3.2	87.5	9.4
1A		44.21	13.97	86	112	1	sd	C			0.2	0.02	0.09	0.05	0.10	0.03	0.37	0.46	0.01	0.3	0.1	0.9	0.8	0.1
2B		43.39	57.79			1	sd	C			0.5	0.02	0.19	3.11	0.36	0.02	1.5	1.80	0.10	0.4	0.2	3.5	3.1	0.4
2B		62.55	34.23	125	111	8	sd.	C			0.9	0.12	0.26	0.08	1.07	0.03	0.55	0.08	0.01	0.9	0.2	0.2	0.3	0.2
2B		62.54	34.20	125	111	9	sd.*	C			0.0	0.26	0.03	0.17	0.01	0.17	0.00	0.05	0.26					
2B		62.82	34.50	125	111	10	sd.*	C			0.0	0.26	0.02	0.16	0.01	0.16	0.00	0.04	0.26					
2B		62.49	34.72	125	110	11	sd.*	C			0.0	0.09	0.02	0.07	0.01	0.20	0.00	0.04	0.26					
2B		62.43	34.21	125	110	12	sd.*	C			0.0	0.12	0.02	0.09	0.01	0.25	0.00	0.04	0.26					
2B		62.12	34.55	125	110	13	sd.*	C			0.0	0.07	0.02	0.07	0.01	0.23	0.00	0.03	0.26					
2B		54.02	45.66	111	90	2	sd	C			0.4	0.02	0.22	2.96	0.18	0.02	0.7	0.79	0.03	0.3	0.1	1.5	1.3	0.2
2B		54.76	43.23	111	90	2	sd	R			0.6	0.03	0.09	0.03	0.19	0.01	0.6	0.76	0.02	0.7	0.2	1.5	1.2	0.3

CordX and CordY: the eletronprobe coordinate for thin sections

RefX and RefY: the reference coordinate relative to the position of the clinopyroxenite vein (see Plate 2 and Plate 5)

sd.': standard deviation of point averages.

sd.*': Counting statistics of electroprobe for single point.

Table 5: (Con'd)																								
Thin Sect.	Piece	Cord X	Cord Y	Ref X	Ref Y	Gr.	Pts.	Loc	Gr.size(mm)		SiO2	TiO2	Al2O3	Cr2O3	FeO	MnO	MgO	CaO	Na2O	Total	[Mg]	Wo	En	Fs
RC27-9-6-2 OPX Composition																								
2B		22.85	21.97	134	60	3	sd	I			0.3	0.03	0.19	0.04	0.25	0.02	0.8	1.00	0.03	0.3	0.2	2.0	1.7	0.3
2C	2	44.28	46.43	82	64	1	sd.	C			0.2	0.01	0.09	0.02	0.13	0.02	0.28	0.25	0.02	0.3	0.2	0.5	0.4	0.2
2C	2	44.50	45.78	82	64	1	sd.	R			0.4	0.02	0.39	0.08	0.09	0.03	0.41	0.26	0.03	0.3	0.2	0.5	0.6	0.1
2B		42.72	37.86	122	64	4	sd.				0.3	0.02	0.31	0.12	0.20	0.02	0.62	0.89	0.29	0.6	0.2	1.7	1.4	0.3
2B		42.66	38.10	122	64	5	sd.*				0.0	0.26	0.02	0.24	0.01	0.17	0.00	0.05	0.26					
2B		43.03	38.25	121	64	6	sd.*				0.0	0.26	0.02	0.16	0.01	0.17	0.00	0.06	0.26					
2B		42.77	38.12	122	64	7	sd.*				0.0	0.26	0.02	0.26	0.01	0.14	0.00	0.05	0.26					
3A	3	65.84	66.05	26	7	1	sd.	B			0.3	0.02	0.27	0.04	0.12	0.02	0.47	0.30	0.02	0.4	0.2	0.6	0.7	0.2
3B		25.74	34.12	64	21	4	sd.	I			0.2	0.02	0.17	0.03	0.20	0.02	0.7	0.99	0.03	0.4	0.0	0.0	0.0	0.0
3B		62.90	46.95	77	-18	2	sd.	C			0.2	0.03	0.26	0.03	0.15	0.02	0.3	0.41	0.03	0.4	0.3	0.8	0.8	0.3
3B		63.60	46.60	77	-18	2	sd.	R			0.5	0.01	0.12	0.05	0.20	0.02	0.8	0.89	0.00	0.3	0.1	1.7	1.4	0.2
3B		64.18	38.63	65	-21	3	sd.	C			0.6	0.04	0.27	0.09	0.47	0.01	1.8	2.43	0.08	0.4	0.2	4.7	4.1	0.6
3B		64.90	39.63	65	-21	3	sd.	R			0.3	0.01	0.13	0.07	0.17	0.01	0.5	0.65	0.03	0.2	0.1	1.3	1.0	0.2
3B		69.48	30.02	59	-25	1	sd.	C			0.3	0.02	0.23	0.07	0.10	0.02	0.6	0.83	0.00	0.4	0.2	1.6	1.5	0.2
3C	1	60.20	32.48	131	20	1	sd.	C			0.2	0.02	0.12	0.05	0.12	0.02	0.44	0.42	0.01	0.2	0.2	0.8	0.8	0.2
RC27-9-6-5 OPX Composition																								
						1	10	C	2.75	1.5	53.9	0.09	5.71	0.76	6.59	0.11	31.11	2.29	0.02	100.6		4.5	85.3	10.1
						1	sd	C			0.3	0.03	0.13	0.04	0.50	0.02	1.49	2.13	0.02	0.4		4.3	3.6	0.7
RC 27-9-6-8 OPX Composition (from Johnson, thesis 1990)																								
											54.6	0.09	5.50	0.70	6.42	0.15	33.03	1.11	0.02	101.6	90.1	2.2	88.2	9.6
CordX and CordY: the eletronprobe coordinate for thin sections																								
RefX and RefY: the reference coordinate relative to the position of the clinopyroxenite vein (see Plate 2 and Plate 5)																								
sd.': standard deviation of point averages.																								
sd.*': Counting statistics of electroprobe for single point.																								

Table 6: Major element abundances for olivine from the RC 27-9.

Thin Sect.	Piece	Cord X	Cord Y	Ref X	Ref Y	Gr.	Pts.	Loc	Gr.size(mm)		SiO2	TiO2	Al2O3	Cr2O3	FeO	MnO	MgO	CaO	NiO	Total	[Mg]
RC27-9-6-2 Olivine Composition																					
1A		38.42	9.06	92	116	1	5	B	0.31		40.4	0.00	0.00	0.01	9.91	0.13	49.46	0.02	0.33	100.2	89.9
2B		62.91	34.45	125	111	6	1	B			41.5				9.30	0.10	50.24	0.02	0.31	101.4	90.6
2B		33.46	27.38	127	67	1	5	B			41.7	0.02	0.03	0.01	9.71	0.14	50.1	0.05	0.34	102.0	90.2
2B		42.69	38.37	121	64	2	1	B			41.4				9.68	0.14	49.79	0.03	0.33	101.4	90.2
2B		42.47	38.01	122	63	3	1	B			41.7				9.61	0.16	49.87	0.02	0.32	101.7	90.3
2B		42.74	37.81	122	64	4	1	B			41.5				9.50	0.15	49.52	0.02	0.29	101.0	90.3
2B		42.77	38.16	122	64	5	1	B			41.7				9.59	0.12	49.94	0.02	0.33	101.8	90.3
2C	1	11.27	26.82	61	98	6	5	B	0.4		40.4	0.00	0.00	0.02	9.74	0.12	50.21	0.03	0.34	100.9	90.2
2C	1	20.74	36.24	71	90	5	5	B	0.16		40.4	0.00	0.00	0.02	9.71	0.13	50.17	0.03	0.33	100.8	90.2
2C	2	49.60	33.23	76	77	1	5	B	0.3		40.5	0.00	0.00	0.01	9.58	0.11	49.77	0.01	0.32	100.3	90.3
2C	2	43.59	42.09	82	68	4	5	B	0.14		40.4	0.00	0.00	0.02	9.60	0.14	49.75	0.02	0.34	100.3	90.2
2C	4	49.35	30.47	81	56	2	5	B	0.3		40.5	0.00	0.00	0.02	9.51	0.12	49.44	0.02	0.33	99.9	90.3
2C	4	48.35	19.02	79	44	3	5	B	0.2		40.5	0.00	0.00	0.04	9.60	0.14	49.28	0.01	0.33	99.9	90.2
3A	3	33.77	75.85	28	-6	1	5	B	0.28		40.4	0.00	0.00	0.02	9.55	0.13	49.04	0.02	0.35	99.5	90.2
3B		14.80	71.47	79	33	4	5	B	0.2		40.6	0.00	0.00	0.02	9.74	0.13	49.60	0.02	0.34	100.4	90.1
3B		26.88	61.81	69	19	9	5	B	0.3		40.2	0.00	0.00	0.02	9.60	0.13	50.02	0.01	0.35	100.4	90.3
3B		40.60	41.69	50	6	5	5	B	0.5	0.5	40.4	0.00	0.00	0.01	9.76	0.15	49.47	0.03	0.32	100.1	90.0
3B		47.19	67.90	76	0	8	5	B	0.6		40.3	0.00	0.01	0.01	9.64	0.13	49.47	0.02	0.34	99.9	90.1
3B		53.75	63.31	72	-8	6	5	B	0.25		40.1	0.00	0.00	0.01	9.74	0.13	49.62	0.04	0.32	99.9	90.1
3B		53.01	37.43	67	-10	1	5	B			41.5	0.01	0.01	0.00	9.71	0.12	50.1	0.04	0.35	101.9	90.2
3B		70.25	65.68	75	-23	7	5	B	0.26		40.2	0.00	0.00	0.03	9.56	0.13	49.85	0.01	0.33	100.1	90.3
3B		51.86	38.11			3	1	B			41.4	0.00	0.03	0.02	9.52	0.13	48.9	0.00	0.33	100.4	90.2
3B		48.52	38.74			2	1	B			41.8	0.00	0.02	0.00	9.36	0.13	48.6	0.01	0.34	100.3	90.3
3C		63.58	20.49	129	31	1	6	B	0.73		40.3	0.00	0.00	0.03	9.71	0.14	49.97	0.03	0.32	100.5	90.2
4A		46.92	53.30	76	-35	1	5	B	0.22		40.5	0.00	0.00	0.01	9.64	0.12	50.33	0.03	0.35	101.0	90.3
4A		55.49	42.74	84	-47	2	5	B	0.19		40.4	0.00	0.00	0.02	9.51	0.13	49.98	0.00	0.36	100.4	90.4
4A		59.06	34.99	87	-54	3	5	B	0.22		40.5	0.00	0.00	0.02	9.60	0.14	50.05	0.01	0.34	100.7	90.3
4A		75.78	23.37	102	-66	4	5	B	0.6		40.5	0.00	0.00	0.02	9.56	0.13	49.89	0.01	0.33	100.5	90.3
1A		38.42	9.06	92	116	1	sd				0.3	0.00	0.00	0.01	0.10	0.02	0.41	0.02	0.01	0.5	0.2
2B		62.91	34.45	125	111	6	sd.*				0.0				0.01	0.26	0.00	0.26	0.07		
2B		33.46	27.38	127	67	1	sd				0.1	0.02	0.01	0.01	0.09	0.03	0.2	0.03	0.01	0.1	0.1
2B		42.69	38.37	121	64	2	sd.*				0.0				0.01	0.17	0.00	0.26	0.07		
2B		42.47	38.01	122	63	3	sd.*				0.0				0.01	0.15	0.00	0.26	0.07		
2B		42.74	37.81	122	64	4	sd.*				0.0				0.01	0.16	0.00	0.26	0.08		
2B		42.77	38.16	122	64	5	sd.*				0.0				0.01	0.21	0.00	0.26	0.07		

CordX and CordY: the eletronprobe coordinate for thin sections

RefX and RefY: the reference coordinate relative to the position of the clinopyroxenite vein (see Plate 2 and Plate 5)

sd.': standard deviation of point averages.

sd.*': Counting statistics of electroprobe for single point.

Table 6: (con'd)

Thin Sect.	Piece	Cord X	Cord Y	Ref X	Ref Y	Gr.	Pts.	Loc	Gr.size(mm)		SiO2	TiO2	Al2O3	Cr2O3	FeO	MnO	MgO	CaO	NiO	Total	[Mg]
RC27-9-6-2 Olivine Composition																					
2C	1	11.27	26.82	61	98	6	sd				0.1	0.01	0.01	0.02	0.14	0.02	0.12	0.01	0.03	0.2	0.1
2C	1	20.74	36.24	71	90	5	sd				0.2	0.00	0.00	0.01	0.10	0.01	0.22	0.01	0.02	0.3	0.1
2C	2	49.60	33.23	76	77	1	sd				0.1	0.00	0.00	0.02	0.09	0.02	0.28	0.01	0.01	0.3	0.1
2C	2	43.59	42.09	82	68	4	sd				0.2	0.00	0.01	0.02	0.23	0.01	0.17	0.01	0.01	0.3	0.2
2C	4	49.35	30.47	81	56	2	sd				0.1	0.00	0.01	0.01	0.10	0.02	0.17	0.01	0.02	0.3	0.1
2C	4	48.35	19.02	79	44	3	sd				0.1	0.00	0.00	0.02	0.16	0.02	0.14	0.01	0.02	0.1	0.2
3A	3	33.77	75.85	28	-6	1	sd				0.2	0.00	0.01	0.02	0.12	0.02	0.15	0.01	0.02	0.4	0.1
3B		14.80	71.47	79	33	4	sd				0.2	0.00	0.00	0.01	0.17	0.00	0.29	0.02	0.02	0.3	0.1
3B		26.88	61.81	69	19	9	sd				0.2	0.00	0.01	0.01	0.12	0.01	0.22	0.01	0.03	0.2	0.1
3B		40.60	41.69	50	6	5	sd				0.3	0.01	0.00	0.02	0.18	0.01	0.27	0.01	0.02	0.3	0.2
3B		47.19	67.90	76	0	8	sd				0.2	0.00	0.01	0.01	0.18	0.01	0.29	0.02	0.01	0.4	0.2
3B		53.75	63.31	72	-8	6	sd				0.1	0.00	0.00	0.02	0.11	0.01	0.33	0.01	0.01	0.4	0.1
3B		53.01	37.43	67	-10	1	sd				0.2	0.00	0.00	0.00	0.14	0.02	0.2	0.02	0.01	0.4	0.1
3B		70.25	65.68	75	-23	7	sd				0.3	0.00	0.00	0.02	0.17	0.01	0.27	0.01	0.02	0.3	0.1
3B		51.86	38.11			3	sd.*				0.0	0.26	0.26	0.26	0.02	0.19	0.0	0.26	0.07		
3B		48.52	38.74			2	sd.*				0.0	0.26	0.26	0.26	0.02	0.19	0.0	0.26	0.07		
3C		63.58	20.49	129	31	1	sd				0.2	0.00	0.00	0.02	0.17	0.02	0.09	0.01	0.02	0.3	0.1
4A		46.92	53.30	76	-35	1	sd.				0.3	0.00	0.00	0.01	0.11	0.02	0.56	0.01	0.02	0.4	0.2
4A		55.49	42.74	84	-47	2	sd.				0.1	0.00	0.00	0.02	0.14	0.01	0.45	0.01	0.02	0.3	0.2
4A		59.06	34.99	87	-54	3	sd.				0.2	0.00	0.00	0.01	0.10	0.02	0.16	0.02	0.02	0.1	0.1
4A		75.78	23.37	102	-66	4	sd.				0.5	0.00	0.01	0.02	0.20	0.01	0.52	0.01	0.03	0.5	0.2
RC27-9-6-5 Olivine Composition																					
						1	6	B	?	?	40.5	0.01	0.01	0.00	10.32	0.11	49.43	0.03	0.35	100.7	89.5
						2	6	B	0.1	0.05	40.7	0.01	0.01	0.03	9.85	0.11	49.98	0.04	0.39	101.2	90.0
						1	sd	B			0.2	0.01	0.01	0.00	0.07	0.01	0.07	0.01	0.02	0.2	0.1
						2	sd	B			0.3	0.01	0.02	0.01	0.11	0.02	0.31	0.01	0.02	0.2	0.1
RC 27-9-6-8 Olivine Composition (from Johnson, thesis 1990)																					
											41.1	0.00	0.01	0.02	9.55	0.10	50.03	0.03	0.35	101.2	90.3
CordX and CordY: the eletronprobe coordinate for thin sections																					
RefX and RefY: the reference coordinate relative to the position of the clinopyroxenite vein (see Plate 2 and Plate 5)																					
sd.': standard deviation of point averages.																					
sd.*': Counting statistics of electroprobe for single point.																					

Table 7: Major element abundances for spinel from the RC 27-9.

Thin Sect.	Piece	Cord X	Cord Y	Ref X	Ref Y	Gr.	Pts.	Loc	Gr.size(mm)		SiO2	TiO2	Al2O3	Cr2O3	FeO	MnO	MgO	CaO	NiO	Total	[Fe3+]	[Mg]	[Cr]
RC27-9-6-2 Spinel Composition																							
1A		44.86	12.93	85	112	1	5	B	0.12	0.03	0.41	0.18	25.83	41.01	21.89	0.28	11.71	0.00	0.09	101.4	3.5	52.5	51.6
2B		64.83	37.23	120	101	1	5	B			0.05	0.33	23.8	42.2	21.3	0.35	13.1	0.02	0.11	101.1	6.4	59.3	54.3
2C	1	18.06	27.25	62	91	4	5	B	0.26	0.14	0.00	0.33	28.13	38.67	19.53	0.34	13.64	0.07	0.27	101.0	4.8	61.2	48.0
2C	1	24.85	54.88	90	84	3	5	B	0.42	0.08	0.00	0.17	38.57	28.31	16.98	0.28	16.22	0.09	0.33	101.0	4.5	69.0	33.0
2C	2	47.45	19.94	75	64	1	5	B	0.2	0.1	0.00	0.04	40.14	28.35	15.82	0.15	16.53	0.00	0.22	101.2	3.0	69.2	32.2
2C	4	40.85	26.80	72	51	2	5	B	1	0.4	0.00	0.18	40.18	27.11	16.64	0.27	16.24	0.06	0.32	101.0	3.7	68.5	31.2
3A	3	44.39	70.13	16	-2	1	5	B	2	0.75	0.00	0.28	34.66	32.68	17.88	0.18	15.29	0.00	0.14	101.1	4.0	65.5	38.7
3B		13.64	44.20	53	33	4	5	B	0.96	0.12	0.00	0.30	34.18	33.71	18.13	0.32	14.70	0.06	0.29	101.7	3.6	63.6	39.8
3B		15.48	24.57	53	29	3	1	B			0.04	0.09	39.1	28.1	15.8	0.15	16.3	0.02	0.17	99.7	3.3	69.1	32.5
3B		23.86	77.00	85	22	5	5	B	0.5	0.1	0.00	0.22	38.28	29.37	16.57	0.29	15.89	0.08	0.33	101.0	3.4	67.6	34.0
3B		43.12	68.04	76	3	9	5	B	0.1	0.8	0.00	0.19	43.67	24.08	15.17	0.26	16.88	0.06	0.36	100.7	2.6	70.2	27.0
3B		53.63	52.24	82	-9	1	1	B			0.05	0.02	43.4	23.6	15.8	0.15	16.8	0.04	0.18	100.0	3.3	69.9	26.7
3B		59.22	69.13	77	-13	7	5	B	0.33	0.1	0.00	0.15	42.11	25.29	15.51	0.28	16.95	0.07	0.35	100.7	3.5	70.9	28.7
3B		68.68	73.90	83	-22	8	5	B	0.15	0.1	0.00	0.18	41.19	26.31	16.39	0.28	16.10	0.07	0.33	100.8	3.1	67.8	30.0
3B		69.04	37.78	70	-26	2	3	B			0.10	0.10	39.1	28.7	16.3	0.16	16.5	0.01	0.17	101.1	3.5	66.9	33.0
3B		40.41	56.82			6	5	B	0.11	0.07	0.00	0.19	40.31	27.13	16.35	0.28	16.21	0.10	0.34	100.9	3.4	68.5	31.1
3C	3	63.16	30.23	94	8	1	6	B	0.85	0.3	0.00	0.03	40.64	27.45	15.29	0.13	16.91	0.03	0.15	100.6	3.2	70.7	31.3
4A		49.86	50.99	78	-37	1	5	B	0.5	0.22	0.00	0.18	40.02	26.89	16.63	0.27	16.48	0.07	0.33	100.9	4.2	69.5	31.1
4A		39.20	43.79	67	-44	2	5	B	0.24	0.04	0.00	0.14	41.13	26.43	15.74	0.26	16.86	0.08	0.38	101.0	3.7	70.7	30.1
4A		60.61	32.56	87	-57	3	5	B	0.36	0.2	0.00	0.17	41.46	26.21	15.89	0.25	16.81	0.06	0.37	101.2	3.6	70.2	29.9
1A		44.86	12.93	85	112	1	sd	B			0.93	0.01	0.75	1.35	0.41	0.03	0.20	0.00	0.02	0.2	2.0	1.7	1.6
2B		64.83	37.23	120	101	1	sd	B			0.02	0.02	0.2	0.2	0.2	0.01	0.1	0.01	0.02	0.3	0.4	0.4	0.3
2C	1	18.06	27.25	62	91	4	sd	B			0.00	0.01	0.39	0.46	0.23	0.01	0.17	0.00	0.02	0.2	0.2	0.7	0.6
2C	1	24.85	54.88	90	84	3	sd	B			0.00	0.02	1.29	1.40	0.64	0.05	0.42	0.01	0.02	0.4	0.2	1.5	1.8
2C	2	47.45	19.94	75	64	1	sd	B			0.00	0.02	1.19	1.25	0.33	0.03	0.24	0.00	0.03	0.2	0.3	0.7	1.6
2C	4	40.85	26.80	72	51	2	sd	B			0.00	0.01	0.68	0.72	0.12	0.03	0.28	0.01	0.04	0.3	0.3	0.8	0.9
3A	3	44.39	70.13	16	-2	1	sd	B			0.01	0.02	0.58	0.83	0.37	0.01	0.18	0.00	0.03	0.7	0.1	0.7	1.0
3B		13.64	44.20	53	33	4	sd	B			0.00	0.01	0.13	0.26	0.16	0.02	0.29	0.00	0.01	0.6	0.5	0.9	0.2
3B		15.48	24.57	53	29	3	sd.*	B			0.26	0.22	0.0	0.0	0.0	0.19	0.0	0.26	0.17				
3B		23.86	77.00	85	22	5	sd	B			0.00	0.00	1.33	1.37	0.65	0.03	0.65	0.03	0.03	0.1	0.3	2.1	1.8
3B		43.12	68.04	76	3	9	sd	B			0.00	0.01	0.89	0.88	0.33	0.02	0.22	0.01	0.02	0.2	0.3	0.6	1.1
3B		53.63	52.24	82	-9	1	sd.*	B			0.26	0.26	0.0	0.0	0.0	0.19	0.0	0.26	0.16				
3B		59.22	69.13	77	-13	7	sd	B			0.00	0.01	1.33	1.05	0.41	0.02	0.36	0.01	0.03	0.2	0.2	0.9	1.5
3B		68.68	73.90	83	-22	8	sd	B			0.00	0.01	0.61	0.42	0.48	0.02	0.12	0.01	0.03	0.3	0.4	0.3	0.6
3B		69.04	37.78	70	-26	2	sd	B			0.02	0.01	0.2	0.3	0.1	0.02	0.2	0.01	0.03	0.4	0.3	3.5	0.4
3B		40.41	56.82			6	sd	B			0.00	0.02	1.10	1.09	0.20	0.03	0.24	0.03	0.03	0.1	0.2	0.7	1.4
3C	3	63.16	30.23	94	8	1	sd.	B			0.00	0.02	3.78	3.56	1.34	0.03	1.04	0.04	0.04	0.4	0.4	2.9	4.6
4A		49.86	50.99	78	-37	1	sd.	B			0.00	0.01	0.71	1.03	0.16	0.02	0.15	0.01	0.03	0.4	0.2	0.5	1.2
4A		39.20	43.79	67	-44	2	sd.	B			0.00	0.01	0.82	0.80	0.18	0.02	0.11	0.01	0.03	0.3	0.1	0.3	1.0
4A		60.61	32.56	87	-57	3	sd.	B			0.00	0.01	3.43	3.48	1.30	0.02	1.05	0.01	0.03	0.5	0.4	3.2	4.6
RC27-9-6-5 Spinel Composition																							
						1	6	B	1.2	0.4	0.00	0.32	46.56	20.61	13.81	0.25	17.87	0.07	0.41	99.91	2.5	73.4	22.9
						1	sd	B			0.00	0.09	2.30	2.26	0.60	0.02	0.44	0.02	0.03	0.51	0.4	1.1	2.8
RC 27-9-6-8 Spinel Composition (from Johnson, thesis 1990)																							
											0.00	0.06	52.40	15.54	14.61	0.12	19.27	0.01	0.37	100.4		73.1	16.6
RC 27-9-6-2 Spinel Composition (from Snow, thesis 1993)																							
											0.08	0.08	38.03	27.79	11.56*	0.15	17.02		0.19	99.36	4.8	72.4	32.9
CordX and CordY: the eletronprobe coordinate for thin section.																							
RefX and RefY: the reference coordinate relative to the position of the clinopyroxenite vein (see Plate 2 and Plate 5)																							
sd.': standard deviation of point averages.																							
sd.*: Counting statistics of electroprobe for single point.																							

Table 8: Major element abundances for plagioclase and the adjacent minerals from RC 27-9.

Thin Sect.	Piece	Cord X	Cord Y	Ref X	Ref Y	Gr.	Pts.	Loc	Gr.size(mm)	SiO2	TiO2	Al2O3	Cr2O3	FeO	MnO	MgO	CaO	Na2O	K2O	P2O5	NiO	Total	[Mg]	En	Fs	Wo	An	Ab	Or
Plagioclase (area1)																													
2B		42.70	37.94	122	64	1	1			54.0		30.37		0.15			12.19	4.86	0.08			101.7					57.9	41.7	0.4
2B		42.71	38.22	121	64	2	1			53.8		30.37		0.16			12.29	4.99	0.09			101.7					57.4	42.1	0.5
2B		42.66	38.41	122	64	3	1			53.6		30.25		0.19			12.43	4.83	0.08			101.4					58.5	41.1	0.4
2B		42.70	37.94	121	64	1	sd.*			0.0		0.01		0.24			0.01	0.02	0.16										
2B		42.71	38.22	122	64	2	sd.*			0.0		0.01		0.23			0.01	0.02	0.14										
2B		42.66	38.41	122	64	3	sd.*			0.0		0.01		0.20			0.01	0.02	0.16										
Amphibole (area1)																													
2B		42.64	37.84	122	64	1	1			44.4	1.59	12.33	1.46	3.82	0.02	18.15	12.59	2.99	0.46			97.8	89.5	61.9	7.3	30.8			
							sd.*			0.0	0.02	0.01	0.06	0.03	0.26	0.01	0.01	0.02	0.05										
Orthopyroxene (area1)																													
2B		42.72	37.86	122	64	4	1			56.7	0.02	1.12	0.08	6.77	0.15	34.74	0.45	0.00				100.0	90.1	89.4	9.8	0.8			
2B		42.66	38.10	122	64	5	1			57.9	0.04	0.90	0.13	6.93	0.15	36.47	0.34	0.00				102.8	90.3	89.8	9.6	0.6			
2B		43.03	38.25	121	64	6	5			57.5	0.10	1.81	0.57	6.22	0.15	33.99	1.29	0.13				101.6	90.7	88.5	9.1	2.4			
2B		42.77	38.12	122	64	7	1			58.1	0.02	0.97	0.07	6.28	0.19	35.00	0.38	0.00				101.0	90.8	90.2	9.1	0.7			
2B		42.72	37.86	122	64	4	sd.			0.3	0.02	0.31	0.12	0.20	0.02	0.62	0.89	0.29				0.6	0.2	1.4	0.3	1.7			
2B		42.66	38.10	122	64	5	sd.*			0.0	0.26	0.02	0.24	0.01	0.17	0.00	0.05	0.26											
2B		43.03	38.25	121	64	6	sd.*			0.0	0.26	0.02	0.16	0.01	0.17	0.00	0.06	0.26											
2B		42.77	38.12	122	64	7	sd.*			0.0	0.26	0.02	0.26	0.01	0.14	0.00	0.05	0.26											
Clinopyroxene (area1)																													
2B		42.64	37.82	122	64	2	1			54.8	0.24	2.20	0.71	2.30	0.11	17.53	23.93	0.40				102.3	93.1	48.7	3.6	47.7			
							sd.*			0.0	0.09	0.01	0.04	0.03	0.22	0.01	0.01	0.11											
Olivine (area1)																													
2B		42.69	38.37	121	64	2	1			41.4				9.68	0.14	49.79	0.03				0.33	101.4	90.2						
2B		42.47	38.01	122	63	3	1			41.7				9.61	0.16	49.87	0.02				0.32	101.7	90.3						
2B		42.74	37.81	122	64	4	1			41.5				9.50	0.15	49.52	0.02				0.29	101.0	90.3						
2B		42.77	38.16	122	64	5	1			41.7				9.59	0.12	49.94	0.02				0.33	101.8	90.3						
2B		42.69	38.37	121	64	2	sd.*			0.0				0.01	0.17	0.00	0.26				0.07								
2B		42.47	38.01	122	63	3	sd.*			0.0				0.01	0.15	0.00	0.26				0.07								
2B		42.74	37.81	122	64	4	sd.*			0.0				0.01	0.16	0.00	0.26				0.08								
2B		42.77	38.16	122	64	5	sd.*			0.0				0.01	0.21	0.00	0.26				0.07								
Plagioclase (area2)																													
2B		62.39	34.66	125	110	4	1			54.7		29.33		0.09		0.03	11.30	5.23	0.10			100.8					54.1	45.3	0.6
2B		63.15	34.75	125	111	5	1			54.7		29.91		0.12		0.01	11.76	5.16	0.10			101.8					55.4	44.0	0.6
2B		62.67	34.42	125	111	6	1			54.9		29.86		0.03		0.00	11.59	5.24	0.08			101.7					54.8	44.8	0.4
2B		62.51	34.33	125	111	7	1			54.9		29.78		0.08		0.00	11.89	5.22	0.06			101.9					55.6	44.1	0.3
2B		62.56	34.16	126	111	8	1			54.6		29.84		0.05		0.00	11.86	5.18	0.11			101.7					55.5	43.9	0.6
2B		62.48	34.15	126	110	9	1			53.6		30.64		0.10		0.00	12.79	4.53	0.06			101.7					60.7	38.9	0.4
2B		62.39	34.66	125	110	4	sd.*			0.0		0.01		0.26		0.26	0.01	0.02	0.13										
2B		63.15	34.75	125	111	5	sd.*			0.0		0.01		0.26		0.26	0.01	0.02	0.13										
2B		62.67	34.42	125	111	6	sd.*			0.0		0.01		0.26		0.26	0.01	0.02	0.16										
2B		62.51	34.33	125	111	7	sd.*			0.0		0.01		0.26		0.26	0.01	0.02	0.19										
2B		62.56	34.16	125	111	8	sd.*			0.0		0.01		0.26		0.26	0.01	0.02	0.13										
2B		62.48	34.15	126	110	9	sd.*			0.0		0.01		0.26		0.26	0.01	0.02	0.19										

CordX and CordY: the eletronprobe coordinate for thin section

RefX and RefY: the reference coordinate relative to the position of the clinopyroxenite vein (see Plate 2 and Plate 5)

sd.': standard deviation of point averages.

sd.*: Counting statistics of electroprobe for single point.

Table 8: (Continued)

Thin Sect.	Piece	Cord X	Cord Y	Ref X	Ref Y	Gr.	Pts.	Loc	Gr.size(mm)		SiO2	TiO2	Al2O3	Cr2O3	FeO	MnO	MgO	CaO	Na2O	K2O	P2O5	NiO	Total	[Mg]	En	Fs	Wo	An	Ab	Or
Amphibole (area2)																														
2B		63.08	34.67	125	111	2	1				45.1	2.03	12.69	1.01	3.75	0.04	18.28	12.20	2.94	0.59			98.7	89.7	62.7	7.2	30.1			
2B		62.53	34.22	125	111	3	1				44.8	2.12	13.61	1.47	4.13	0.04	18.18	12.30	3.19	0.50			100.3	88.7	62.0	7.9	30.1			
2B		62.60	34.09	126	111	4	1				45.0	2.26	12.74	1.04	3.71	0.07	18.28	12.53	3.09	0.47			99.2	89.8	62.2	7.1	30.7			
2B		62.50	34.26	125	111	5	1				44.8	1.75	12.68	0.97	3.73	0.08	18.60	12.52	3.11	0.44			98.7	90.0	62.7	7.0	30.3			
2B		62.74	34.42	125	111	6	1				44.8	1.85	12.56	0.95	4.08	0.08	18.40	12.44	3.13	0.46			98.7	89.0	62.1	7.7	30.2			
2B		63.08	34.67	125	111	2	sd.*				0.0	0.02	0.01	0.08	0.03	0.26	0.01	0.01	0.02	0.04										
2B		62.53	34.22	125	111	3	sd.*				0.0	0.02	0.01	0.06	0.03	0.26	0.01	0.01	0.02	0.05										
2B		62.60	34.09	126	111	4	sd.*				0.0	0.02	0.01	0.07	0.03	0.26	0.01	0.01	0.02	0.04										
2B		62.50	34.26	125	111	5	sd.*				0.0	0.02	0.01	0.08	0.03	0.26	0.01	0.01	0.02	0.05										
2B		62.74	34.42	125	111	6	sd.*				0.0	0.02	0.01	0.08	0.03	0.26	0.01	0.01	0.02	0.05										
Orthopyroxene (area2)																														
2B		62.55	34.23	125	111	8	1				58.0	0.02	0.76	0.11	6.46	0.16	35.05	0.45	0.00				101.0	90.6	89.9	9.3	0.8			
2B		62.54	34.20	125	111	9	1				58.2	0.05	1.17	0.11	6.50	0.17	35.31	0.53	0.00				102.0	90.6	89.8	9.3	1.0			
2B		62.82	34.50	125	111	10	1				57.7	0.25	1.46	0.32	6.34	0.13	34.94	0.65	0.00				101.8	90.8	89.7	9.1	1.2			
2B		62.49	34.72	125	110	11	1				57.8	0.16	1.29	0.23	6.32	0.10	35.12	0.60	0.00				101.6	90.8	89.8	9.1	1.1			
2B		62.43	34.21	125	110	12	3				57.9	0.21	1.34	0.32	5.82	0.15	35.02	0.48	0.01				101.7	90.8	90.0	9.1	0.9			
2B		62.12	34.55	125	110	13	1				57.4	0.31	1.61	0.31	6.21	0.11	34.59	0.78	0.00				101.3	90.9	89.8	9.0	1.5			
2B		62.55	34.23	125	111	8	sd.				0.9	0.12	0.26	0.08	1.07	0.03	0.55	0.08	0.01				0.9	0.2	0.3	0.2	0.2			
2B		62.54	34.20	125	111	9	sd.*				0.0	0.26	0.03	0.17	0.01	0.17	0.00	0.05	0.26											
2B		62.82	34.50	125	111	10	sd.*				0.0	0.26	0.02	0.16	0.01	0.16	0.00	0.04	0.26											
2B		62.49	34.72	125	110	11	sd.*				0.0	0.09	0.02	0.07	0.01	0.20	0.00	0.04	0.26											
2B		62.43	34.21	125	110	12	sd.*				0.0	0.12	0.02	0.09	0.01	0.25	0.00	0.04	0.26											
2B		62.12	34.55	125	110	13	sd.*				0.0	0.07	0.02	0.07	0.01	0.23	0.00	0.03	0.26											
Olivine (area2)																														
2B		62.91	34.45	125	111	6	1				41.5				9.30	0.10	50.24	0.02				0.31	101.4	90.6						
2B		62.91	34.45	125	111	6	sd.*				0.0				0.01	0.26	0.00	0.26				0.07								
Plagioclase (area3)																														
3A	3	40.35	70.70	20	-7	1	6	B	0.1	0.05	49.8		32.60		0.12		0.05	15.24	3.00	0.00			100.9					73.7	26.3	0.0
						1	sd				0.8		0.33		0.03		0.07	0.63	0.38	0.00			0.3					3.2	3.2	0.0
Clinopyroxene (area3)																														
3A	3	40.96	70.57	22	-2	3	20	B	6	3	52.0	0.46	4.96	1.61	3.35	0.11	18.67	22.69	0.51				104.4	90.9	52.9	5.3	41.8			
3A	3	40.87	70.26	22	-2	4	10	lam	?	?	51.5	0.25	4.99	1.59	2.72	0.11	15.70	22.55	0.57				100.0	91.1	47.0	4.6	48.5			
3A	3	40.96	70.57	22	-2	3	sd	B			1.0	0.42	0.33	0.38	0.85	0.03	3.57	17.90	0.15				17.1	0.5	11.9	1.5	13.3			
3A	3	40.87	70.26	22	-2	4	sd	lam.			0.2	0.02	0.09	0.04	0.17	0.02	0.42	0.60	0.04				0.3	0.3	1.1	0.3	1.4			
RC27-9-6-5 Plagioclase																														
						1	6	B	0.15	0.05	47.2		33.62		0.10		0.06	17.02	1.84	0.01			99.87					83.7	16.3	0.0
						1	sd				0.4		0.28		0.03		0.10	0.18	0.19	0.02			0.49					1.5	1.5	0.0

CordX and CordY: the eletronprobe coordinate for thin sections

RefX and RefY: the reference coordinate relative to the position of the clinopyroxenite vein (see Plate 2 and Plate 5)

sd.': standard deviation of point averages.

sd.*: Counting statistics of electroprobe for single point.

sd.*: Counting statistics of electroprobe for single point.

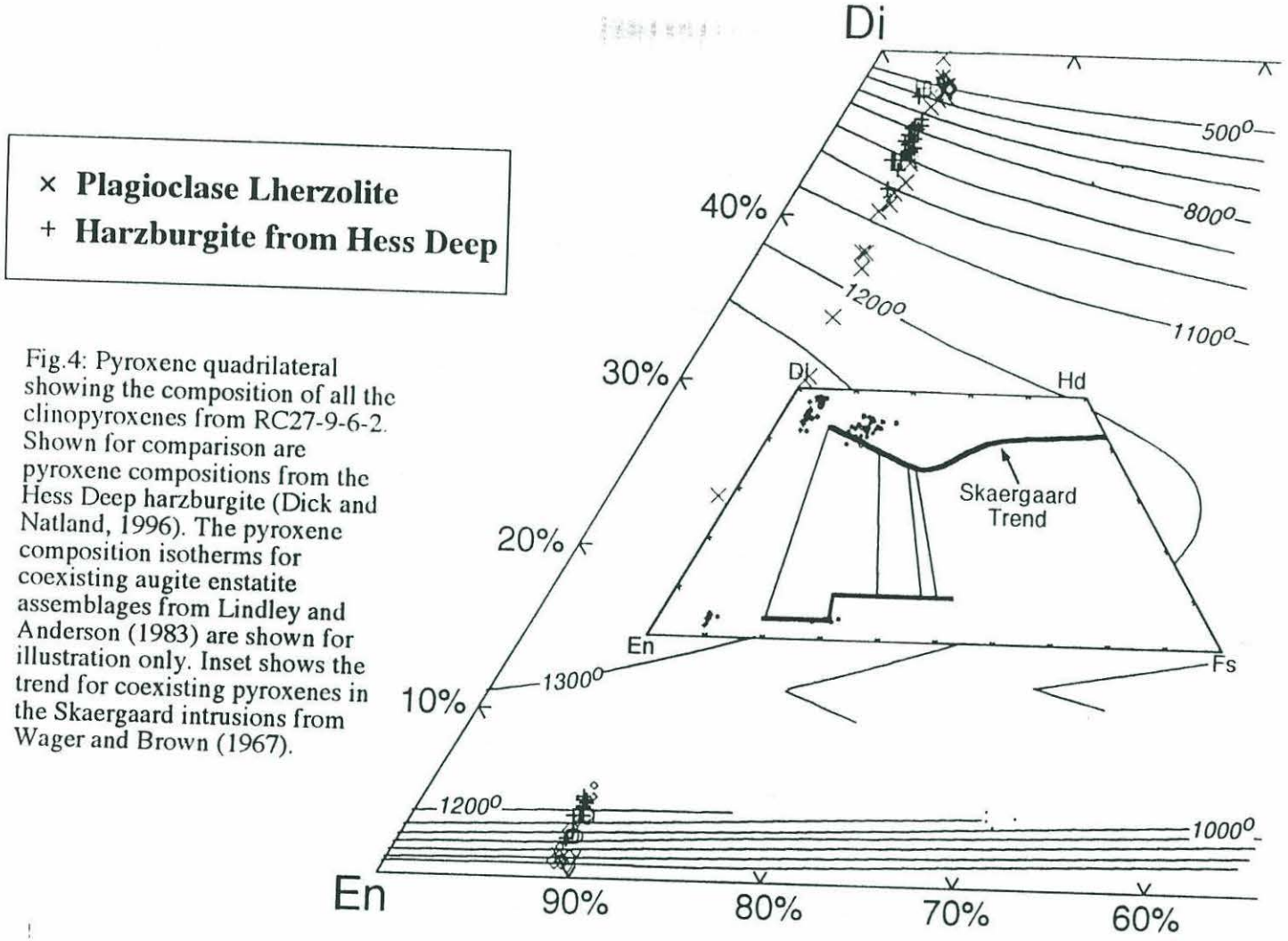

Fig.4: Pyroxene quadrilateral showing the composition of all the clinopyroxenes from RC27-9-6-2. Shown for comparison are pyroxene compositions from the Hess Deep harzburgite (Dick and Natland, 1996). The pyroxene composition isotherms for coexisting augite enstatite assemblages from Lindley and Anderson (1983) are shown for illustration only. Inset shows the trend for coexisting pyroxenes in the Skaergaard intrusions from Wager and Brown (1967).

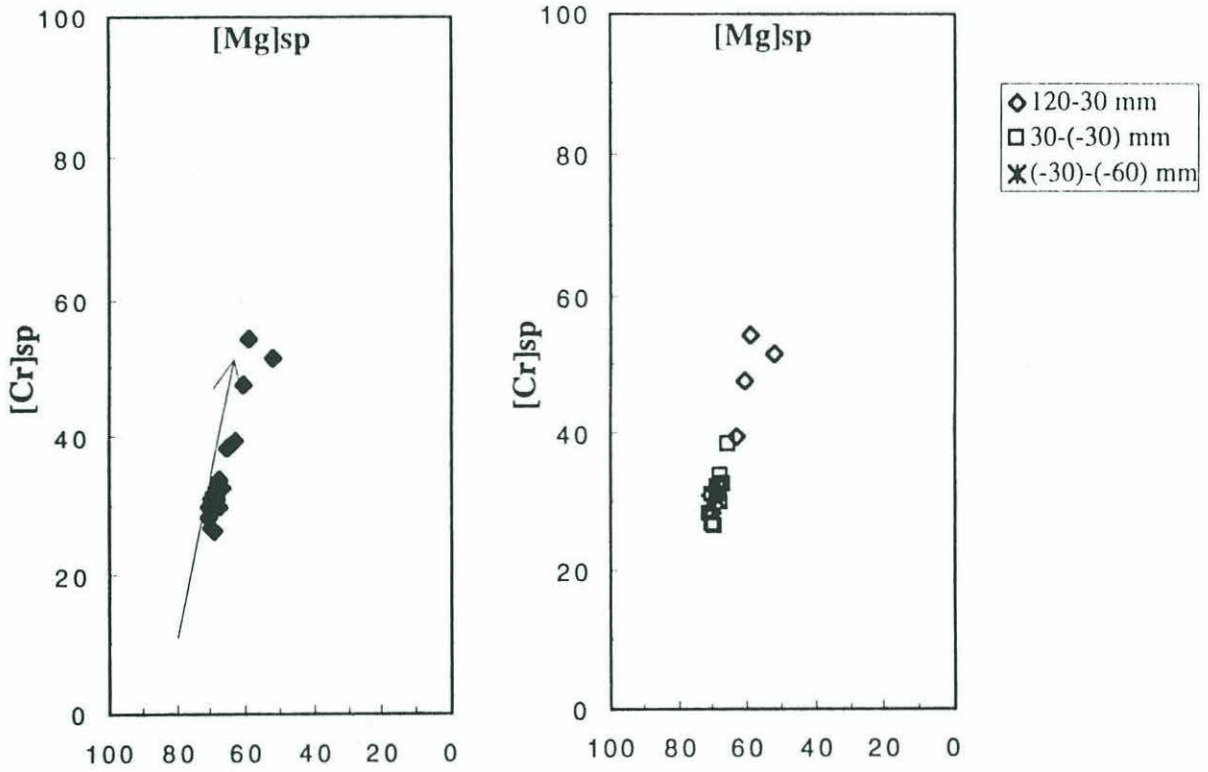

Fig.5: Compositions of spinels plotted on the Cr-Al-Mg-Fe(2+) face of the spinel composition prism (Irving, 1965, 1967). The compositional arrow for abyssal peridotites is from Dick and Bullen (1984). The Y-axis is two times longer than the X-axis to reflect the relative proportions of R(2+)and R(3+) cations.

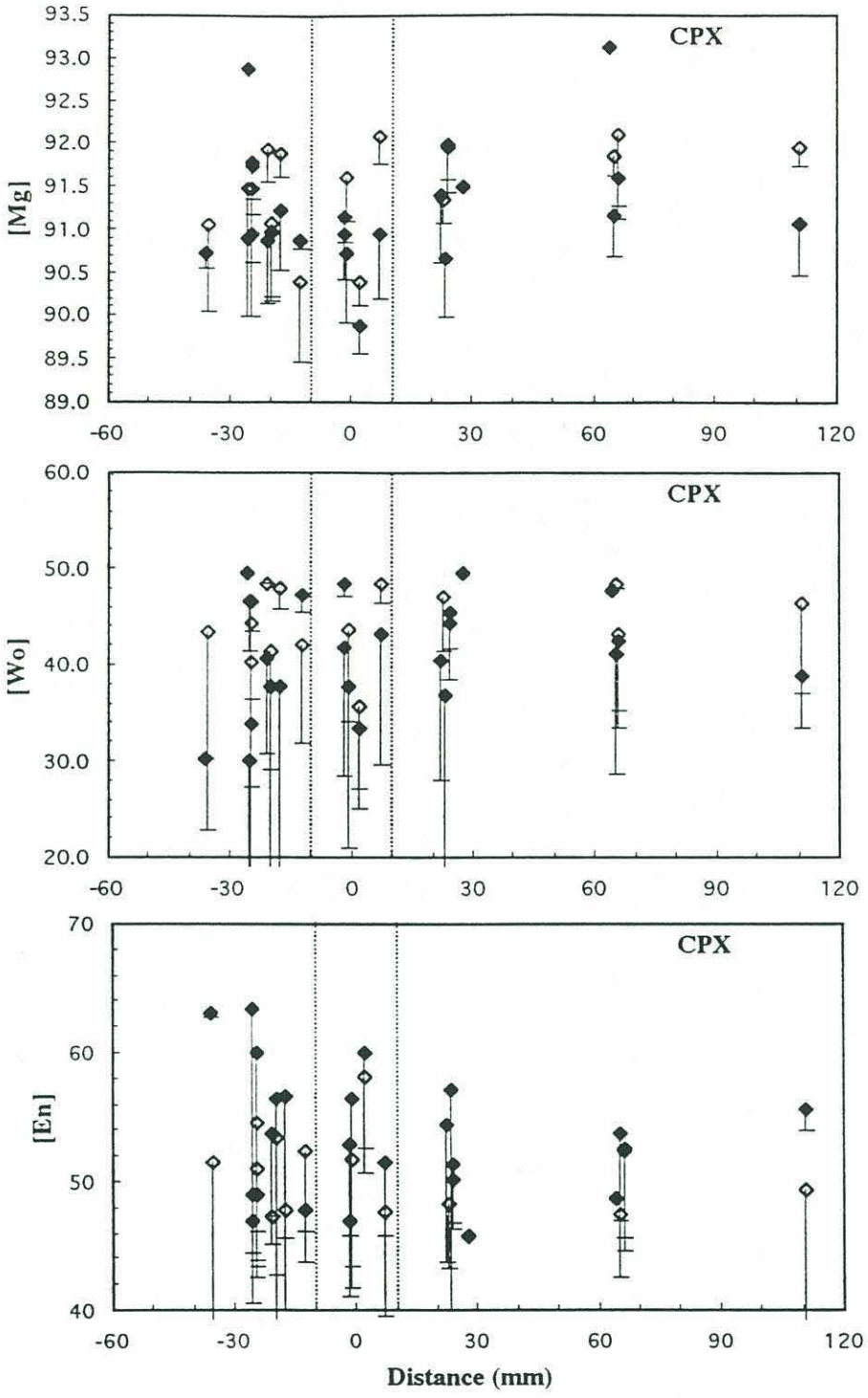

Fig.6: Compositional variation of clinopyroxenes with distance for sample RC27-9-6-2. Errors are plotted as standard deviations for averaged analyses. Core and rim data for each clinopyroxene grain are separated by solid and open symbols. The clinopyroxene vein is located at the center at 0 mm. Possible affected regions of the pyroxenite vein are indicated by the dashed lines.

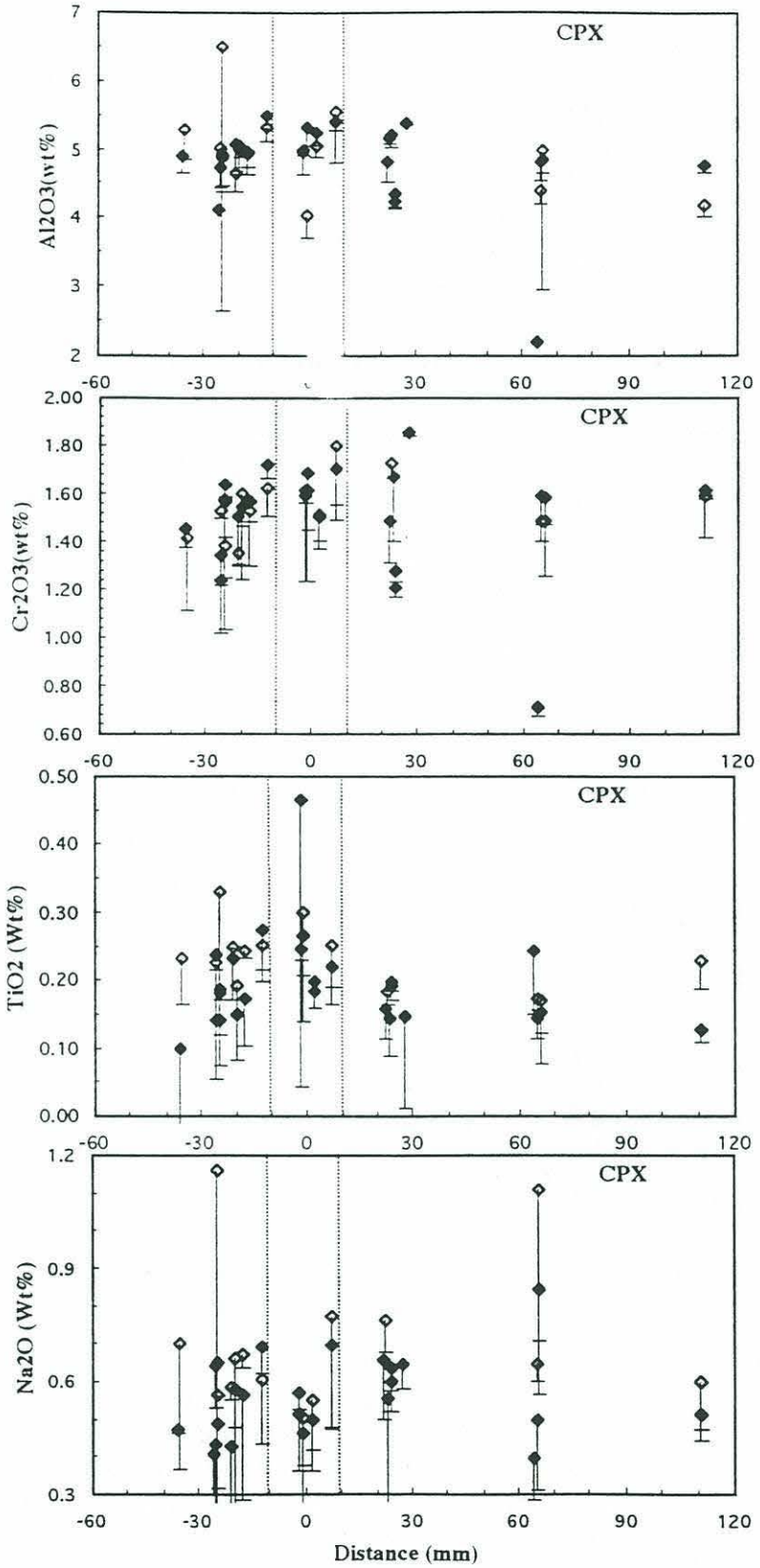

Fig.7: Compositional variation of clinopyroxene with distance for sample RC27-9-6-2. Errors and symbols are the same as in Fig.5.

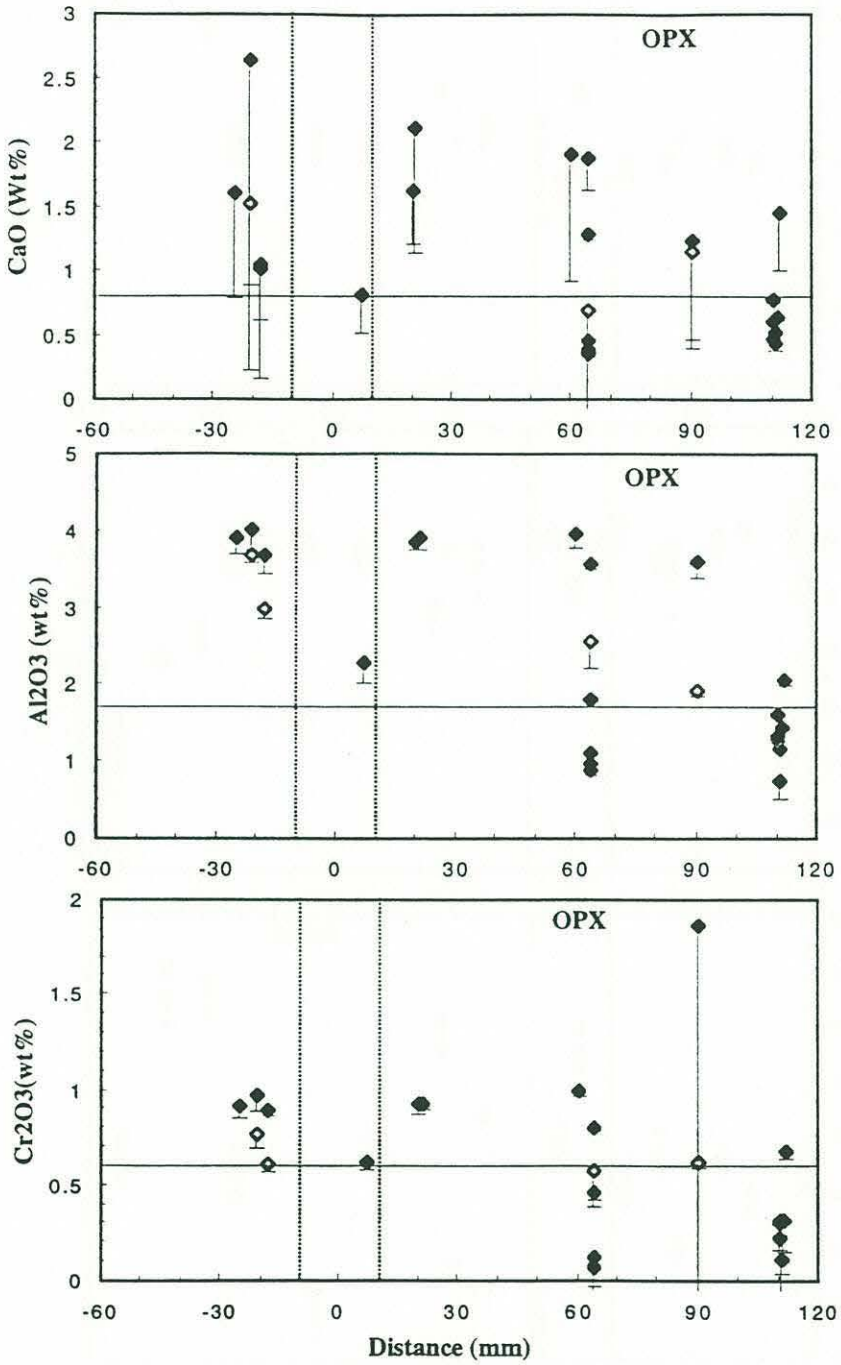

Fig.9: Compositional variation of orthopyroxene with distance for sample RC 27-9-6-2. The horizontal lines roughly separate the Opx adjacent to the plagioclase from the Opx in the rest of the sample. Errors and symbols see Fig.5.

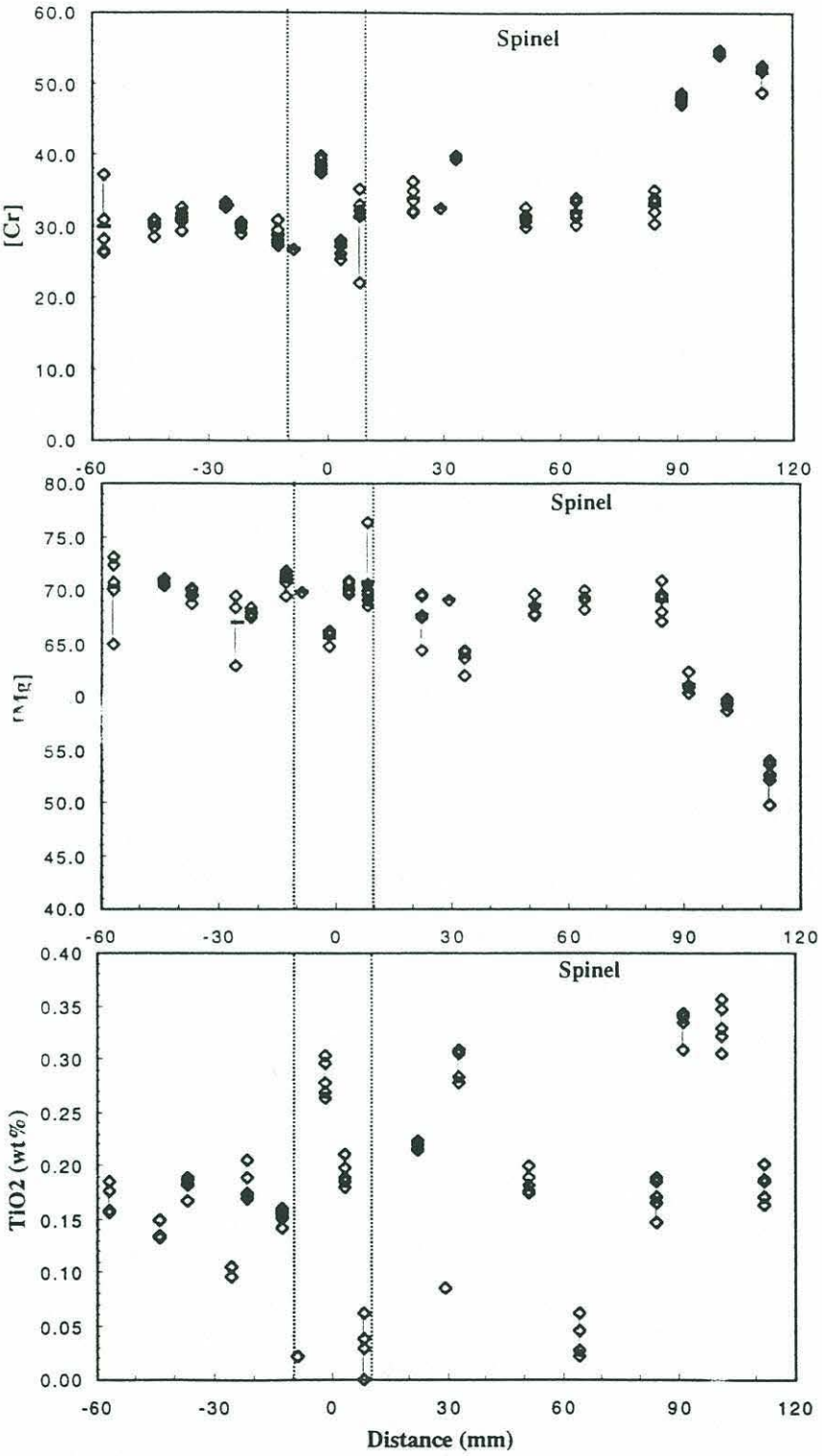

Fig.10: Compositional variation of spinel with distance for sample RC 27-9-6-2. Each separate point of analysis of a single grain is plotted and connected with a tie line. The average for each single grain is shown by the horizontal dotted line. The clinopyroxene vein is located at the center, at 0 mm. Possible regions affected by the pyroxenite vein are indicated by the dash lines.

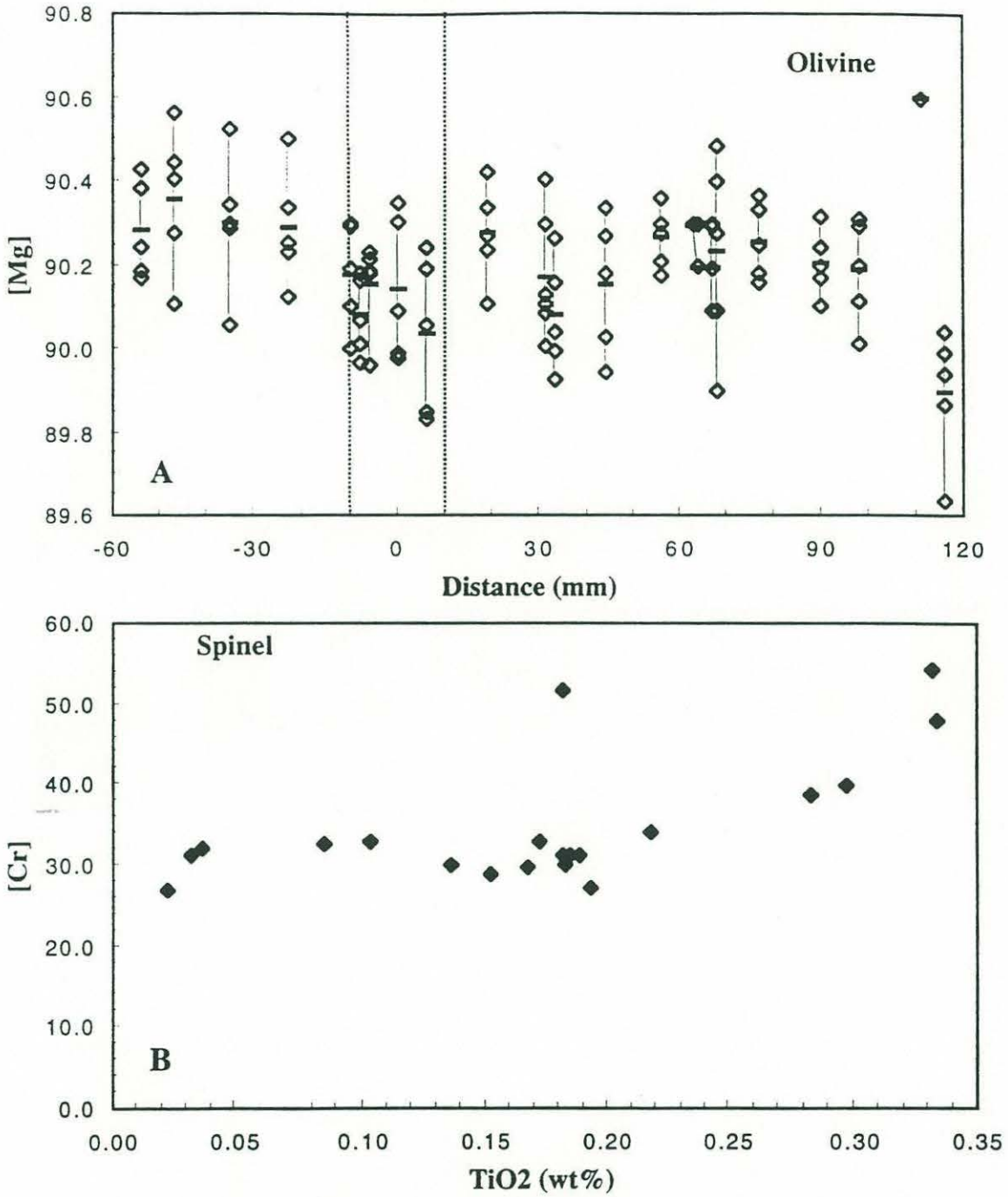

Fig.11: A. Compositional variation of olivine with distance for sample RC 27-9-6-2. Each separate point of analysis of a single olivine grain is plotted and connected with a tie line. The average for each single grain is shown by a red horizontal line. The clinopyroxene vein is located at the center, at 0 mm. Possible regions affected by the pyroxenite vein are indicated by the dash lines. B. The Cr number ($[Cr]=Cr^{3+}/(Cr^{3+}+Fe^{3+})$) vs. TiO_2 content in spinel from RC 27-9-6-2.

6. GEOCHEMISTRY

6.1 REE Patterns of Clinopyroxene From The Peridotite RC 27-9-6-2

The REE results are summarized in Table 9.

Fig. 12 shows the rare earth element (REE) patterns of core and rim of clinopyroxene relative to their positions relative to the clinopyroxenite vein. Abyssal clinopyroxene compositions from the Indian Ocean (Johnson et al., 1990) are also shown for comparison (Fig. 13). Overall, this sample is not as depleted in LREE as normal abyssal clinopyroxenes . The (Ce/Yb)n ratio ranges from 0.17 to 0.54 in clinopyroxene near the vein, and ranges from 0.75 to 2.35 in Cpx away from the vein (compared to ratios of 0.003 to 0.58 for the abyssal peridotite Cpx from Johnson et al. (1990)). Unlike most of the Cpxs from depleted mantle, the Cpx from thin section 2C and 1A have basically flat to enriched REE patterns. All the clinopyroxene core data have slightly more depleted HREE compositions than normal abyssal Cpx. One striking feature of this sample is the difference in concentrations from core to rim for the Cpx outside of the vein (Fig. 13), and the largest difference is shown in thin section 2C (Plate 5). In contrary, the Cpx near and in the vein have quite homogeneous rim-to-core ratios for the whole spectrum of REEs. Cpx from RC27-9-6-5 falls in the normal range of abyssal Cpx, with (Ce/Yb)n ranging from 0.05 (core ratio) to 0.18 (rim ratio), representing a sharp increase from the core to the rim in LREE concentrations.

Fig. 14 shows both the melt compositions in equilibrium with the Cpx and the range of abyssal basalts from the same dredged location from Johnson et al. (1990) for comparison. It should be noted that the abyssal basalts may represent the aggregated melts from different melting episodes (Johnson et al., 1990), and are not necessarily in equilibrium with the abyssal Cpxs in the mantle residue. The abyssal basalts in this area have Mg numbers lower than 60, indicating that the melts have undergone both olivine and plagioclase fractionation. Considering the olivine fractionation correction only, it takes about 25 weight percent olivine to convert the REE abundances of a AII basalt from 25 times chondrite back to about 20 times chondrite concentration, which is still two times higher than the most depleted equilibrated melt in the sample. Fractionation correction on plagioclase could probably bring the concentration down a little without introducing an obvious Eu anomaly in the residual melt. It is clear that most of the Cpx data are not in equilibrium with the basalts from this area, especially the Cpx that are away from the clinopyroxenite vein. Cpxs from thin section 3A have similar patterns to that of the basalts, but with lower abundances. It is possible that these are derived from primitive melt from this area. The other Cpx have

Table 9: Clinopyroxene REE and other trace element abundances																				
Thin Sect.	RefX	RefY	Gr.	Pts.	Loc.	La	Ce	Nd	Sm	Eu	Dy	Er	Yb	Ti	V	Cr	Sr	Y	Zr	Ti/Zr
RC27-9-6-2 (this study)																				
1A	83	111	1	1	C1	0.751	2.278	1.570	0.414	0.246	1.054	0.535	0.708	532	199	8218	24..	2.9	2.2	239
1A	83	111	1	1	C2	1.259	3.767	1.896	0.738	0.214	0.901	0.636	0.642	648	212	8789	24.7	3.4	3.1	207
1A	83	111	1	1	R1	1.010	3.955	3.621	0.965	0.449	2.078	1.085	1.366	822	260	5894	12.1	9.1	13.6	60
1A	83	111	1	1	R2	1.992	7.431	5.407	1.890	0.499	2.624	1.464	1.603	1038	268	8346	14.3	9.6	17.1	61
2C	86	66	1	1	C	0.491	1.706	1.077	0.400	0.143	0.611	0.340	0.351	671	171	7373	19.7	1.6	3.3	202
2C	86	66	1	1	R	3.372	7.631	2.707	0.722	0.249	1.050	0.745	0.837	599	215	6547	27.7	3.4	1.8	329
3A			1	1	R	0.140	0.591	0.937	0.486	0.331	1.181	0.642	0.841	1166	250	9545	10.0	6.0	4.6	252
3A	19	-1	2	1	R	0.143	0.531	0.958	0.410	0.282	1.211	0.681	0.683	1194	237	8537	7.8	5.4	4.0	297
3A	19	-1	2	1	C	0.101	0.364	0.565	0.291	0.160	0.710	0.467	0.509							
3A	22	-2	3	1	I	0.140	0.605	1.178	0.426	0.326	1.578	0.804	0.911							
3C	129	24	1	1	C1	0.342	1.317	1.270	0.666	0.259	1.024	0.810	0.626	888	222	8879	33.5	5.1	3.9	226
3C	129	24	1	1	C2	0.320	1.152	1.213	0.547	0.238	0.955	0.597	0.616	888	255	8305	32.8	5.8	4.3	205
3C	129	24	1	1	R	0.330	1.335	1.477	0.693	0.255	1.122	0.706	0.673	949	240	7566	34.2	5.3	3.7	255
3C	131	22	2	1	C	0.335	1.207	1.354	0.615	0.280	1.177	0.617	0.716	1163	249	6429	30.1	5.6	4.4	263
3C	131	22	2	1	R	0.323	1.174	1.469	0.632	0.274	1.292	0.803	0.769	1043	237	6333	28.6	5.2	4.0	259
RC27-9-6-2 (Snow, 1993)																				
				?	avg.		1.60	1.77	0.95	0.35	1.49	0.92	0.97	1369	295	8870	30.35		6.32	217
RC27-9-6-5 (this study)																				
				1	C	0.089	0.234	0.432	0.521	0.240	1.704	1.061	1.257							
				1	R	0.284	1.021	1.054	0.812	0.191	1.949	1.177	1.412							
RC27-9-6-3 (Johnson et al., 1990)																				
				21	avg.		0.04	0.47	0.62	0.33	1.93	1.17	0.78	1525	305	7051	1.2		2.1	726
RC27-9-6-8 (Johnson et al., 1990)																				
				24	avg.		0.03	0.57	0.76	0.39	2.67	1.72	1.74	1702	338	6959	0.6		1.7	1001

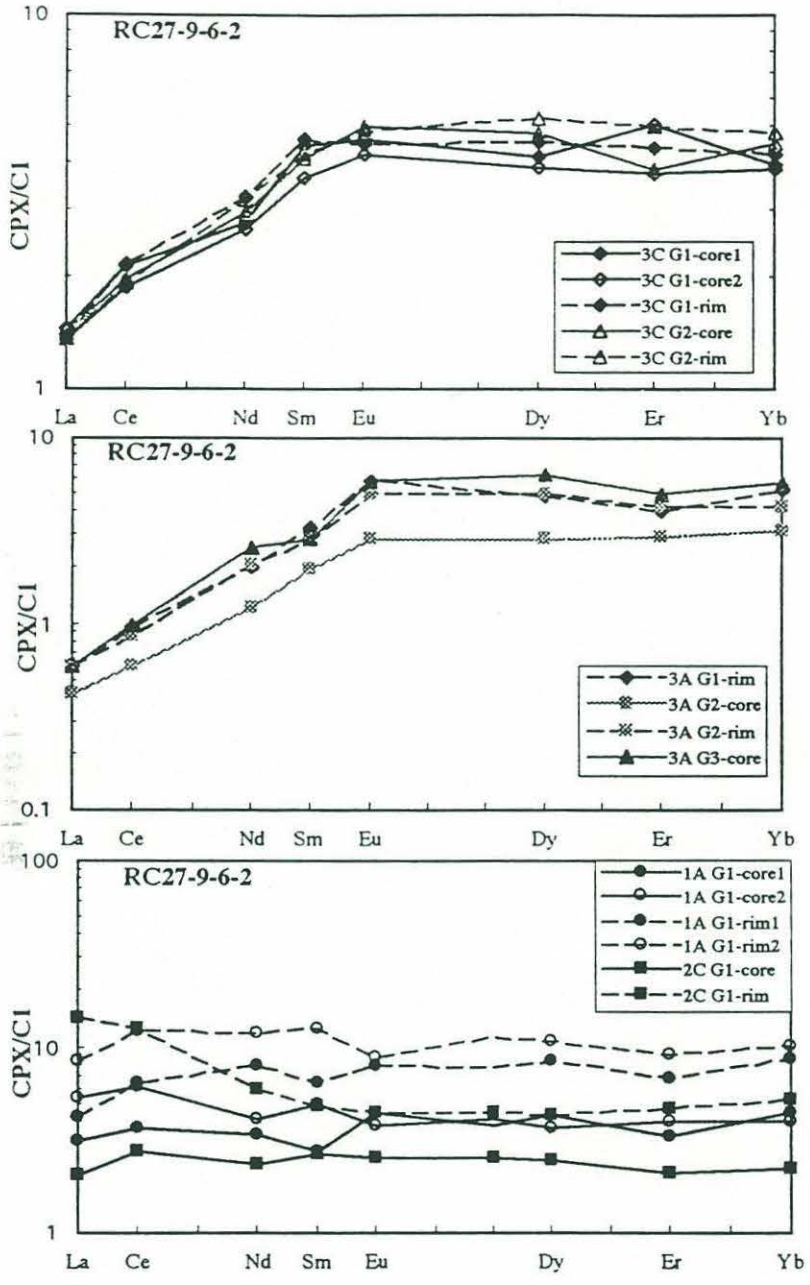

Fig.12: REE in diopsides from RC 27-9-6-2. All REE concentrations are normalized to C1 chondrites (Anders and Grevesse, 1989).

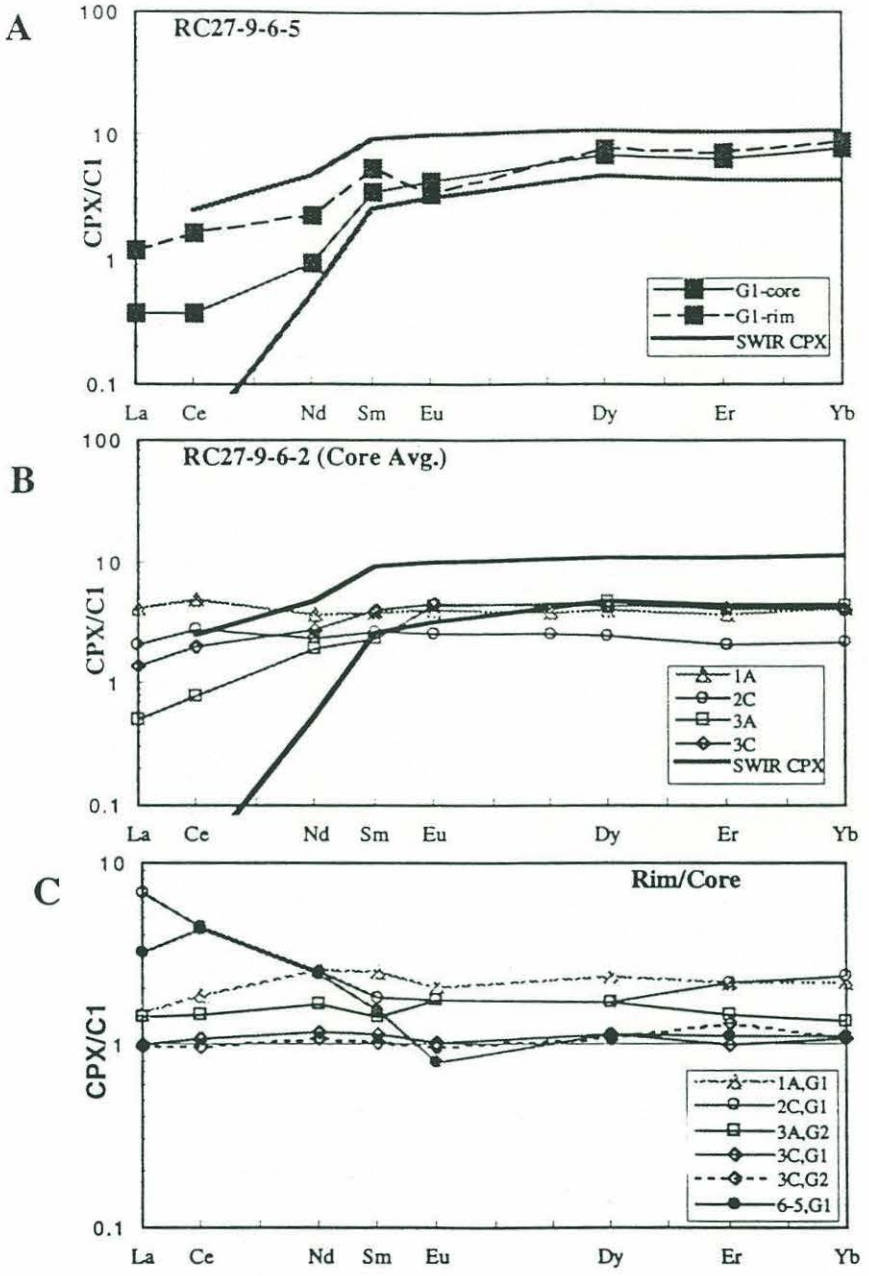

Fig.13: A. REE concentration in diopsides from RC 27-9-6-5 normalized to C1 chondrites (Anders and Grevesse, 1989). Shown for comparison is the field of Southwest Indian Ridge harzburgite Cpx sampled far from mantle hot spots from Johnson et al. (1990). B. The averaged REE in diopsides from RC 27-9-6-2. There is a tendency for LREE enrichment, going from the pyroxenite vein to the lherzolite. C. The averaged rim/core ratios in diopsides from RC 27-9-6-2 and RC 27-9-6-5. Samples from 2C and RC 27-9-6-5 show the largest enrichment in LREE.

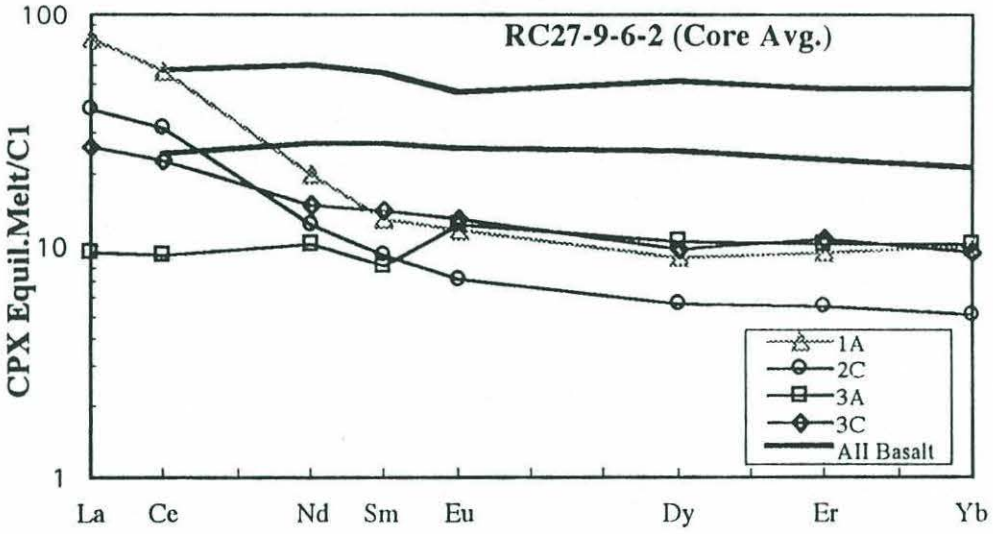

Fig.14: Calculated equilibrium liquid compositions for diopsides from RC 27-9-6-2. Also shown for comparison is the field of basalt compositions from the Atlantis II Fracture Zone from Johnson and Dick (1992). Cpx partition coefficients are from Kelemen et al. (1993).

too enriched LREE concentrations to be in equilibrium with the associated basalts. Melting models based on Johnson et al. (1990) suggest that, for most of the data, different sources or degrees of melting are needed to explain most of the trace element patterns by either batch or aggregated fractional melting models, as well as the discrepancy of concentrations between core and rim for single clinopyroxene grains. For example, Cpx 1A rim has a similar pattern and abundance to a melt that could be in equilibrium with the Cpx from 3A, while the melt from Cpx 1A is so LREE-enriched that it requires a very small degree of melting from a depleted source. Contrary to Johnson et al's (1990) data, the evolutionary history of clinopyroxenes in this sample is probably more complicated than that of most other abyssal peridotites, which are multiply depleted residues.

6.2 Melt-Rock Reaction Process Versus Melting with Residual Garnet: Interpretation of Ti, Zr and REE data

An alternative way to explain the variations of REE patterns is by a melt-rock reaction process (Kelemen et al., 1992; Dick and Natland, 1996). It is evident that some spinels from gabbroic segregations in the East Pacific Rise near the Hess Deep are affected by melt-rock reaction (Dick and Natland, 1996). The variation in TiO content in spinel is too large to be accounted for by simple melting and fractionation processes. The explanation of such a variation may be melt-rock reaction and trapped melt. While the TiO_2 content in spinel is elevated by both crystallization from trapped melt and the incompatibility in the residue, the large variation in TiO_2 content reflects the compositions of the liquids migrating through the dunite after the melt-rock reaction. During such a process, the melt-rock reaction has a huge impact on the trace element concentrations in the melt, while most of the major element concentrations, such as the Mg number, are still buffered by fractionation of olivine and orthopyroxene. Since the melt dissolves clinopyroxene and precipitates olivine and orthopyroxene in the cooling region, Kelemen et al. (1992) showed that Ti/Ti* (=2*Ti(N)/(Dy(N)+Eu(N)) in clinopyroxene decreases because of the differences in partition coefficients between clinopyroxene and the other silicate minerals for titanium and the adjacent rare earth elements. They also showed that the increases in both Nd and Yb concentrations during melt-rock interaction are on the one hand caused by the fractionation of olivine and orthopyroxene, and on the other hand by a decrease of melt mass in the conductive cooling region.

Shown in Fig. 15 are both the variations of Ti versus Zr, and Ti/Ti* versus Zr/Zr* of the clinopyroxenes. Data from Johnson et al. (1990) in the Southwest Indian Ocean Ridge are also shown for comparison. It is obvious that the titanium concentrations in the Cpx of this study are lower than in other samples from this region. In general, the further away from

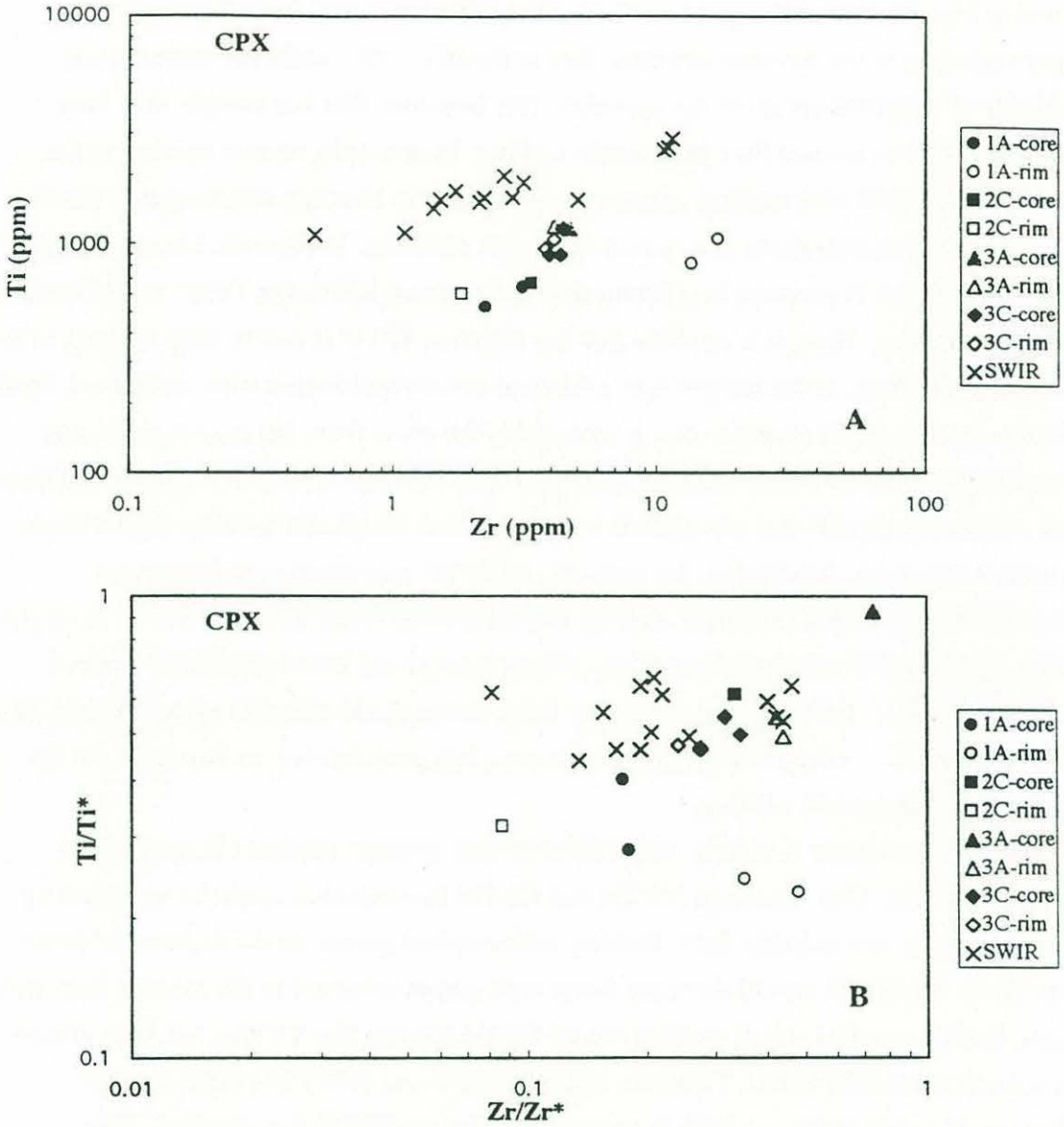

Fig.15: A. Ti vs. Zr contents in diopsides from RC 27-9-6-2. Data from Southwest Indian Ridge harzburgites (Johnson et al., 1990) are shown for comparison. B. Ti/Ti* vs. Zr/Zr* in diopsides from RC 27-9-6-2. Ti* is calculated from 2*Ti(N)/(Dy(N)+Eu(N)), and Zr* is calculated from 2*Zr(N)/(Dn(N)+Sm(N)).

the vein position (3A), the more depleted the concentrations are. The same tendency is also shown in the variation of Ti/Ti*. The variation of the titanium anomaly and (Ce/Yb)n is shown in Fig. 16. One striking feature is that the clinopyroxenes from this study have larger variations in the titanium anomaly than in the (Ce/Yb)n, while the other abyssal peridotite clinopyroxenes show the opposite. This indicates that this sample may have undergone other processes than just mantle melting. In principle, mantle melting in the garnet stability field with residual garnet would deplete the titanium concentration much faster than the concentrations of adjacent rare earth elements. In contrast, because spinel has a much higher Ti partition coefficient than the adjacent REEs, the Ti/Ti* would increase during the melting. Thus, it is possible that the negative Ti/Ti* is due to deep melting in the garnet stability field, or the sample was infiltrated and reequilibrated with melts from depth. Because the Atlantis II fracture zone is reasonably far away from hot spot regions, and other samples from this same area did not show REE evidence of residual garnet (Johnson et al., 1990), the chance that this sample is derived from the garnet stability region is not favored at this point. In addition, the variation of Ti/Ti* is probably too large to be accounted for by simple fractional melting in the garnet stability field. However, as shown in Fig. 16, the Ti/Ti* of all of the abyssal clinopyroxenes are lower than the fractional melting trend (F from the spinel stability field. Given the incomplete understanding of the melting mechanism and the migration process, it is probably too early to rule out the influence of deep mantle melting.

The Cpx have higher (Ce/Nd)n and (Nd/Yb)n than average abyssal clinopyroxenes (Figs. 16 and Fig. 17)). The high Nd-Yb and Ce-Nd fractionation could be provided by melting the garnet stability field. Melting with residual garnet would deplete Nd faster than Yb, so the Nd/Yb would decrease faster with garnet involved in the melting than with spinel. Both garnet and spinel melting would fractionate the Sm-Yb pair, but with almost the same fractionation factor. Thus, the high (Ce/Nd)n and (Nd/Yb)n indicates less influence of garnet melting, which is contrary to what the Ti/Ti* data implied. This dilemma for mantle melting partly builds on the uncertainties of the physical processes involved in the garnet-spinel transition zone.

Alternatively, based on Kelemen et al. (1992), melt-rock reaction could increase (Nd/Yb)n, and at the same time decrease Ti/Ti*. In the following discussion, I will try to model the melt-rock interaction by an assimilation-fractional crystallization (AFC) process as proposed by DePaolo (1982). The same modeling has also adopted by Kelemen et al. (1992) in the search for evidence of melt-rock reaction in orogenic peridotites. The usage of simple AFC modeling is promoted by the similarity between melt-rock reaction in a closed system and the cooling process in a magma chamber. The driving forces for both

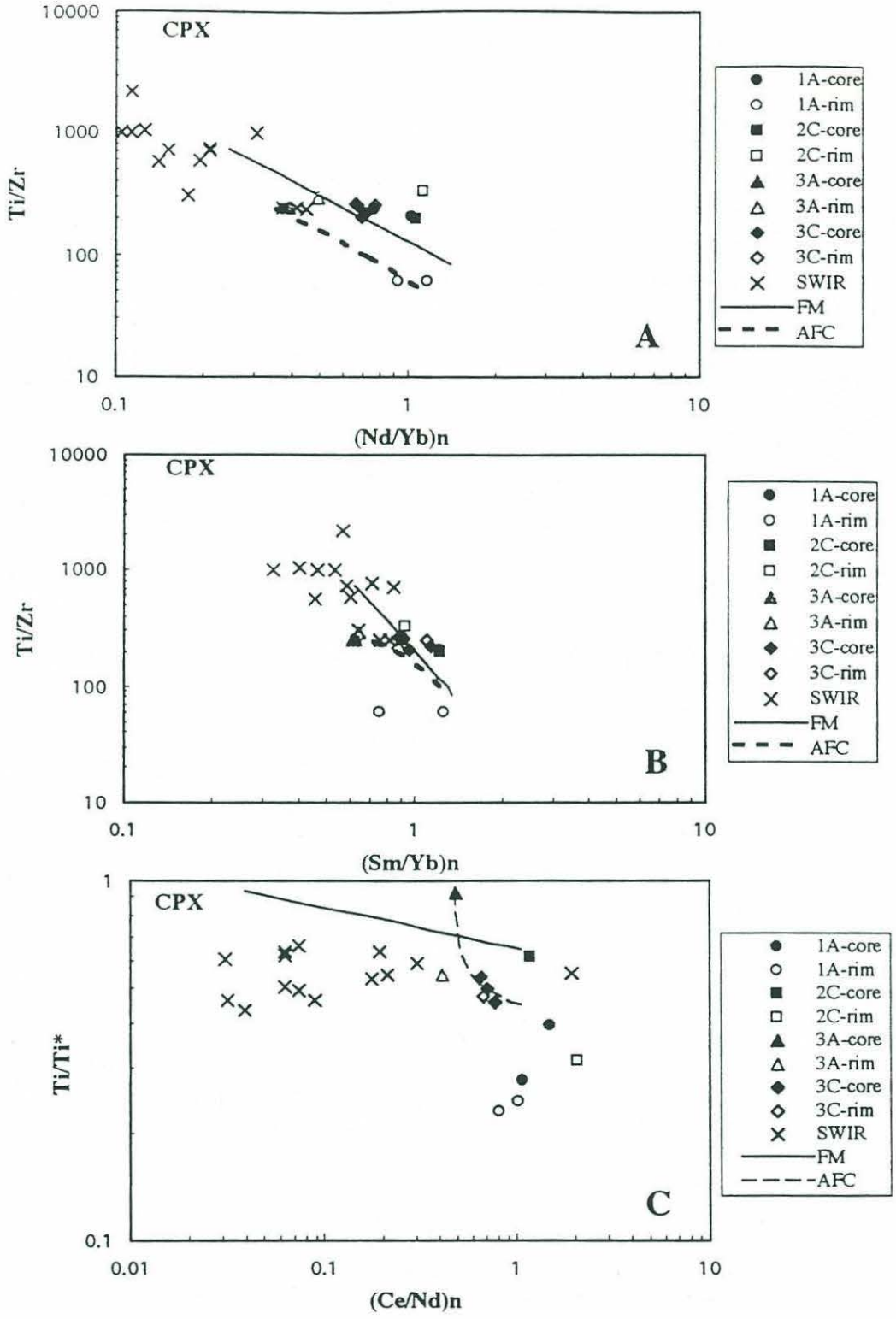

Fig.16: A. Ti/Zr vs. (Nd/Yb)n, and B. (Sm/Yb)n and C. Ti/Ti* vs. (Ce/Nd)n for diopsides from RC 27-9-6-2 and RC 27-9-6-5. Also shown for comparison are data of Southwest Indian Ridge harzburgite Cp̄xs from Johnson et al. (1990). The solid line is a fractional melting model trend based on Johnson et al. (1990). The thick, dash line is an AFC model curve calculated using the parameters listed in Table 10.

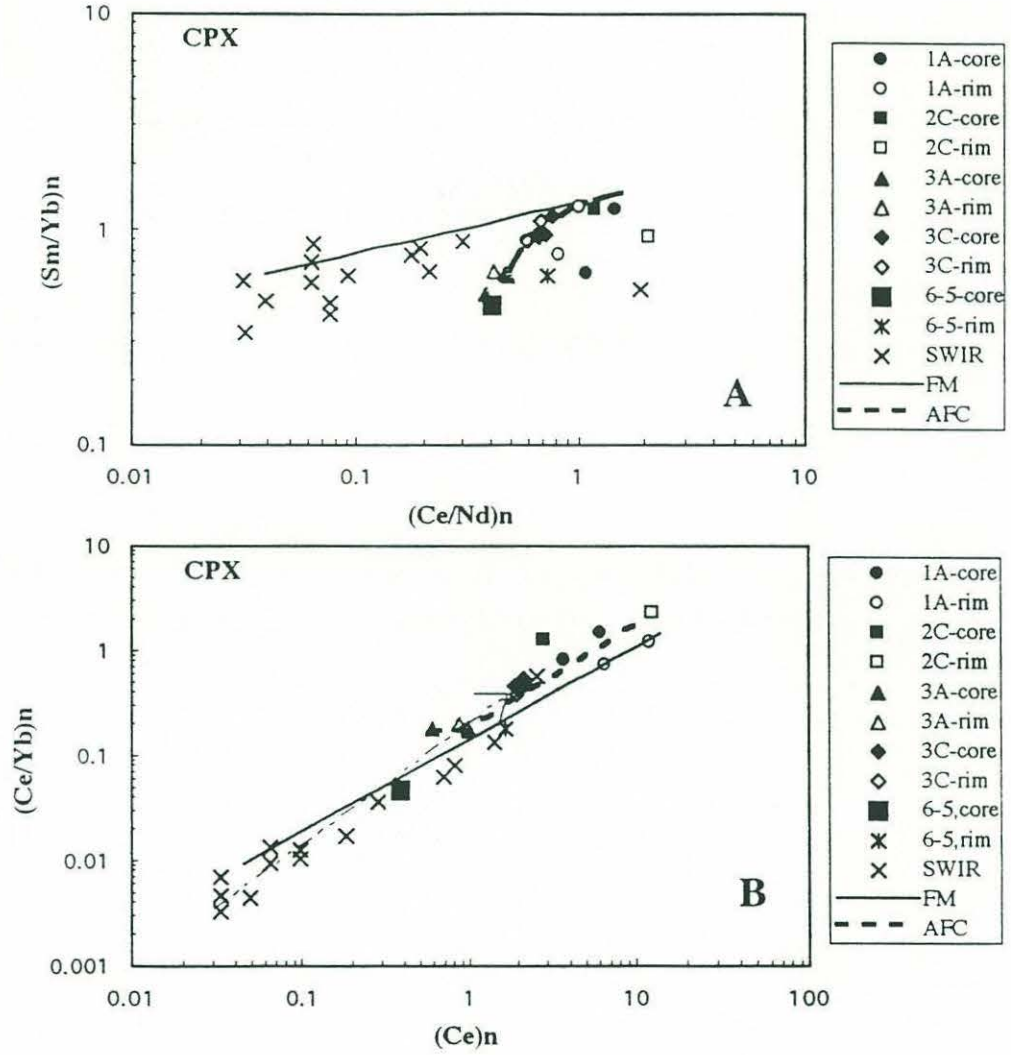

Fig.17: A. (Sm/Yb)n vs. (Ce/Nd)n and B. (Ce/Yb)n vs. (Ce)n for diopsides from RC 27-9-6-2 and RC 27-9-6-5. SWIR data, FM and AFC model trends are as in Fig.15. Also shown in dashed arror is the refertilization model trend from Elthon (1992).

processes, however, are different. In the traditional AFC model, a batch of magma assimilates the wall rock by exchanging the latent heat of fractional crystallization of the magma, and the composition of magma for each instantaneous step is dependent on both the concentration of the assimilant and the cumulate. Since the volume of the assimilant is infinite, the magma would never reach a steady state for the elements with partition coefficients less than 1. Thus, for the LIL trace elements, the AFC result is a single event after the magma is consumed completely. On the other hand, the melt-rock reaction process mainly depends on the chemical disequilibrium between the reactant and the assimilant, indicating a possible intermediate stage for the assimilant to be in equilibrium with the reactants in an open system. Therefore, it is more suitable to describe the melt-rock reaction process with a model which is capable of modeling multistages instead of a single event. Since the physical process for the melt-rock reaction is not well understood yet, it is probably still a good choice to extract the first order information through the AFC process. A combination of AFC and chromatographic models is probably closer to the real situation. Given the uncertainty in the parameters in both models, I choose to use the simple AFC model, to simplify the entire modeling and to make the modeling clear.

The AFC trend (Fig. 16 and Fig. 17) is the 'cumulate' trend which represents the clinopyroxene (crystal) compositions in equilibrium with the 'melt'. Also shown in the figures is the residual Cpx composition from fractional melting (FM trend) in the spinel stability field. Both the data from this study and from the abyssal clinopyroxenes (Johnson et al., 1990) are plotted for comparison. The parameters for both of the models are summarized in Table 10. For the AFC model, the melt composition was taken to be that in equilibrium with the Cpx in thin section 3A, which is the most depleted melt in this sample (and is probably also in equilibrium with the primitive MORB from this area, as discussed before). The pyrolite mantle composition for the fractional melting model is too enriched to be the source of depleted suboceanic mantle, but instead of investing a lot of effort to find the right composition for it, I concentrated my attention on the difference between the fractional melting model and the AFC model. Non-modal fractional melting depletes the LREE/MREE ratios faster than it does the MREE/HREE ratios. The AFC process enriches the melt in both LREE and MREE, since the melt mass decreases while the melt precipitates olivine and orthopyroxene. Even if the product precipitates more clinopyroxene component than the reactant, the enrichment is still obvious. Therefore, the effect of the AFC process is totally opposite to fractional melting, in the current case. As mentioned before, the AFC process has a profound effect on both the titanium anomaly and the titanium concentration (Kelemen et al., 1992) (Fig. 16). The Cpx composition spreads vertically along the Ti/Ti* axis, with little variation in (Ce/Nd)n. It is hard to envision a simple melting process which

Table 10: The parameters for the AFC and FM models.

	C(0)	D(ol)	D(opx)	D(cpx)	D(sp)	D(0)	D(P)	D(ppt)	Ca)n	Cm)n
Ce	2.5	0.000007	0.005	0.0858	0.0006	0.0156	0.0583	0.0114	0.0045	6.9875
Nd	2.5	0.00007	0.009	0.1873	0.0006	0.0359	0.1310	0.0246	0.0808	6.6045
Zr	2.5	0.0005	0.014	0.1234	0.07	0.0314	0.1061	0.0193	0.0539	9.5106
Sm	2.5	0.0007	0.02	0.291	0.0006	0.0577	0.2065	0.0399	0.3546	6.7004
Eu	2.5	0.00095	0.03	0.35	0.0006	0.0711	0.2516	0.0494	0.5611	8.1492
Ti	2.5	0.015	0.14	0.384	0.15	0.1257	0.3624	0.0895	0.6572	7.0000
Dy	2.5	0.004	0.06	0.442	0.0015	0.0974	0.3289	0.0692	0.8417	6.5576
Er	2.5	0.009	0.07	0.387	0.003	0.0928	0.2955	0.0681	0.9357	7.5491
Yb	2.5	0.023	0.1	0.43	0.0045	0.1155	0.3351	0.0891	0.7922	7.4407
Phase Proportions										
OL						0.4676	-0.4464	0.639		0.671
OPX						0.2788	0.5534	0.227		0.256
CPX						0.1780	0.6722	0.120		0.066
SP						0.0756	0.2230	0.014		0.006

The r factor (ratio of the assimilating rate to the crystallizing rate) in the AFC model is 0.97 in present calculation.

C(0): stating source compositions for fractional melting (FM) model

D(0): Source mode and partition coefficient for fractional melting (FM) model, adopted from Kelemen et al., (1992).

D(P): Melting mode and partition coefficient for fractional melting (FM) model, adopted from Kelemen et al., (1992).

D(minerals): partition coefficients are adopted from Kelemen et al. (1993)

D(ppt): partition coefficients for the product (the cumulate) in AFC model

the mode of the product is adopted from the lherzolite Vulc5: 41-15 (8) from Johnson et al. (1990)

Ca)n: chondrite normalized REE concentration for the wallrock (the assimilant) in AFC model

data is converted from the clinopyroxene concentration from RC 27-9-6-3 (Johnson et al., 1990)

Cm)n: chondrite normalized concentration for the melt (the assimilant) in AFC model

data is converted from the clinopyroxene composition of Cpx 3A in this study

is able to produce such a data array. In terms of the titanium anomaly, it is easier to model this with the AFC process. Although not perfect, the AFC trend shows the tendency, that as the melt migrates outward from the vein, the effect of the reaction between the melt and the adjacent lherzolite is to cause the light rare earth element concentrations to increase, while the melt mass decreases. The effect is larger with distance. As shown in Fig. 16, the AFC trend passes through the data points from 3A to 3C, suggesting that the reaction zone may be on the scale of one centimeter. As clinopyroxenes in thin sections 2C and 1A are often off the AFC model trend, and noting the occurrence of plagioclase, rutile and ilmenite in thin section 2B, this may suggest the combined effects of melt-rock reaction and trapped melt in a zone a few centimeters away from the vein. It should be remembered that this sample is a plagioclase lherzolite with about 0.4 wt% of plagioclase (Snow, 1993). If the vein clinopyroxene and the trace element variations are truly the evidence of melt-rock reaction, this scenario indicates not only the process itself, but also the dynamic consequence of such a process. It should be noted that it is still difficult to constrain the whole data array by a single process because of the scatter of the data. This scatter could be caused by analytical errors, as well as uncertainties in the parameters chosen for the models. At this point, however, the melt-rock reaction process is favored, for it reproduces the trace element variations better than the other processes.

6.3 Refertilization of Depleted Peridotites

Elthon (1992) suggested an alternative way to explain the chemical trend of abyssal clinopyroxenes, by refertilization of highly depleted mantle by MORB melt at low pressure. The current study provides an opportunity to verify this refertilization process. The arrow in Fig. 17 indicates one of the refertilization trends from Elthon (1992). It is clear that the arrow points toward more enriched LREE concentration and passes through most of the data points of this study. On the other hand, both the refertilization and the fractional melting trends cannot perfectly explain the distribution of normal abyssal clinopyroxenes from the SWIR. As discussed above, given the uncertainties in the parameters for the modeling, it is premature to argue that all of the abyssal peridotites have been somewhat influenced by migrating melts. For the current study, the refertilization process does offer one more aspect to consider the melt-rock reaction and the melt impregnation processes.

7. THE EFFECT OF SEA WATER ALTERATION

Normally, abyssal peridotites are severely serpentinizied and altered by sea water. Most previous studies have focused on high temperature and high pressure metamorphic grade alteration as well as on very low temperature sea water weathering. Few studies have concentrated on the serpentinization process, partly because of its ambiguous relationship to the tectonic setting and the pattern of hydrothermal fluid circulation.

7.1 Serpentinization

A previous study by Kimball et al. (1985) showed that abyssal peridotites have undergone a series of episodes of alteration, through high temperature metamorphism involving amphibole phases, to very low temperature sea water weathering. The later alteration events may overprint previous episodes, in the form of replacement of mineral grains and crosscutting veins. Some of the high temperature metamorphic products would be unstable at lower temperature and gradually retrograde to other mineral assemblages; some would remain as metastable phases, depending on the composition of the products and the environment that provides the source for that specific composition. In hydration processes such as serpentinization, a stable mineral assemblage at certain temperature and pressure is not the only controlling factor; the kinetics of mineral reaction and dissolution are important as well. It is not unusual to find a number of unequilibrated phases present during serpentinization , which violates the phase rule in that these are excess phases present at transition periods (Sanford, 1981). In their closed-system experiments, Janecky and Seyfried (1986) found that some alteration products such as brucite and talc, common at the lower range of temperature, are metastable. Over longer periods of time, it is unclear whether these minerals would be stabilized or be transformed into more stable phases. Equilibrium between alteration assemblages and altering solutions is harder to maintain in a natural open system. Therefore, the mineral assemblages observed in altered abyssal peridotites might represent each single episode of an alteration event, and the relationship between them is often ambiguous.

For instance, alteration phases which are frequently present such as magnetite, talc, chlorite, hematite, tremolite-actinolite, magnesite and aragonite are not all present in Janecky and Seyfried's experiments. Magnetite, which is frequently found coexisting with serpentine in natural rocks, is not present in the lherzolite/harzburgite-sea water experiments, since the redox conditions favor precipitation of hematite instead of magnetite. Their results also showed that the alteration processes depend not only on pressure, temperature, composition of altering solution and mineral proportions of the rocks, but also on the kinetics of mineral dissolution

rate, the mechanism of the alteration (structure controlled), and the stability of each phase. A more detailed study is needed to understand how each phase assemblage forms under specific conditions. Although it is not the focus of this study, I will try to use some of the ideas from previous studies to interpret the mineral assemblages found in this sample, with a focus on the origins of the magnetite and the sulfides.

Petrographically, most of the magnetite in this sample is found at the center of alteration veins, formed either as discontinuous thin veinlets or as veinlets with skeletal forms. Some magnetite is found associated with amphibole and chromite, which indicates that the magnetite is reprecipitated in the vein after the serpentine and amphibole, or as replacements after the amphibole and chromite. Some discrete sulfides disseminated in serpentine veins have magnetite rims, and some others have been altered to iron-oxides in their cleavages. Texturally, these magnetites in the abyssal peridotites are of metamorphic origin. During high temperature metamorphism (T>600°C), the dominant hydration reaction is clinopyroxene altering to hornblende or hornblende + antigorite (Kimball et al., 1985). There is no report of magnetite coforming along with this reaction. It is generally believed that the non-magmatic magnetite is formed during the serpentinization of ultramafic rocks, which is at slightly less than 500°C. Iron is released during the serpentinization through the reactions of olivine and orthopyroxene with fluid to form Mg-rich serpentine. In theory, magnetite may be found to be associated with n alloys, since the reactions release H^+ and thus locally produce a reducing environment. Therefore, it is suspected that the metal alloys found in ophiolites are associated with magnetite during the serpentinization (Abrajano et al., 1988). Several lines of observation (Charlou and Donval, 1993; Berndt et al., 1996) also relate the emission of hydrogen and/or methane gas from ultramafic complexes, to the serpentinization, using the same rationale as above.

Closed-system experiments and calculations (Janecky and Seyfried, 1986) showed that at the very late stage of serpentinization, the oxygen fugacity decreases while pH increases to a very high value, and there is a significant amount of magnetite precipitated. Moody (1976) found that the Fe partitioning between brucite and magnetite is strongly dependent on the acidity of the conditions. Several other experiments (Johnson and Bauman, 1978; Tamura et al., 1976; Smith et al., 1982) also showed that at low temperature, the oxidation kinetics of Fe has a very strong pH dependence. Janecky and Seyfried's experiments showed that both the pH value and the redox conditions are controlled by the chemical reaction paths. It is likely that the iron released from the silicates is oxidized to form magnetite at relatively alkaline conditions and at the same time, the reactions consume oxygen to reduce the surrounding environment. Two competing reactions occur during the serpentinization at the expense of H_2O. The initial magnetite precipitation may thus be controlled by the pH rather than by Fe redox kinetics.

Because serpentinization is by nature a hydration reaction of silicate minerals, each reaction stage may be reflected in the amount of magnetite precipitated and the Fe content in associated minerals such as serpentine and brucite.

The magnetite precipitation is associated with an increase of pH value, and a decrease of SiO_2. O'Hanley and Dyar (1993) analyzed $^4Fe(III)$ and $^6Fe(III)$ in serpentine minerals (utilizing Mossbauer spectroscopy) and their relationships with modal magnetite. They showed that the formation and consumption of magnetite depends on the activity of SiO_2 in the fluid at high oxygen fugacity. The SiO_2 content of the solution is also strongly inversely correlated with the late stage pH value variation in two of Janecky and Seyfried's closed-system hydrothermal experiments (1986), which were conducted with Mg and Mg-SO_4 free solutions having undergone reaction with basalts. Significant amounts of magnetite were found only in these two experiments, which suggests that the magnetite precipitated more efficiently in such an alkaline and reacted environment. Most of O'Hanley and Dyar's sample are recrystallized serpentinites from continental terrains, which may not be a good analogue of the oceanic setting to understand hydration mechanisms. The oceanic environment is usually considered to be an open system with an infinite supply of water and reactants during the serpentinization. However, based on the results of both studies above, it is possible that the serpentinization is retarded at the reaction front due to either a volume increase or an exothermic process, or possibly both of them. Once the serpentinization is slowed down, the fluid that is out of equilibrium with the surroundings could precipitate magnetite by the consumption of early-formed lizardite and brucite in the presence of excess SiO_2 (O'Hanley and Dyar, 1993). This suggests that it is possible that some of the serpentinization in abyssal peridotite is isochemical. In other words, the only material added into the system is H_2O, and mass is conserved during the hydration reaction(s) for the whole system.

Frost (1985) suggested that if the activity of hydrogen ($a(H_2)$) is high enough, FeNi alloys or Fe(0) could be precipitated with or at the expense of magnetite. Frost suggested that the reducing agent during the serpentinization was due to the activity of H_2O in the fluids, and consequently, H2 gas. Sanford (1981) proposed a phase relationship under the $P(H_2O) <$ P(total) condition to explain serpentine assemblages in serpentinite. These studies all point to the idea that in a semi-open system, the hydraulic pressure at the reaction front in an open structure and the permeability of the protoliths have profound effects on the mineral assemblages formed by hydration reactions. This implies that the formation of iron oxides and metal alloys depends not only on the supply and composition of the fluids, but also on the location where the required chemical elements are active. Metal alloys, especially the PGE alloys in ophiolites and alpine peridotites, are believed to be formed during late

serpentinization, or during the recrystallization stage after the serpentinization (O'Hanley, 1996), while the continual supply of fluids may reverse the reducing processes to form these minerals. Therefore, as far as the open structure of transform faults as concerned, it is no surprise to find the absence of metal and PGE alloys.

7.2 Major and Trace Element Variations of Bulk Rocks

Major and trace element abundances in the bulk rocks are summarized in Table 11.

Fig. 18 plots the trace elements versus the amount of water for the bulk rock analyses. In general, LOI is used to represent H_2O^+ in rocks; the latter is usually used as an indicator of the degree of hydration during alteration processes. In this study, the amount of water was analyzed by a gas chromographic method and represents both H_2O^+ and H_2O^-. During processes such as sea water alteration in mafic rocks near hydrothermal veins, some mobile elements such as Ba and Sr are found positively correlated to H_2O^+, indicating that these elements are being affected by the hydration processes. In contrast, the so called immobile elements such as Ti and Cr should still maintain the original bulk rock composition and should not correlate with H_2O^+. On the other hand, in a closed system, the degree of mobility of the mobile elements will not necessarily correlate with the H_2O^+, the degree of hydration. Consider a closed system (except for water): the amount of water added is used to hydrate olivine, assuming that olivine is much more sensitive to alteration than pyroxenes. Thus the larger the amount of water added, the larger the amount of olivine is hydrated. The amount of water more or less represents the amount of olivine present in the rock. If we look at it in this way, it is not difficult to rationalize the negative correlation between Ba, Sr and water, and the positive correlation for Ni. It suggests that the larger the amount of olivine in the rock (mode of olivine), the more depleted is this rock, and the higher the Ni and the lower the Ba and Sr.

Fig. 19 plots some trace and major elements versus MgO for the bulk rock analyses. Most of the data represent normal correlation seen for magmatic processes, such as clinopyroxene and olivine fractionation. Although this sample has gone through severe serpentinization, it does not show as much low temperature alteration by sea water as do mafic rocks in bulk rock analyses. Fig. 20 shows major element variation diagrams. It is clear that most of the data points fall in the central region or on the connecting lines between silicate minerals. This suggests that some of the bulk composition variations between each portion of this sample can be explained by the variations in the proportions of the minerals. This figure also shows that the major variations between sample portions is in the content of clinopyroxene. This sample contains minor aragonite on the outer surface (sub-sample A). The high CaO value in this portion may be caused either by some incorporation of the pyroxenite vein or the presence of

Table 11: Major and trace element abundances for the whole rock fractions from different slabs.

	Slab 3					Slab 1			RC27-9-6-2
	AB3	C3	D3	E3	F3	D1	E1	F1	(Snow, 1993)
Major elements (wt%)									
Unnormalized Results									
SiO_2	46.93	45.50	45.07	44.58	44.64				46.27
Al_2O_3	2.51	1.56	1.43	1.48	2.09				1.49
TiO_2	0.073	0.028	0.025	0.065	0.072				0.05
FeO	7.64	8.09	7.99	8.21	7.32				8.46
MnO	0.130	0.136	0.136	0.135	0.124				0.13
CaO	4.43	1.76	1.57	1.76	5.94				1.38
MgO	32.88	38.75	39.18	38.54	33.26				40.79
K_2O	0.05	0.02	0.01	0.01	0.01				0.02
Na_2O	0.38	0.18	0.12	0.12	0.24				0.1
P_2O_5	0.010	0.008	0.005	0.012	0.005				0.01
Total	95.03	95.93	95.54	94.91	93.70				98.7
H_2O	7.02	7.18	7.45	7.36	8.02	7.67	6.41	5.98	7.06–
CO_2	0.104	0.082	0.092	0.071	0.154	0.172	0.172	0.249	
S	0.066	0.086	0.082	0.080	0.079	0.085	0.112	0.065	
Normalized Results									
SiO_2	49.38	47.33	47.18	46.97	47.64				
Al_2O_3	2.64	1.63	1.50	1.56	2.23				
TiO_2	0.077	0.029	0.026	0.068	0.077				
FeO	8.04	8.43	8.36	8.65	7.81				
MnO	0.137	0.142	0.142	0.142	0.132				
CaO	4.66	1.83	1.64	1.85	6.34				
MgO	34.60	40.39	41.01	40.61	35.50				
K_2O	0.05	0.02	0.01	0.01	0.01				
Na_2O	0.40	0.19	0.13	0.13	0.26				
P_2O_5	0.011	0.008	0.005	0.013	0.005				
Trace elements (ppm)									
Ni	1794	1997	2056	2025	1707				2101
Cr	4564	2848	2779	2672	4031				2603
Sc	12	5	9	7	15				
V	87	54	52	53	83				57
Ba*	2.72	1.15	0.39	0.99	0.49				
Rb*	0.44	0.24	0.07	0.36	0.13				2
Sr*	11	6	4	4	10				6
Zr	14	13	8	12	10				9
Y*	5.02	1.30	0.74	1.67	2.80				1
Hf*	0.14	0.11	0.03	0.10	0.09				
Nb*	0.66	0.24	0.03	0.09	0.05				
Ga	5	0	2	1	2				
Cu	72	52	58	50	33				30
Zn	54	46	50	47	42				43
Pb*	0.71	0.13	0.08	0.12	0.09				
Th*	0.04	0.05	0.01	0.03	0.01				
–: LOI, loss on ignition									
*: data from ICP-MS analysis, others are all from XRF analysis except H_2O, CO_2 and S.									

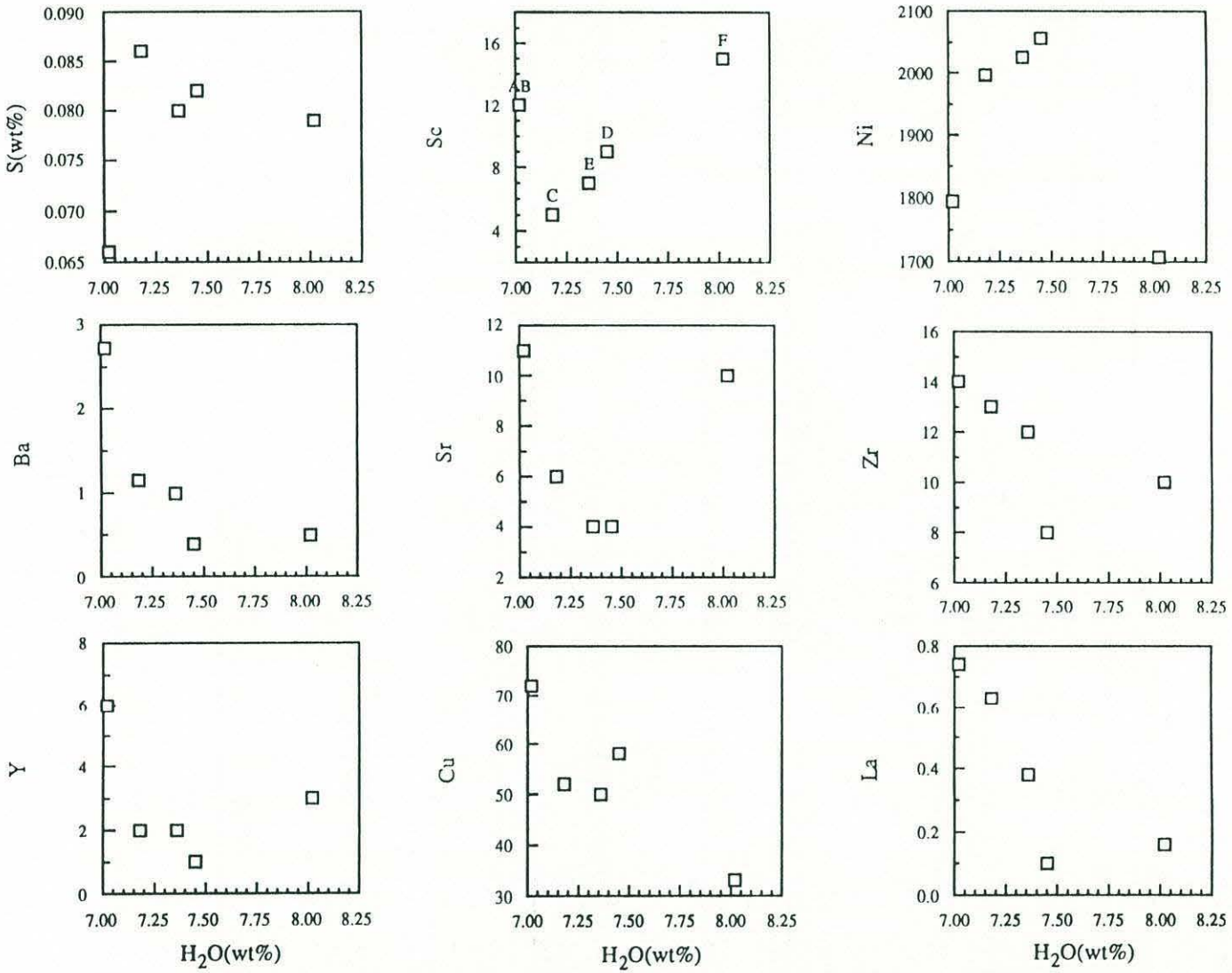

Fig.18: Major and trace element concentrations vs. water content in the bulk samples from abyssal peridotite RC 27-9-6-2. Trace element concentrations are in ppm. Water contents in the trace element plots are from Slab 3.

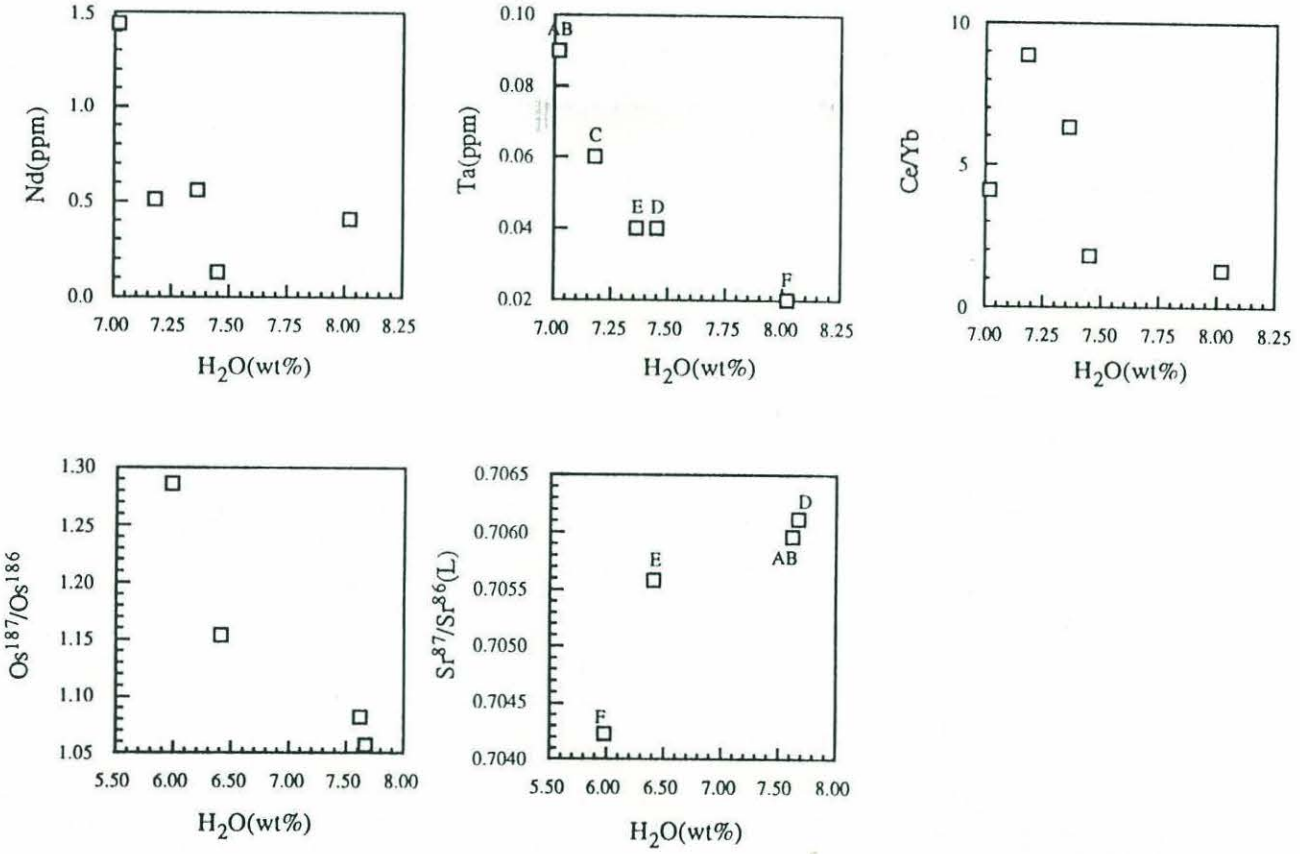

Fig.18 (Con'd) Trace element concentrations and isotopic ratios vs. water contents in bulk samples from abyssal peridotite RC 27-9-6-2. Water contents in the isotopic ratio plots are from Slab 1.

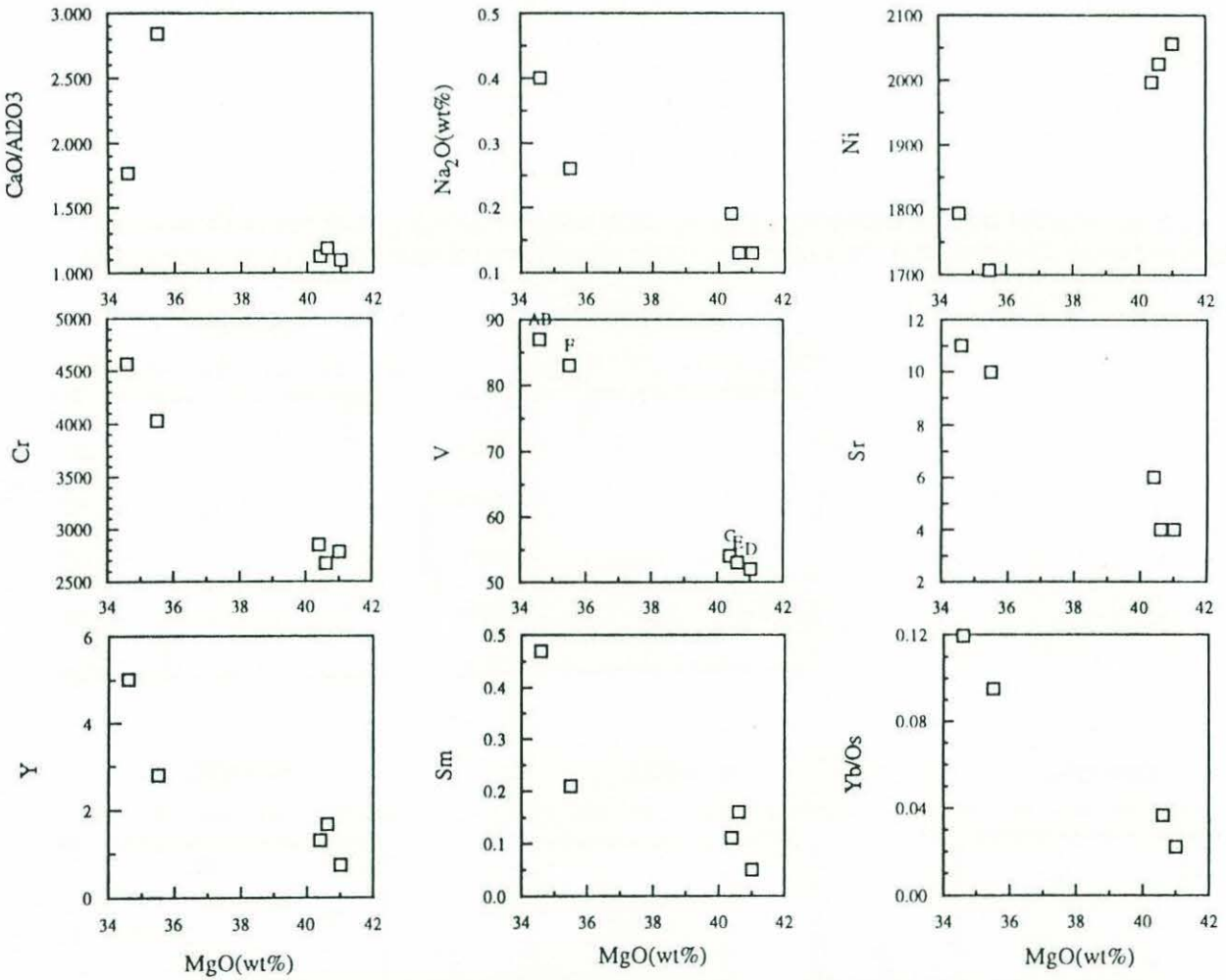

Fig.19: Major and trace element contents vs. MgO (wt%) in bulk samples from abyssal peridotite RC 27-9-6-2. Trace element concentrations are in ppm. Both the major and trace elements data are from Slab 3.

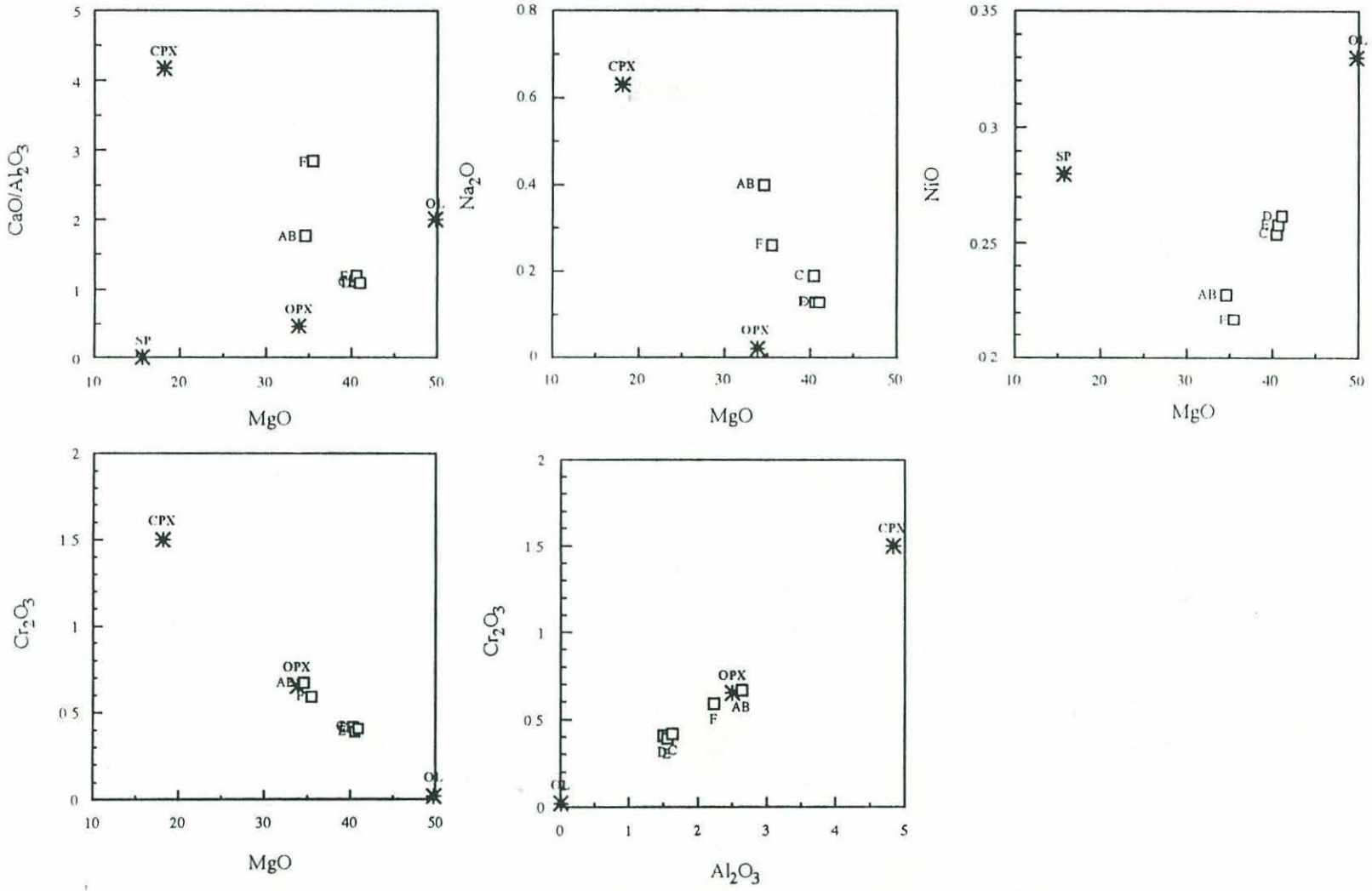

Fig.20: Major element variation diagrams for whole rocks from RC 27-9-6-2. All elements are in wt%. Mineral compositions for spinel (SP), olivine (OL), orthopyroxene (OPX) and clinopyroxene (CPX) are averaged electronprobe analyses listed in Tables 4 through 7. Whole rock data are from Slab 3.

aragonite. The bulk analysis of Sr concentration and Sr isotopic ratio indicates the presence of sea water phases (Fig. 21). The highest unleached Sr concentration and $^{87}Sr/^{86}Sr$ is in the A/B portion of the sample, and these are roughly correlated with the CO_2 concentration in the bulk rock. The Sr concentration and $^{87}Sr/^{86}Sr$ after dilute HCl leaching are still very high in the A/B portion. This suggests that the Sr data reflect both magmatic (the pyroxenite vein) and hydrothermal compositions.

The idea of a nearly isochemical alteration can also be tested by a least square fit for the bulk rock analysis using the individual mineral composition from electron probe analysis. If the process is isochemical, we should be able to recover a reasonable proportion of minerals (the mode) from the whole rock data. The method does not prove that the process is truly isochemical, but it will be difficult to produce a reasonable mode if the sample has undergone severe alteration and has mineral compositions changed by adding significant sea water component. It should be emphasized that this method is simply an algebraic translation, it does not include any assumption on the initial mineral proportions. Any mineralogical constraint on this method would lead it toward a norm calculation, which is not the purpose here. To first order, if this calculation does not come up with a reasonable result, the idea of a isochemical process can be ruled out. Table 12 summarizes the results of whole rock proportions, both away from the vein, and in the vein segment. The calculation gives pretty optimal results, suggesting that it is possible that even though this sample has gone through severe alteration and serpentinization, chemically it is still very conservative. This means that we might still be able to extract meaningful magmatic processes data, such as elemental concentration ratios and Os isotopic ratios, from this sample.

7.3 A note regarding 'orphan Sr'

Snow (1993) analyzed another half of this boulder, and found anomalously high Sr isotopic ratios, in the magnetic fractions-the locations of the orphan strontium-87. My study, however, did not found any $^{87}Sr/^{86}Sr$ ratios higher than sea water, either in different sized magnetic separations or in different portions of the bulk rock (Table 2). It is possible that the 'orphan Sr-87' is locally concentrated in part of this boulder, but it is hard to envision that this rock is only partly affected by such an infiltration mechanism, without totally different permeability, porosity and mineralogy. The unusually high Sr isotopic ratios in ultramafic rocks from the sea floor is rarely documented in the literature, suggesting that it is an uncommon phenomenon. If the anomalously high $^{87}Sr/^{86}Sr$ could be substantiated, it represents an important type of infiltration process operating on the sea floor, and it provides a new way to look at alteration mechanisms. Unfortunately it has not been verified in this study, and it remains a mystery.

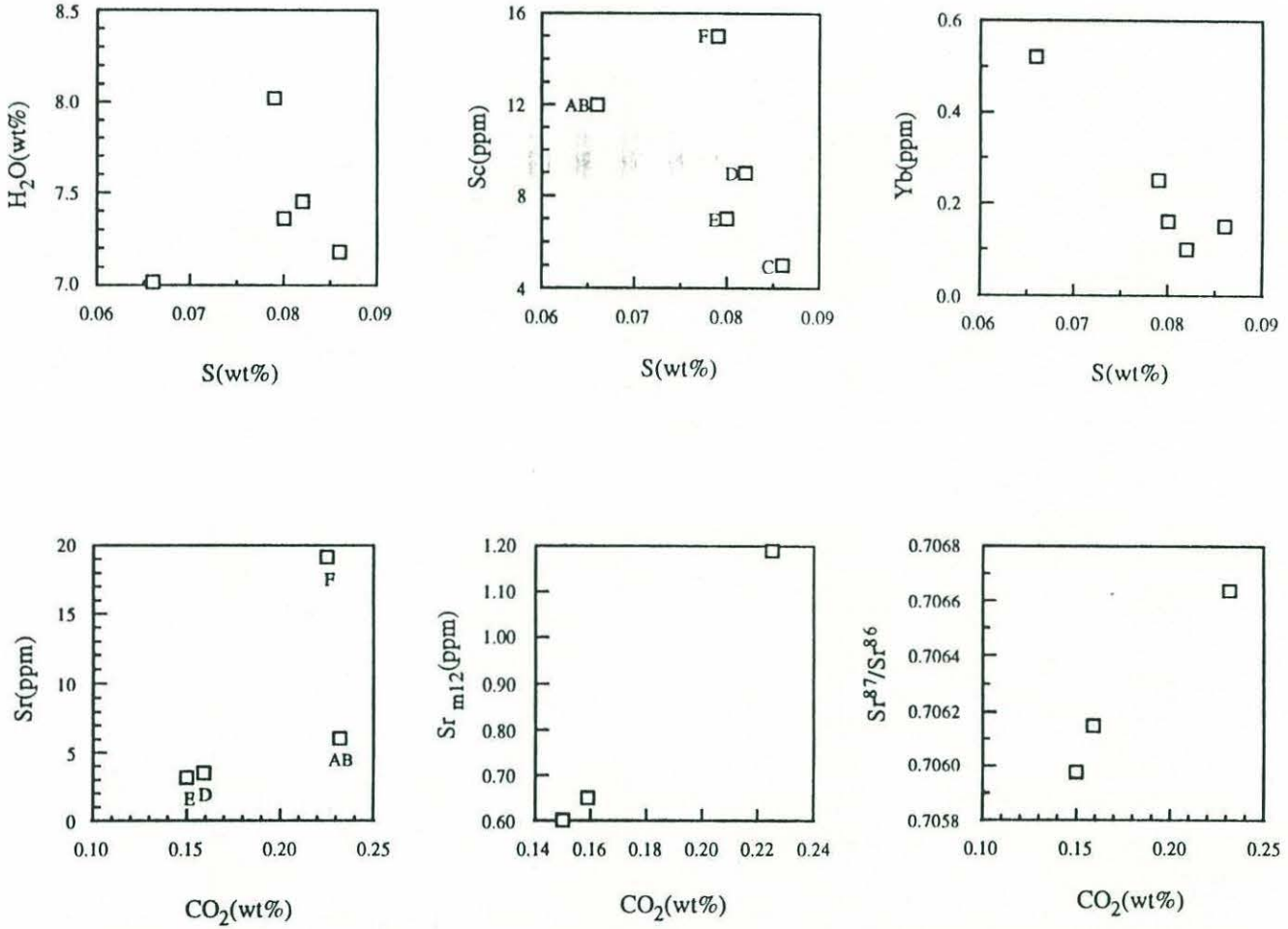

Fig 21: Elemental variation diagrams for sulfur (S, wt%) and CO2 (wt%) contents in whole rock analyses from RC 27-9-6-2. Data in the sulfur variation diagrams are from Slab 3, while the data in the CO2 variation diagrams are from Slab 1. Sr(m12) represents the Sr concentration in magnetic separation from 157 to 286 μm. Both Sr and Srm12 concentrations are from isotope dilution analysis.

Table 12: The composition of minerals and bulk rock fractions for the mass balance calculation.

RC27-9-6-2								
Input							**output**	
Whole rock excluding the vein								
	CPX	OPX	OL	SP	PLAG	Melt	Melt1	Melt2
SiO2	52.30	56.60	40.80	0.04	54.30	47.16	46.872	46.871
TiO2	0.19	0.09	0.00	0.18	0.00	0.04	0.048	0.048
Al2O3	4.84	2.50	0.01	37.09	30.40	1.56	1.588	1.598
Cr2O3	1.50	0.65	0.02	30.23	0.00	0.40	0.612	0.601
FeO	3.07	6.25	9.60	17.21	0.11	8.48	7.875	7.871
MnO	0.09	0.13	0.13	0.26	0.00	0.14	0.127	0.127
MgO	18.10	33.86	49.77	15.64	0.01	41.02	40.900	40.901
CaO	20.21	1.15	0.02	0.05	12.01	1.77	1.7[illegible]	[illegible]751
Na2O	0.63	0.02	0.00		5.03	0.15	0.048	0.053
K2O					0.08	0.01	0.000	0.000
P2O5								
NiO			0.33	0.28		0.26	0.179	0.179
Total	100.93	101.25	100.68	100.98	101.58	101.00	100.000	100.000
Phase proportions								
CPX							6.49	6.44
OPX							38.76	38.63
OL							53.89	51.01
SP							0.86	0.82
PLAG								0.09
Pyroxenite vein								
	CPX	OPX	OL	SP		Melt	Melt1	Melt2
	52.20	56.10	40.30	0.00		48.51	45.469	48.419
	0.26	0.09	0.00	0.28		0.08	0.116	0.104
	4.72	2.29	0.00	34.66		2.44	2.080	2.462
	1.61	0.62	0.03	32.68		0.63	0.707	1.037
	3.21	6.54	9.71	17.88		7.93	6.751	6.933
	0.12	0.18	0.14	0.18		0.13	0.130	0.149
	18.41	33.38	49.97	15.29		35.05	35.657	35.189
	19.41	0.81	0.03	0.00		5.50	8.695	5.451
	0.49	0.02	0.00	0.00		0.33	0.219	0.137
						0.03	0.000	0.000
			0.32	0.14		0.22	0.176	0.119
	100.43	100.03	100.50	101.11		100.84	100.000	100.000
Phase proportions								
CPX							44.90	26.68
OPX								35.18
OL							55.19	36.97
SP							-0.09	1.18
PLAG								

8. SULFIDES

Not much attention has been paid to the sulfides in abyssal peridotites, because of the intensive alteration and the very depleted nature of the rocks. Since sulfides are a major reservoir for Os in alpine-type peridotites, the sulfides in abyssal peridotites, especially possible residual sulfides retained in the suboceanic mantle after partial melting events, may play an important role in the retention of Os and other PGEs in the depleted mantle. Because of the altered nature of this sample and the immature analysis technique, this study is mainly based on a general interpretation of sulfide morphology and composition, and I try to compare these to previous studies of alpine peridotites. It is hard to tackle the details of sulfide genesis as related to the influence of serpentinization and the higher reaction rate of sulfides relative to silicates and oxides (Barton, 1970). Under segregation cooling or serpentinization, some sulfides would quickly rehomogenize any initial compositional zoning. The initial sulfide compositions may be overprinted by subsequent events. Many previous studies of both alpine-type peridotites and xenoliths from alkali basalts report the primary composition of sulfides based on sulfide inclusions in silicates and chrome spinel. These minerals act as barriers to protect the sulfides from subsequent alteration events. The sulfides which are enclosed in silicates are believed to represent trapped immiscible melts, enclosed by secondary grain growth of silicates in the upper mantle (Lorand 1987) after the melting event. On the other hand, the sulfides which occur as interstitial phases with curvilinear margins molded around silicates represent the solidification of immiscible sulfide liquids that are in equilibrium with the silicate phases (Garuti et al. 1984; Lorand 1987). The latter are much more likely to be affected by later metamorphic events.

8.1 Mineralogy and Occurrence

Sulfide analysis results are summarized in Table 13.

There are three types of sulfide occurrence noted in sample RC27-9-6-2. Corresponding to previous studies of alpine peridotites, sulfides occur as interstitial grains, as inclusions within pyroxenes (Lorand 1989a, 1989b, 1989c), and as single grains between the islands of olivine in the alteration veins. The interstitial sulfides are the most abundant sulfide occurrence (Type I) (Plate 7 and Plate 8). Normally they are trapped between two pyroxenes or pyroxene and spinel; fewer are found between pyroxene and olivine. The curvilinear margins between silicates and sulfides, roughly 120° along the grain boundaries in the triple junctions, indicate that they may be primary in origin. Interstitial sulfides are predominantly composed of nickel-iron-bearing sulfides. Because of the relatively broad beam analysis, the stoichiometry of the sulfides is not very precise, nor can the multi-

Table 13: Sulfide composition from thin sections 2B and 3B, RC 27-9-6-2.

2B	Cord		Ref		Wt%					At%					Ratios								
	X	Y	X	Y	Fe	Co	Ni	Cu	S	Fe	Co	Ni	Cu	S	Fe/Ni	Ni/Fe	Cu/Fe	Cu/Ni	Cu/S	Fe/S	Fe/(Fe+Cu)	Ni/S	Ni/(Fe+Ni+Cu)
s-1	67.31	56.86	100.72	102.02	32.34	0.27	19.94	15.63	31.81	26.79	0.21	15.72	11.38	45.90	1.705	0.587	0.425	0.724	0.248	0.584	0.702	0.342	0.292
s-2	68.29	51.65	105.93	103.00	43.66	0.48	21.60	1.71	32.55	35.54	0.37	16.73	1.23	46.14	2.125	0.471	0.035	0.073	0.027	0.770	0.967	0.362	0.313
s-3	67.99	47.02	110.56	102.70	41.64	0.56	27.14	0.16	30.50	34.34	0.44	21.29	0.12	43.81	1.613	0.620	0.003	0.005	0.003	0.784	0.997	0.486	0.382
s-4	66.77	37.84	119.75	101.48	30.23	0.51	20.03	15.02	34.21	24.67	0.39	15.55	10.77	48.62	1.587	0.630	0.437	0.693	0.222	0.507	0.696	0.320	0.305
s-5	65.60	54.53	103.05	100.31	29.53	0.65	37.59	0.03	32.20	24.20	0.50	29.31	0.02	45.97	0.826	1.211	0.001	0.001	0.000	0.526	0.999	0.637	0.547
s-6	64.42	57.71	99.87	99.13	28.64	0.19	6.35	30.60	34.21	23.60	0.15	4.98	22.16	49.10	4.740	0.211	0.939	4.451	0.451	0.481	0.516	0.101	0.098
s-7	63.17	45.75	111.83	97.88	35.52	0.53	30.94	0.04	32.97	28.90	0.41	23.95	0.03	46.72	1.207	0.829	0.001	0.001	0.001	0.619	0.999	0.513	0.453
s-8	62.30	45.68	111.91	97.02	31.73	0.08	13.81	20.44	33.93	26.01	0.06	10.77	14.73	48.44	2.415	0.414	0.566	1.367	0.304	0.537	0.638	0.222	0.209
s-9	63.34	45.09	112.49	98.06	30.05	0.40	36.92	0.08	32.54	24.57	0.31	28.71	0.05	46.35	0.856	1.169	0.002	0.002	0.001	0.530	0.998	0.620	0.538
s-15	62.01	44.92	112.66	96.72	1.16	3.06	61.99	0.09	33.70	0.95	2.38	48.41	0.07	48.19	0.020	50.717	0.071	0.001	0.001	0.020	0.934	1.005	0.979
s-16	61.79	45.96	111.62	96.51	30.63	0.00	0.05	35.37	33.96	25.33	0.00	0.04	25.71	48.92	679.13	0.001	1.015	689.28	0.526	0.518	0.496	0.001	0.001
s-17	61.74	45.94	111.64	96.45	31.80	0.17	13.89	18.97	35.17	25.83	0.13	10.74	13.54	49.76	2.406	0.416	0.524	1.261	0.272	0.519	0.656	0.216	0.214
s-18	61.68	46.02	111.56	96.40	29.17	0.00	0.10	37.19	33.55	24.23	0.00	0.08	27.15	48.54	302.13	0.003	1.120	338.53	0.559	0.499	0.472	0.002	0.002
s-10	63.53	33.97	123.61	98.25	33.90	0.44	31.30	0.50	33.86	27.45	0.34	24.11	0.36	47.75	1.138	0.878	0.013	0.015	0.007	0.575	0.987	0.505	0.464
s-11	61.60	33.52	124.06	96.31	34.74	0.71	27.07	3.74	33.75	28.19	0.54	20.89	2.67	47.70	1.349	0.741	0.095	0.128	0.056	0.591	0.914	0.438	0.404
s-12	61.13	33.58	124.00	95.84	38.19	0.51	28.17	0.08	33.06	31.02	0.39	21.76	0.05	46.77	1.425	0.702	0.002	0.002	0.001	0.663	0.998	0.465	0.412
s-13	61.56	34.89	122.69	96.27	27.82	0.16	8.65	28.85	24.51	22.87	0.13	6.76	20.84	49.40	3.381	0.296	0.911	3.081	0.422	0.463	0.523	0.137	0.134
s-19	61.39	50.50	107.08	96.11	38.08	0.81	27.81	0.36	32.94	30.96	0.62	21.51	0.26	46.65	1.439	0.695	0.008	0.012	0.006	0.664	0.992	0.461	0.408
s-20	60.38	56.40	101.18	95.09	49.55	0.26	12.10	3.43	34.67	39.74	0.20	9.23	2.42	48.42	4.304	0.232	0.061	0.262	0.050	0.821	0.943	0.191	0.180
s-21	60.69	55.51	102.07	95.40	27.62	0.50	37.40	0.11	32.37	22.63	0.39	30.70	0.08	46.20	0.737	1.357	0.003	0.003	0.002	0.490	0.997	0.665	0.575
s-22	60.68	55.50	102.08	95.40	31.45	0.32	21.78	14.15	32.31	25.95	0.25	17.09	10.26	46.44	1.518	0.659	0.395	0.600	0.221	0.559	0.717	0.368	0.321
s-23	57.81	30.87	126.71	92.52	30.47	0.04	0.26	34.58	34.65	25.08	0.03	0.21	25.01	49.67	121.93	0.008	0.997	121.60	0.504	0.505	0.501	0.004	0.004
s-24	57.81	30.87	126.71	92.53	39.39	0.50	26.47	0.38	33.26	31.95	0.38	20.42	0.27	46.99	1.564	0.639	0.008	0.013	0.006	0.680	0.992	0.435	0.388
s-25	56.64	29.53	128.05	91.35	4.06	0.24	2.47	68.55	24.68	3.69	0.21	2.14	54.83	39.13	1.728	0.579	14.843	25.643	1.401	0.094	0.063	0.055	0.035
s-26	57.28	32.36	125.22	91.99	1.22	0.23	62.69	0.55	35.32	0.99	0.17	48.46	0.39	49.99	0.021	48.753	0.392	0.008	0.008	0.020	0.719	0.969	0.972
s-27	57.17	32.80	124.78	91.88	0.32	0.13	64.64	0.13	33.78	1.09	0.10	50.45	0.09	48.28	0.022	46.452	0.086	0.002	0.002	0.022	0.920	1.045	0.977
s-28	56.08	38.08	119.50	90.79	3.52	2.24	59.86	0.03	34.35	2.87	1.74	46.51	0.02	48.86	0.062	16.187	0.008	0.000	0.000	0.059	0.992	0.952	0.941
s-29	54.92	35.70	121.88	89.63	3.10	14.34	35.29	5.76	41.51	2.43	10.65	26.30	3.96	56.66	0.092	10.841	1.633	0.151	0.070	0.043	0.380	0.464	0.805
s-30	54.93	35.67	121.91	89.64	2.14	6.39	41.60	8.28	41.59	1.68	4.75	31.04	5.71	56.82	0.054	18.485	3.398	0.184	0.100	0.030	0.227	0.546	0.808
s-31	53.14	53.42	104.17	87.85	18.22	1.12	39.92	4.75	35.99	14.68	0.85	30.59	3.37	50.50	0.480	2.084	0.229	0.110	0.067	0.291	0.814	0.606	0.629
s-32	53.01	37.73	119.85	87.73	1.09	0.04	63.00	0.53	35.34	0.89	0.03	48.69	0.38	50.01	0.018	54.756	0.426	0.008	0.008	0.018	0.701	0.973	0.975
s-33	53.35	58.86	98.72	88.06	37.44	0.23	29.47	0.06	32.80	30.47	0.18	22.82	0.04	46.50	1.335	0.749	0.001	0.002	0.001	0.655	0.999	0.491	0.428
s-34	53.06	27.08	130.50	87.77	15.57	0.01	0.23	57.62	26.58	13.81	0.00	0.19	44.92	41.08	72.221	0.014	3.253	234.93	1.094	0.336	0.235	0.005	0.003
s-35	52.36	40.54	117.05	87.07	24.14	0.67	41.65	0.08	33.47	19.66	0.51	32.27	0.06	47.50	0.609	1.641	0.003	0.002	0.001	0.414	0.997	0.679	0.621
s-36	50.67	29.10	128.49	85.38	27.82	0.64	21.25	15.66	34.63	22.67	0.49	16.47	11.21	49.15	1.376	0.727	0.495	0.681	0.228	0.461	0.669	0.335	0.327
s-37	49.41	25.98	131.60	84.12	34.49	0.63	30.88	0.05	33.94	27.90	0.48	23.76	0.04	47.82	1.174	0.852	0.001	0.002	0.001	0.583	0.999	0.497	0.460
s-39	48.74	44.57	113.01	83.46	40.23	0.14	20.11	0.02	39.49	31.36	0.11	14.91	0.02	53.61	2.103	0.476	0.000	0.001	0.000	0.585	1.000	0.278	0.322
s-40	47.46	43.97	113.61	82.17	30.47	0.02	0.25	34.30	34.97	25.02	0.01	0.19	24.75	50.02	130.13	0.008	0.989	128.72	0.495	0.500	0.503	0.004	0.004
s-41	45.74	46.48	111.11	80.46	30.10	0.55	36.41	0.15	32.79	24.57	0.42	28.27	0.11	46.63	0.869	1.151	0.004	0.004	0.002	0.527	0.996	0.606	0.534

Table 13: (Con'd) Sulfide composition from thin sections 2B, RC 27-9-6-2.																								
2B	Cord		Ref		Wt%						At%					Ratios								
	X	Y	X	Y	Fe	Co	Ni	Cu	S	Fe	Co	Ni	Cu	S	Fe/Ni	Ni/Fe	Cu/Fe	Cu/Ni	Cu/S	Fe/S	Fe/(Fe+Cu)	Ni/S	Ni/(Fe+Ni+Cu)
s-42	45.75	46.49	111.09	80.46	30.38	0.92	35.27	0.12	33.31	24.71	0.71	27.29	0.09	47.20	0.906	1.104	0.004	0.003	0.002	0.524	0.996	0.578	0.524
s-43	46.25	44.01	113.57	80.97	22.46	0.54	38.79	4.60	33.61	18.34	0.42	30.13	3.30	47.80	0.609	1.643	0.180	0.110	0.069	0.384	0.847	0.630	0.582
s-44	44.39	38.50	119.08	79.10	26.79	0.54	38.17	1.40	33.10	21.87	0.42	29.64	1.00	47.06	0.738	1.355	0.046	0.034	0.021	0.465	0.956	0.630	0.564
s-45	44.35	38.49	119.09	79.06	27.57	0.13	17.00	23.04	32.26	22.92	0.11	13.45	16.83	46.70	1.704	0.587	0.734	1.252	0.360	0.491	0.577	0.288	0.253
s-50	41.97	22.55	135.03	76.68	29.26	0.28	14.81	21.15	34.50	23.93	0.22	11.52	15.20	49.14	2.078	0.481	0.635	1.320	0.309	0.487	0.612	0.234	0.227
s-51	38.89	37.91	119.67	73.60	29.02	0.61	3.45	32.09	34.84	23.83	0.47	2.69	23.17	49.84	8.854	0.113	0.972	8.607	0.465	0.478	0.507	0.054	0.054
s-52	33.32	39.06	118.52	68.03	36.83	0.42	26.06	3.63	33.05	30.00	0.33	20.19	2.60	46.89	1.486	0.673	0.087	0.129	0.055	0.640	0.920	0.431	0.383
s-53	32.07	19.79	137.79	66.79	37.54	0.41	28.95	0.07	33.02	30.51	0.32	22.38	0.05	46.74	1.363	0.734	0.002	0.002	0.001	0.653	0.998	0.479	0.423
s-54	32.39	19.58	138.00	67.10	5.30	2.34	51.57	0.84	39.94	4.18	1.75	38.66	0.58	54.83	0.108	9.260	0.140	0.015	0.011	0.076	0.877	0.705	0.890
s-55	30.33	37.65	119.93	65.04	41.86	0.32	24.56	0.00	33.26	33.91	0.25	18.92	0.00	46.92	1.792	0.558	0.000	0.000	0.000	0.723	1.000	0.403	0.358
s-56	29.57	38.30	119.29	64.28	64.40	0.00	0.03	0.00	35.57	50.96	0.00	0.02	0.00	49.02	2600.0	0.000	0.000	0.000	0.000	1.040	1.000	0.000	0.000
s-57	28.32	37.41	120.17	63.03	35.13	0.55	24.98	4.78	34.55	28.38	0.42	19.20	3.39	48.61	1.478	0.676	0.120	0.177	0.070	0.584	0.893	0.395	0.377
s-58	28.60	17.85	139.73	63.31	30.11	0.00	0.20	34.82	34.87	24.76	0.00	0.15	25.16	49.93	161.8	0.006	1.016	164.5	0.504	0.496	0.496	0.003	0.003
s-59	26.85	39.16	118.42	61.56	44.13	0.36	21.00	0.25	34.26	35.49	0.28	16.07	0.18	47.99	2.209	0.453	0.005	0.011	0.004	0.740	0.995	0.335	0.311
s-60	26.86	39.16	118.42	61.58	33.16	0.52	29.49	0.70	36.13	26.47	0.39	22.39	0.49	50.25	1.182	0.846	0.019	0.022	0.010	0.527	0.982	0.446	0.454
s-61	26.76	39.18	118.40	61.47	26.71	0.00	0.11	41.49	31.68	22.55	0.00	0.09	30.78	46.58	245.4	0.004	1.365	335.0	0.661	0.484	0.423	0.002	0.002
s-62	26.73	39.15	118.43	61.44	38.53	0.36	27.55	0.08	33.48	31.21	0.27	21.22	0.06	47.24	1.470	0.680	0.002	0.003	0.001	0.661	0.998	0.449	0.404
s-63	27.38	36.41	121.17	62.10	34.70	1.15	25.85	5.27	33.04	28.32	0.89	20.06	3.78	46.96	1.411	0.709	0.133	0.188	0.080	0.603	0.882	0.427	0.385
s-64	25.14	31.57	126.01	59.86	27.80	0.11	9.03	28.59	34.48	22.85	0.09	7.06	20.65	49.36	3.237	0.309	0.904	2.926	0.418	0.463	0.525	0.143	0.140
s-65	25.18	31.60	125.98	59.89	34.30	0.03	2.75	26.51	36.41	27.74	0.03	2.11	18.84	51.28	13.120	0.076	0.679	8.910	0.367	0.541	0.596	0.041	0.043
s-66	25.19	31.63	125.95	59.90	30.19	0.16	7.39	28.96	33.29	24.99	0.13	5.82	21.07	48.00	4.294	0.233	0.843	3.620	0.439	0.521	0.543	0.121	0.112
s-67	25.16	31.64	125.94	59.88	21.90	0.68	44.97	0.66	31.98	18.06	0.53	35.27	0.48	45.67	0.512	1.953	0.026	0.014	0.010	0.395	0.974	0.772	0.656
s-68	24.97	31.45	126.14	59.68	30.10	0.00	0.00	34.58	35.31	24.68	0.00	0.00	24.91	50.41		0.000	1.010		0.494	0.489	0.498	0.000	0.000
s-69	24.98	31.29	126.29	59.69	25.95	0.00	10.02	29.40	34.63	21.33	0.00	7.83	21.24	49.59	2.723	0.367	0.996	2.711	0.428	0.430	0.501	0.158	0.155
s-70	24.83	31.63	125.95	59.54	33.70	0.23	27.35	0.09	38.64	26.47	0.17	20.43	0.06	52.87	1.295	0.772	0.002	0.003	0.001	0.501	0.998	0.386	0.435
s-71	24.77	31.61	125.97	59.49	26.71	0.33	34.37	4.68	33.91	21.73	0.25	26.60	3.35	48.06	0.817	1.224	0.154	0.126	0.070	0.452	0.867	0.553	0.515
s-72	24.54	31.62	125.96	59.25	30.46	0.03	0.08	34.23	35.20	24.97	0.02	0.06	24.67	50.27	389.0	0.003	0.988	384.2	0.491	0.497	0.503	0.001	0.001
s-74	23.98	26.15	131.44	58.69	32.88	0.47	29.48	0.05	37.12	26.08	0.35	22.25	0.04	51.28	1.172	0.853	0.001	0.002	0.001	0.509	0.999	0.434	0.460
s-75	23.97	26.17	131.41	58.68	31.07	0.51	35.17	0.05	33.21	25.28	0.39	27.22	0.04	47.07	0.929	1.077	0.001	0.001	0.001	0.537	0.999	0.578	0.518
s-77	17.28	43.17	114.41	52.00	40.70	0.44	25.16	0.14	33.56	32.93	0.34	19.36	0.10	47.28	1.701	0.588	0.003	0.005	0.002	0.696	0.997	0.409	0.370
s-78	17.26	43.23	114.35	51.98	32.21	0.24	25.06	7.82	34.68	26.07	0.18	19.29	5.56	48.89	1.351	0.740	0.213	0.288	0.114	0.533	0.824	0.395	0.379
s-79	14.34	27.41	130.17	49.05	10.66	0.00	0.01	63.35	25.98	9.55	0.00	0.01	49.90	40.54	1005.3	0.001	5.225	5252.1	1.231	0.236	0.161	0.000	0.000
s-80	14.36	27.39	130.19	49.08	29.36	0.00	4.73	31.57	34.34	24.18	0.00	3.70	22.85	49.27	6.528	0.153	0.945	6.169	0.464	0.491	0.514	0.075	0.073
s-81	14.36	27.59	129.99	49.07	37.80	0.32	27.93	0.59	33.36	30.66	0.25	21.55	0.42	47.12	1.423	0.703	0.014	0.020	0.009	0.651	0.986	0.457	0.409
s-82	12.03	55.54	102.04	46.74	24.59	0.26	9.06	30.04	36.05	20.05	0.20	7.03	21.53	51.19	2.853	0.350	1.074	3.063	0.421	0.392	0.482	0.137	0.145
s-83	12.05	55.55	102.03	46.76	23.73	0.33	17.87	23.53	34.55	19.46	0.25	13.95	16.96	49.37	1.396	0.716	0.871	1.216	0.344	0.394	0.534	0.282	0.277
s-85	9.25	24.56	133.02	43.96	30.37	0.04	0.17	34.39	35.04	24.93	0.03	0.13	24.81	50.10	187.6	0.005	0.995	186.7	0.495	0.498	0.501	0.003	0.003
s-86	9.23	24.55	133.03	43.94	39.11	0.18	21.79	0.04	38.89	30.61	0.13	16.22	0.03	53.02	1.887	0.530	0.001	0.002	0.000	0.577	0.999	0.306	0.346
s-87	9.19	24.56	133.02	43.90	34.42	0.42	31.98	0.14	33.04	28.00	0.32	24.75	0.10	46.82	1.131	0.884	0.004	0.004	0.002	0.598	0.996	0.529	0.468

Table 13: (Con'd) Sulfide composition from thin section 3B, RC 27-9-6-2.

3B	Cord		Ref		Wt%					At%						Ratios								
	X	Y	X	Y	Fe	Co	Ni	Cu	S	Fe	Co	Ni	Cu	S	Fe/Ni	Ni/Fe	Cu/Fe	Cu/Ni	Cu/S	Fe/S	Fe/(Fe+Cu)	Ni/S	Ni/(Fe+Ni+Cu)
s-1	69.93	62.29	44.00	37.71	23.89	0.08	12.95	27.33	35.74	19.49	0.06	10.05	19.60	50.79	1.939	0.516	1.006	1.950	0.386	0.384	0.499	0.198	0.205
s-3	69.92	62.27	44.02	37.71	45.28	0.41	23.22	5.97	25.12	38.78	0.33	18.91	4.50	37.47	2.051	0.488	0.116	0.238	0.120	1.035	0.896	0.505	0.304
s-4	70.22	62.21	44.09	38.00	21.38	0.00	0.28	46.62	31.72	18.14	0.00	0.22	34.76	46.88	81.701	0.012	1.917	156.6	0.742	0.387	0.343	0.005	0.004
s-5	69.90	61.93	44.36	37.69	29.78	0.02	0.39	34.79	35.02	24.46	0.02	0.30	25.11	50.11	80.326	0.012	1.027	82.472	0.501	0.488	0.493	0.006	0.006
s-7	69.96	61.83	44.46	37.75	10.99	0.35	53.68	0.20	34.77	8.93	0.27	41.47	0.14	49.18	0.215	4.644	0.016	0.003	0.003	0.182	0.984	0.843	0.821
s-9	69.03	58.34	47.96	36.81	39.61	0.68	24.30	0.23	35.18	31.73	0.52	18.52	0.16	49.08	1.713	0.584	0.005	0.009	0.003	0.646	0.995	0.377	0.367
s-10	69.35	57.81	48.48	37.14	31.74	0.34	11.80	22.07	34.05	26.02	0.26	9.21	15.90	48.62	2.827	0.354	0.611	1.727	0.327	0.535	0.621	0.189	0.180
s-11	69.35	57.81	48.48	37.14	31.77	0.33	11.51	22.62	33.76	26.10	0.26	9.00	16.33	48.31	2.902	0.345	0.626	1.816	0.338	0.540	0.615	0.186	0.175
s-11-2	68.13	57.83	48.47	35.91	35.91	0.44	27.32	0.46	35.86	28.69	0.33	20.76	0.33	49.90	1.382	0.724	0.011	0.016	0.007	0.575	0.989	0.416	0.417
s-12	67.79	57.53	48.76	35.58	44.50	0.27	20.25	0.12	34.86	35.64	0.21	15.43	0.08	48.64	2.310	0.433	0.002	0.005	0.002	0.733	0.998	0.317	0.302
s-13	67.81	57.51	48.79	35.59	62.65	0.00	0.08	0.02	37.24	49.09	0.00	0.06	0.02	50.83	827.9	0.001	0.000	0.258	0.000	0.966	1.000	0.001	0.001
s-14-1	67.88	57.29	49.00	35.67	44.99	0.44	18.43	0.10	36.05	35.76	0.33	13.93	0.07	49.91	2.566	0.390	0.002	0.005	0.001	0.716	0.998	0.279	0.280
s-14-2	67.90	57.29	49.00	35.68	45.29	0.35	18.15	0.04	36.18	35.96	0.26	13.71	0.03	50.04	2.624	0.381	0.001	0.002	0.001	0.719	0.999	0.274	0.276
s-15	67.95	57.30	48.99	35.74	32.32	0.20	20.03	13.40	34.05	26.35	0.15	15.54	9.60	48.35	1.696	0.590	0.364	0.618	0.199	0.545	0.733	0.321	0.302
s-16	67.97	57.29	49.00	35.75	29.76	0.06	0.36	35.07	34.75	24.49	0.05	0.28	25.37	49.82	86.539	0.012	1.036	89.630	0.509	0.492	0.491	0.006	0.006
s-17	68.04	57.26	49.04	35.83	42.32	0.46	22.99	0.20	34.04	34.11	0.35	17.62	0.14	47.78	1.935	0.517	0.004	0.008	0.003	0.714	0.996	0.369	0.340
s-18	68.10	57.24	49.05	35.88	36.20	0.65	17.38	5.57	40.21	28.22	0.48	12.89	3.81	54.60	2.190	0.457	0.135	0.296	0.070	0.517	0.881	0.236	0.287
s-19	68.61	57.43	48.87	36.40	25.03	0.20	40.98	0.05	33.74	20.35	0.15	31.69	0.03	47.77	0.642	1.557	0.002	0.001	0.001	0.426	0.998	0.663	0.609
s-20	67.07	43.99	62.30	34.85	22.47	0.48	43.10	0.11	33.85	18.27	0.37	33.34	0.08	47.95	0.548	1.825	0.004	0.002	0.002	0.381	0.996	0.695	0.645
s-21	67.03	45.63	60.66	34.82	12.33	1.21	35.24	14.42	36.79	9.97	0.93	27.09	10.24	51.78	0.368	2.718	1.028	0.378	0.198	0.192	0.493	0.523	0.573
s-22	66.45	46.29	60.01	34.23	29.31	0.00	0.20	34.76	35.63	23.98	0.00	0.23	25.00	50.78	102.4	0.010	1.042	106.7	0.492	0.472	0.490	0.005	0.005
s-23	66.50	46.31	59.98	34.29	21.33	0.49	44.39	0.11	33.68	17.37	0.38	34.40	0.08	47.78	0.505	1.980	0.005	0.002	0.002	0.364	0.995	0.720	0.663
s-24	66.73	47.27	59.02	34.51	29.06	0.34	29.74	0.00	40.86	22.55	0.25	21.96	0.00	55.24	1.027	0.974	0.000	0.000	0.000	0.408	1.000	0.397	0.493
s-25	64.14	64.94	41.35	31.93	29.89	0.37	27.81	0.66	41.28	23.14	0.27	20.48	0.45	55.66	1.130	0.885	0.020	0.022	0.008	0.416	0.981	0.368	0.465
s-26	63.77	62.14	44.16	31.55	33.20	0.33	22.59	9.46	34.41	26.94	0.25	17.44	6.75	48.63	1.545	0.647	0.250	0.387	0.139	0.554	0.800	0.359	0.341
s-27	63.07	61.26	45.03	30.85	35.86	0.39	29.22	0.88	33.65	29.06	0.30	22.52	0.63	47.49	1.290	0.775	0.022	0.028	0.013	0.612	0.979	0.474	0.431
s-28	63.92	60.03	46.27	31.71	61.61	0.00	0.06	0.32	38.01	48.07	0.00	0.05	0.22	51.66	999.5	0.001	0.005	4.518	0.004	0.931	0.996	0.001	0.001
s-29	63.01	59.02	47.28	30.79	32.11	0.29	22.97	11.06	33.57	26.23	0.23	17.85	7.94	47.76	1.470	0.680	0.303	0.445	0.166	0.549	0.768	0.374	0.343
s-31	63.73	52.33	53.96	31.52	25.13	0.51	30.99	0.19	43.17	19.26	0.37	22.60	0.13	57.64	0.853	1.173	0.007	0.006	0.002	0.334	0.993	0.392	0.538
s-32	65.36	20.77	85.52	33.15	39.11	0.29	26.66	0.00	33.94	31.57	0.22	20.48	0.00	47.73	1.542	0.649	0.000	0.000	0.000	0.662	1.000	0.429	0.393

Table 13: (Con'd) Sulfide composition from thin section 3B, RC 27-9-6-2.																							
3B	Cord		Ref		Wt%					At%					Ratios								
	X	Y	X	Y	Fe	Co	Ni	Cu	S	Fe	Co	Ni	Cu	S	Fe/Ni	Ni/Fe	Cu/Fe	Cu/Ni	Cu/S	Fe/S	Fe/(Fe+Cu)	Ni/S	Ni/(Fe+Ni+Cu)
s-33	59.93	25.92	80.37	27.71	31.79	0.05	3.31	31.19	33.66	26.27	0.04	2.60	22.65	48.44	10.092	0.099	0.862	8.702	0.468	0.542	0.537	0.054	0.051
s-34	59.80	25.90	80.39	27.59	35.47	0.33	29.33	1.78	33.09	28.86	0.25	22.70	1.28	46.90	1.271	0.787	0.044	0.056	0.027	0.615	0.958	0.484	0.430
s-35	60.45	50.18	56.11	28.23	59.67	0.00	0.05	0.32	39.96	46.04	0.00	0.04	0.22	53.71	1214.8	0.001	0.005	5.728	0.004	0.857	0.995	0.001	0.001
s-38	61.51	53.17	53.12	29.30	21.04	0.31	20.00	21.24	37.42	16.94	0.24	15.32	15.03	52.48	1.106	0.904	0.887	0.981	0.286	0.323	0.530	0.292	0.324
s-39	58.37	49.16	57.13	26.16	52.43	0.49	24.09	0.09	22.91	45.28	0.40	19.79	0.07	34.46	2.288	0.437	0.002	0.004	0.002	1.314	0.998	0.574	0.304
s-40	57.52	48.71	57.58	25.30	44.36	0.30	20.48	0.09	34.77	35.55	0.23	15.61	0.06	48.54	2.277	0.439	0.002	0.004	0.001	0.732	0.998	0.322	0.305
s-42	56.15	48.03	58.26	23.93	35.26	0.29	25.45	4.54	34.46	28.49	0.22	19.56	3.22	48.50	1.456	0.687	0.113	0.165	0.066	0.587	0.898	0.403	0.382
s-44	54.82	48.00	58.29	22.60	42.81	0.35	23.29	0.14	33.41	34.63	0.27	17.92	0.10	47.08	1.933	0.517	0.003	0.006	0.002	0.736	0.997	0.381	0.340
s-45	58.87	45.54	60.75	26.66	12.19	0.01	0.12	60.20	27.48	10.78	0.01	0.10	46.78	42.33	110.4	0.009	4.341	479.3	1.105	0.255	0.187	0.002	0.002
s-46	58.85	45.56	60.73	26.63	36.79	0.09	13.93	23.28	25.90	31.80	0.07	11.45	17.68	38.99	2.777	0.360	0.556	1.544	0.454	0.816	0.643	0.294	0.188
s-48	58.73	45.67	60.63	26.52	30.25	0.28	34.94	0.47	34.06	24.50	0.21	26.92	0.34	48.04	0.910	1.099	0.014	0.012	0.007	0.510	0.986	0.560	0.520
s-53	52.02	26.29	80.01	19.80	29.73	0.00	0.18	34.32	35.76	24.30	0.00	0.14	24.65	50.90	171.9	0.006	1.015	174.4	0.484	0.477	0.496	0.003	0.003
s-54	50.16	32.23	74.06	17.94	37.78	0.34	27.17	0.58	34.14	30.49	0.26	20.86	0.41	47.99	1.462	0.684	0.013	0.020	0.008	0.635	0.987	0.435	0.403
s-55	49.72	32.79	73.51	17.51	25.31	0.00	0.08	40.91	33.70	21.08	0.00	0.06	29.95	48.90	349.6	0.003	1.421	496.7	0.612	0.431	0.413	0.001	0.001
s-56	51.17	34.50	71.80	18.96	35.33	0.38	28.51	2.12	33.65	28.66	0.29	22.00	1.51	47.54	1.303	0.768	0.053	0.069	0.032	0.603	0.950	0.463	0.422
s-57	50.47	34.87	71.43	18.26	26.37	0.18	40.13	0.13	33.18	21.51	0.14	31.13	0.09	47.13	0.691	1.447	0.004	0.003	0.002	0.456	0.996	0.661	0.590
s-59	50.43	55.33	50.96	18.21	51.12	0.03	9.02	0.04	39.78	39.61	0.03	6.65	0.03	53.68	5.956	0.168	0.001	0.004	0.001	0.738	0.999	0.124	0.144
s-60	50.40	55.27	51.02	18.18	29.94	0.00	1.86	34.34	33.86	24.77	0.00	1.47	24.97	48.79	16.890	0.059	1.008	17.030	0.512	0.508	0.498	0.030	0.029
s-62	50.32	55.24	51.06	18.11	31.89	0.00	0.86	36.12	31.14	26.87	0.00	0.69	26.75	45.70	38.910	0.026	0.996	38.735	0.585	0.588	0.501	0.015	0.013
s-63	50.31	55.17	51.13	18.10	52.53	0.09	7.37	0.01	40.01	40.61	0.07	5.42	0.01	53.89	7.490	0.134	0.000	0.001	0.000	0.754	1.000	0.101	0.118
s-64	50.12	55.42	50.87	17.91	62.58	0.00	0.07	0.11	37.24	49.05	0.00	0.05	0.08	50.83	973.1	0.001	0.002	1.494	0.001	0.965	0.998	0.001	0.001
s-66	50.05	55.45	50.84	17.84	27.24	0.15	39.17	0.00	33.45	22.17	0.11	30.32	0.00	47.40	0.731	1.368	0.000	0.000	0.000	0.468	1.000	0.640	0.578
s-68	22.38	47.55	58.75	-9.83	32.33	1.87	32.06	0.02	33.72	26.21	1.44	24.73	0.01	47.61	1.060	0.943	0.000	0.001	0.000	0.551	1.000	0.519	0.485
s-69	19.21	42.70	63.60	-13.01	27.26	0.04	8.42	29.18	35.09	22.33	0.03	6.56	21.01	50.07	3.403	0.294	0.941	3.202	0.420	0.446	0.515	0.131	0.131
s-71	18.08	32.09	74.21	-14.14	12.74	0.14	53.48	0.09	33.55	10.42	0.11	41.61	0.07	47.80	0.250	3.994	0.006	0.002	0.001	0.218	0.994	0.870	0.799
s-72	13.99	60.93	45.36	-18.23	30.39	1.20	26.22	0.06	42.13	23.39	0.88	19.20	0.04	56.49	1.218	0.821	0.002	0.002	0.001	0.414	0.998	0.340	0.450
s-75	13.16	26.56	79.74	-19.06	29.16	0.00	0.19	35.03	35.62	23.87	0.00	0.15	25.20	50.79	163.3	0.006	1.056	172.4	0.496	0.470	0.486	0.003	0.003
s-76	9.36	59.02	47.27	-22.85	20.87	0.46	44.62	0.28	33.77	17.00	0.36	34.56	0.20	47.89	0.492	2.033	0.012	0.006	0.004	0.355	0.989	0.722	0.668

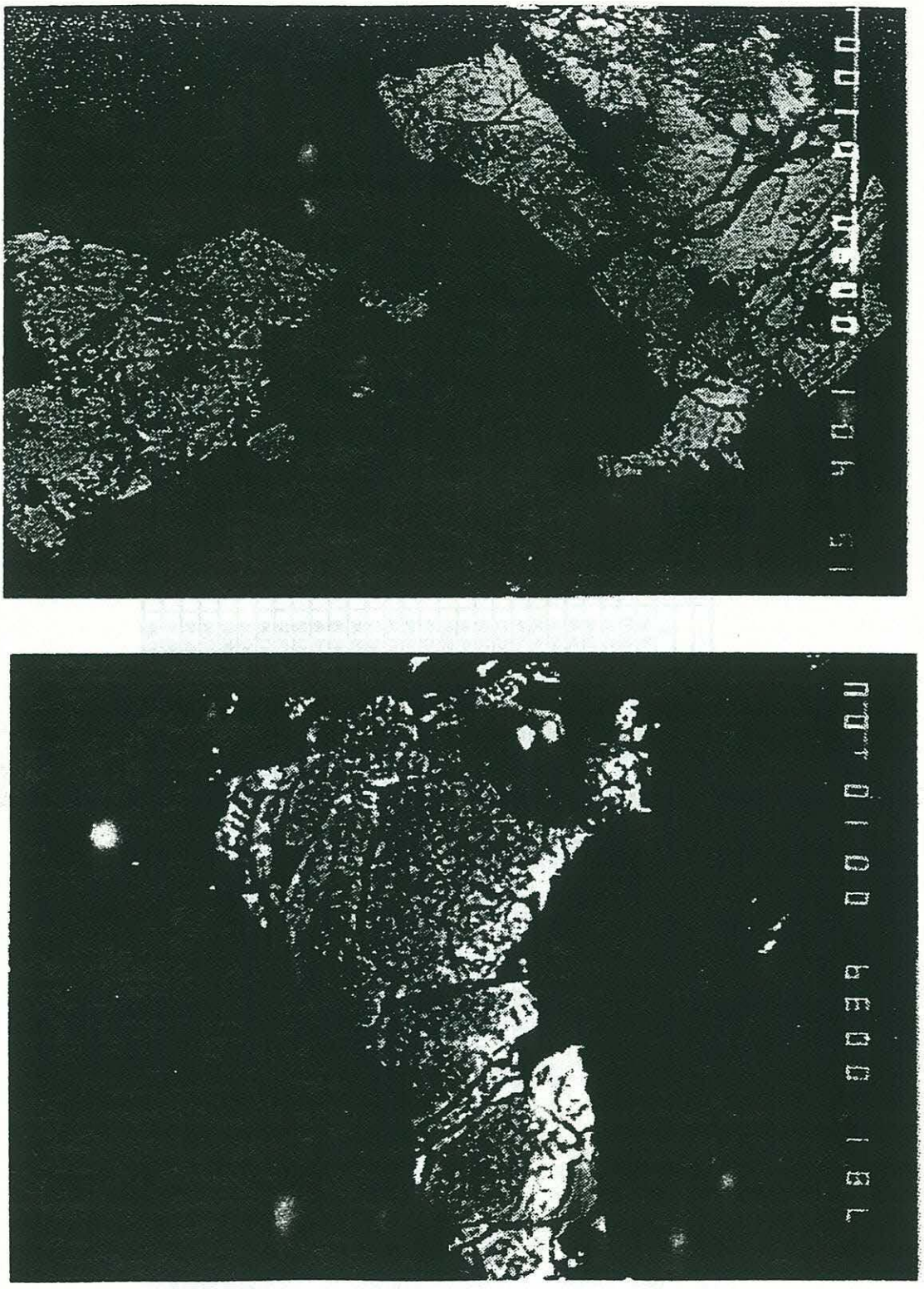

Plate 8: Type I sulfides on grain boundaries between pyroxene and spinel.

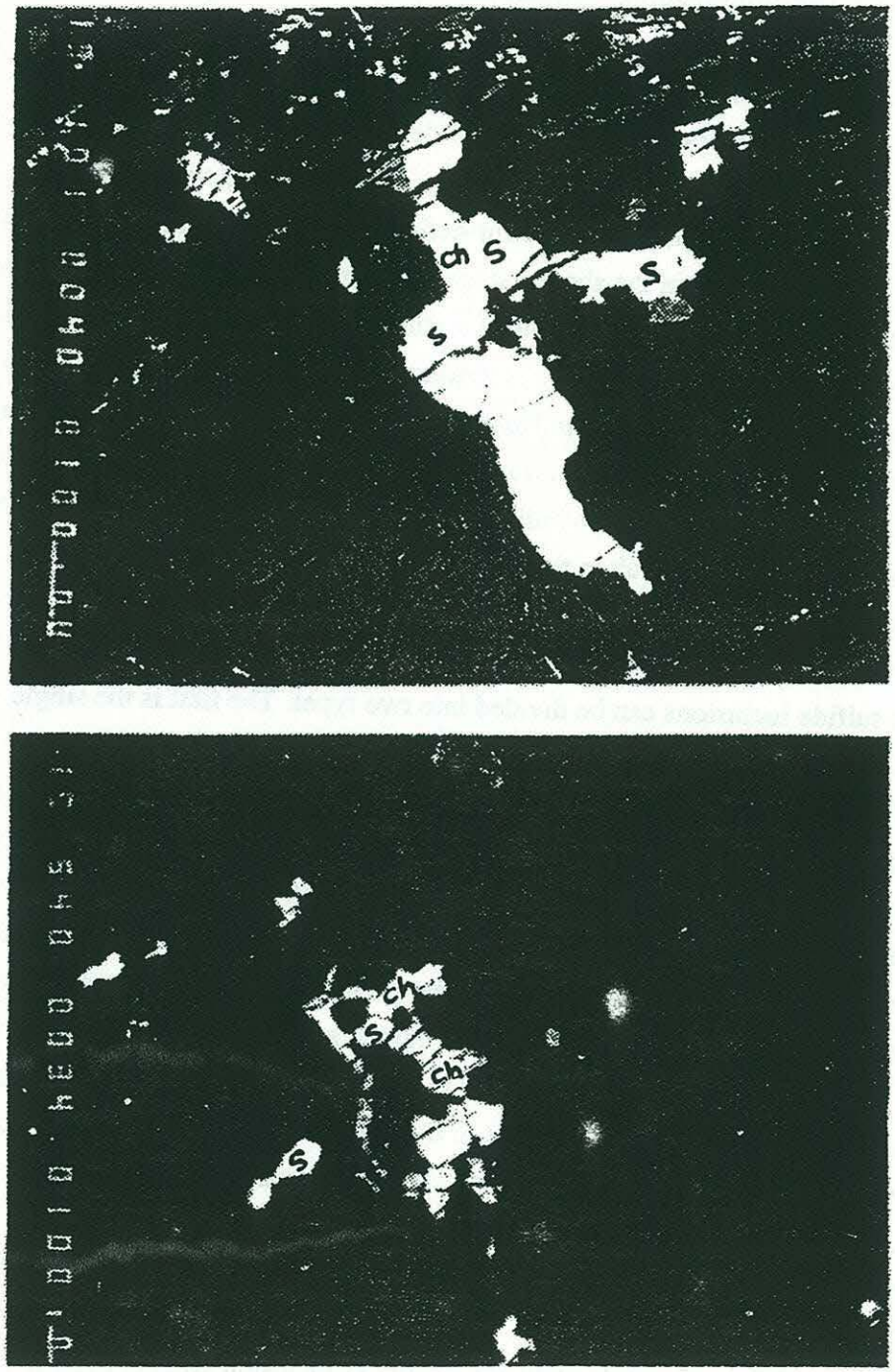

Plate 7: Type I sulfides on grain boundaries between pyroxenes.

mineralogy of the sulfides within one interstitial grain be detected. In order to avoid confusion about the origin of the sulfides, terminology that describes the chemical compositions of the sulfides is used in the following paragraphs instead of phase names. The term 'nickel-iron-bearing' sulfides is used to refer to hexagonal pyrrhotite (po), sulfur-rich or -deficient pentlandite (pn) (or nickel-bearing pyrrhotite), stoichiometric pentlandite, low temperature nickel-bearing hexagonal pyrrhotite, and monoclinic pyrrhotite with nickel. The name 'copper-iron-bearing sulfides' refers to chalcopyrite (cp), and a few low temperature copper sulfides such as bornite (Cu_5FeS_4). The pure iron or nickel sulfides phases such as troilite (tr, FeS), or sulfur-deficient marcasite (mk) and heazlewoodite (hz, Ni_3S_2) are not included in the above categories even though they contain minor amounts of nickel and iron, respectively. In terms of texture, the interstitial sulfides are often associated with hydrothermal alteration veins. Secondary products such as iron oxides and occasionally millerite (NiS) and polydymite (Ni_3S_4) are observed in the cleavage planes or at the margins of the host sulfides. Some of the nickel-iron-bearing sulfides also contain minor copper and trace cobalt in bulk analyses. The more secondary product the sulfides contain, the higher the cobalt in the bulk analysis. Some copper-iron sulfides, such as bornite, are also found associated with nickel-iron-bearing sulfides, while pyrite is rare in this study.

The sulfide inclusions can be divided into two types. The first is the single sulfide inclusion which is enclosed and isolated in pyroxenes, especially in clinopyroxene (Type II-1) (Plate 9). These are oval or rectangular in shape, such as those reported in clinopyroxene megacrysts (Lorand 1989c). No single inclusions have been found in olivine or spinel. It is quite possible that some of the sulfide in olivine has been severely altered to iron oxides. Most of the single inclusions are developed along cleavage planes or exsolution planes of the host clinopyroxene. Usually the sulfides occur in groups either in the neighborhood of exsolution planes, or next to some large sulfides grains which are often open to the alteration veins around the silicate grain boundary. The single sulfide inclusions are often pretty small, most of them are less being than 10 μm in diameter. As a result, it is hard to do a satisfactory analysis on such small scales. Qualitatively, similar to the interstitial sulfides, the single sulfide inclusions are dominantly nickel-iron-bearing sulfides, but copper-iron-bearing sulfides and some low temperature sulfides such as heazlewoodite are also common.

The second type of sulfide inclusion occurs as inclusion arrays (Type II-2) (Plate 10). The arrays are either sub parallel to the pyroxene exsolution planes, or pass through the textural lineations of the host pyroxenes. These inclusion arrays are often found in big orthopyroxene grains. The size for each single inclusion in the arrays is very small, usually

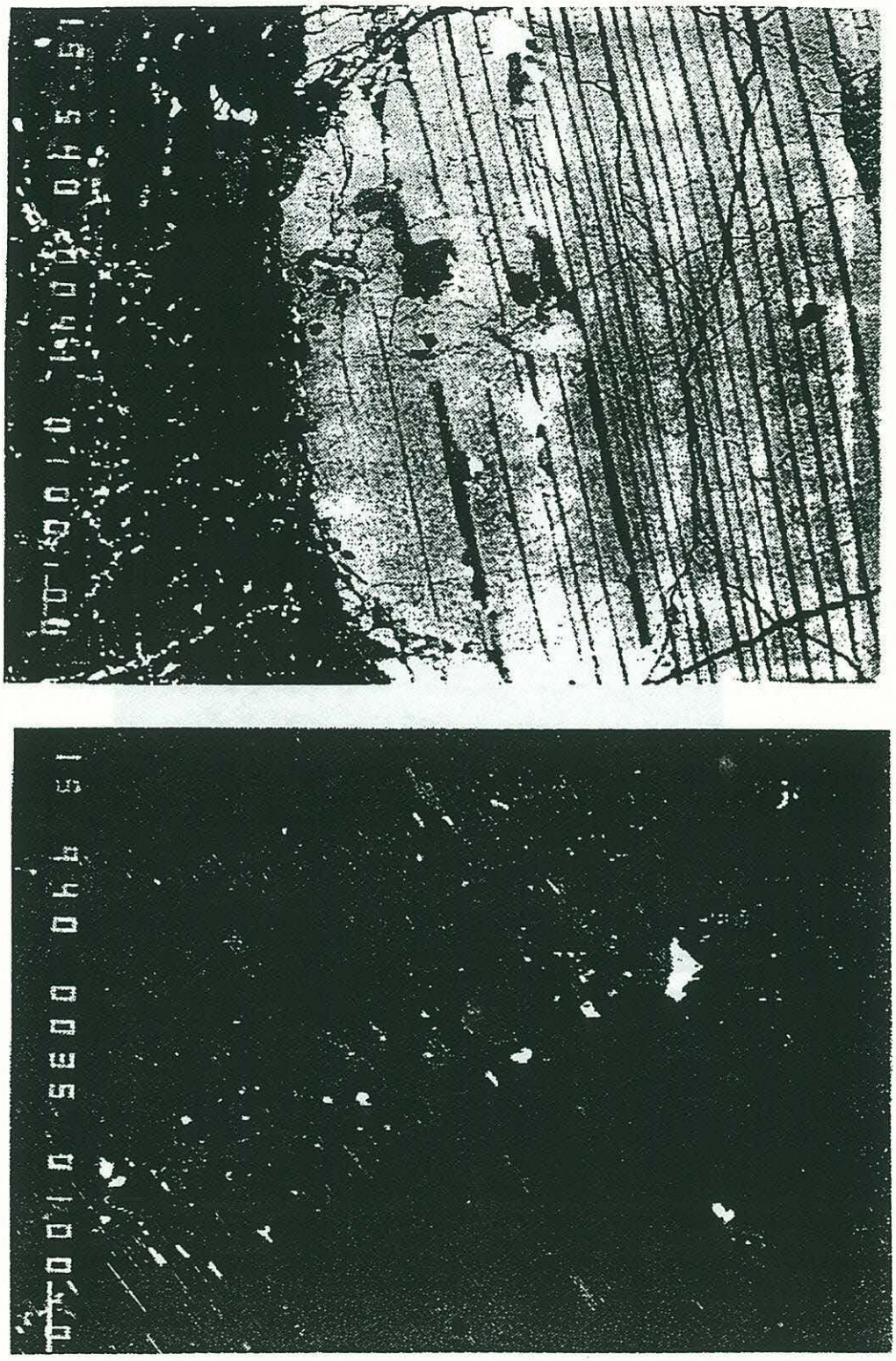

Plate 9: Type II-1 sulfides as inclusions in big pyroxene grains.

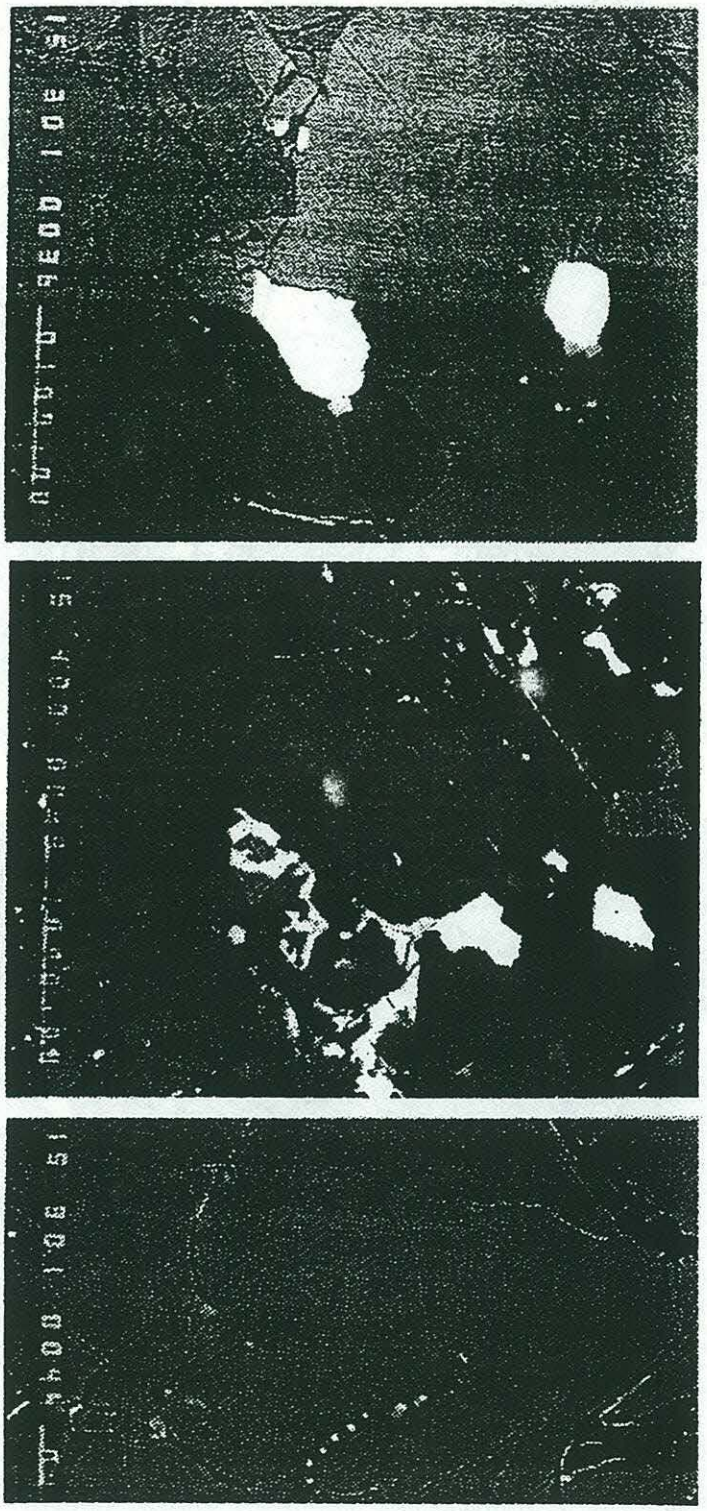

Plate 10: Type II-2 sulfides as inclusions in pyroxene grains.

ranging between 2 μm to less than 1 μm. This makes the analysis even more difficult. EDS scans indicate that the sulfide composition for each single sulfide grain of the array is variable. It is possible that all kinds of sulfides coexist in one array. Some of the arrays are texturally connected to the alteration products in the cleavage planes of the host pyroxene, and some are well away from any signs of alteration, although the latter are rare. It seems that the sulfides closer to the altered cleavages have a higher content of iron and/or nickel, but in general there is no obvious compositional relationship with proximity to alteration planes. Other than the interstitial sulfides and the large inclusion sulfides, it appears that the inclusions in the arrays are pretty mono-mineralic.

The third type of sulfide occurrence is in alteration veins between the olivine islands (Type III) (Plate 11). The shape is often irregular. Electron probe analysis shows that most of these are nickel-iron-bearing sulfides, and they have been altered to iron oxides along the margins and the cleavages. The relationships between the three types of sulfides and their mineralogy are summarized in Table 14 for all the grains that have been qualitatively analyzed. It should be remembered that all of the analyses were conducted in only two thin sections (2B and 3B). The initial idea for doing the analyses was to search for the variability of sulfide phases and their occurrences, in relation to possible primary or secondary origins. Most of the nickel-iron-bearing sulfides and some of the copper-iron-bearing sulfides were skipped for the qualitative analyses and only an EDS identification scan was conducted. These skipped sulfides constitute the majority of sulfides which are not included in Table 14. Thus, the relative proportion of the sulfide phases should not be considered seriously in terms of the compositional differences between the occurrence of the sulfides, and their spatial relationships. It should be pointed out that I did not find copper-iron-bearing sulfides in the clinopyroxenite vein, and this is likely to be statistically significant in a comparison between the vein and the rest of the sample.

8.2 A Note Regarding the Effect of Serpentinization on Sulfides

Garuti et al. (1984) reported that pentlandite can be altered to heazlewoodite and magnetite during low-temperature serpentinization. Pyrite can be altered to secondary pyrrhotite, accompanied by the reaction of mackinawite after pentlandite when the serpentinization is complete (Lorand, 1989a). There are at least two reasons for the high abundance of nickel-bearing sulfides in this sample. First, these sulfides represent exsolutions from the sulfur-poor end of the monosulfide solid solution (MSS). Thus, the predominant nickel-bearing sulfide component results from the residual nature of this sample. Secondly, the sulfide assemblages have undergone sulfur metasomatism during serpentinization, with the sulfur fugacity buffered by the assemblage itself (Eckstrand,

Plate 11: Type III sulfides in the serpentine vein (black area)

Type/ Phases	I	II-1	II-2	III
Cu-Fe sulfides	2	19	6	
Ni-Fe sulfides	19	30	9	2
Iron sulfides	3	2		
Nickel sulfides	4	4		1
Cu- and Ni-Fe sulfides	5	9	5	

Type/ Distance	I	II-1	II-2	III
110-80 mm	11	11	7	2
80-50 mm	8	12	4	1
50-20 mm	13	31	3	
20-(-10) mm		6	4	
(-10)-(-40) mm		4	2	

Distance/ Phases	110-80 mm	80-50 mm	50-20 mm	20-(-10) mm	(-10)-(-40) mm
Cu-Fe sulfides	5	7	10	3	2
Ni-Fe sulfides	14	9	25	6	4
Iron sulfides		1	3	1	
Nickel sulfides	7	1	1		
Cu- and Ni-Fe sulfides	5	6	8		

Table 14: Summary of sulfide abundance in relation to the sulfide compositions, spatial distribution and the sulfide occurrence (type). For sulfide occurrence, see the 'Sulfide' chapter in text. The spatial distribution is based on the reference coordinate.

1975; O'Hanley, 1996), and were subsequently reequilibrated. In fact, Shiga (1987) studied the sulfides from partly to completely serpentinized peridotites form the Kamaichi mining district of northern Japan, and observed that, in partly serpentinized peridotite, the Fe, Ni and Co lost from olivine could be incorporated into secondary pyrrhotite and pentlandite. Magnetite and marcasite are produced along with these reactions, and possibly H_2S gas, which is either liberated or reincorporated into discrete pentlandite, depending on the degree of serpentinization. In such a nearly isochemical process, the nickel content increases in the direction of increasing serpentinization, and this is reflected in the composition of the pentlandite with increasing amounts of nickel relative to iron. In my sample, the iron content can be both higher and lower than nickel in the pentlandite, and the pentlandite can be both sulfur-enriched and sulfur-deficient, suggesting that the serpentinization has not yet been completed; this corresponds to the conclusion drawn from the alteration observations. Therefore, given the textural and compositional evidence from the sulfides, and the occurrence of iron oxides within the sulfide cleavages, it is quite possible that the original magmatic sulfides have been modified compositionally to accommodate the change in chemical environment during serpentinization. Although most of the sulfides could be secondary with respect to the initial high temperature sulfides, they are still very different from hydrothermal sulfides in compositions.

There are some Ni-sulfides such as bornite and millerite occurring as late products at temperatures as low as 300°C (Craig and Scott, 1976), indicating the influence of low temperature weathering event(s). It should be noted here that in thin section 2B, quite a few of the low temperature sulfides such as millerite, hz and mk (tr) have been found around the thin rutile-plagioclase veinlet. The amount of these sulfides in the vicinity of the veinlet is probably larger than in the rest of the sample. We cannot rule out the possibility that this is a magmatic vein, but the appearance of the low-temperature sulfides suggests that the this veinlet has gone through both serpentinization and low temperature weathering.

8.3 Sulfide Compositions

The sulfide compositions from thin sections 2B and 3B are shown in Figs. 22 through 26. Also shown for comparison are the compositional boundaries of the MSS at 600°C and 230°C. The data scatter around the MSS compositional boundaries, and a large proportion of the data falls outside of the MSS boundaries. In comparison to previous studies, most of the sulfide data from Lorand (1989a) are inside the 230°C MSS triangle between Pn, Po and Py on the S-Fe-Ni phase diagram, and his broad beam analysis (to get the bulk sulfide compositions) data are clustered inside the 600°C MSS boundaries. The scattering of the present data may be partly caused by the inadequate analysis technique, and partly caused

by the size of the beam which was too large to focus on single sulfide phases, and thereby covers secondary minerals on the margins. A lot of sulfides on the phase diagrams fall below the pentlandite composition end member, and this could represent the combined effects of sulfur lost during the serpentinization and the presence of secondary sulfides. As discussed above, sulfides reequilibrated during serpentinization would decrease in sulfur and iron content and increase in nickel content, in magmatic sulfide assemblages (Pn+Po+Cp). The broad spectrum between Fe, Ni, and S components in the phase diagrams may as well be a result of the consequence of reequilibration between pentlandite, pyrrhotite and olivine.

There is no obvious correlation found between composition and distance (Figs. 24 and Fig. 25). In order to make these diagrams more accessible, sulfides with Cu contents higher than 5 wt% are not included in the Fig. 24, and Cu contents less than 5 wt% are discarded from the Fig. 25 (these are not considered to be pure nickel-iron-bearing and copper-iron-bearing sulfides, respectively). Since this observation largely depends on the density of sulfide grains for each interval, it should be noted that these relationships can be easily biased by the lack of representativeness of probed sulfides for each interval.

The lack of spatial relationships with the sulfide phases, the dominantly nickel-iron-bearing sulfides in all three types of textural occurrence, and the appearance of low temperature sulfides, all point to the conclusion that the serpentinization has had a thorough influence on this sample. During the serpentinization, not only have the compositions of the sulfides been gradually rehomogenized, but also the mode of the sulfides has changed to cope with the compositional changes. The serpentinization is probably so thorough that only a few of the sulfide inclusions in silicates have survived, with nearly all of the interstitial sulfides showing evidence of textural and compositional alteration. A few sulfides, such as bornite, occur at temperatures lower than 200°C, indicating the low temperature event(s). However, these low temperature event(s) did not completely overwrite the influence of the serpentinization.

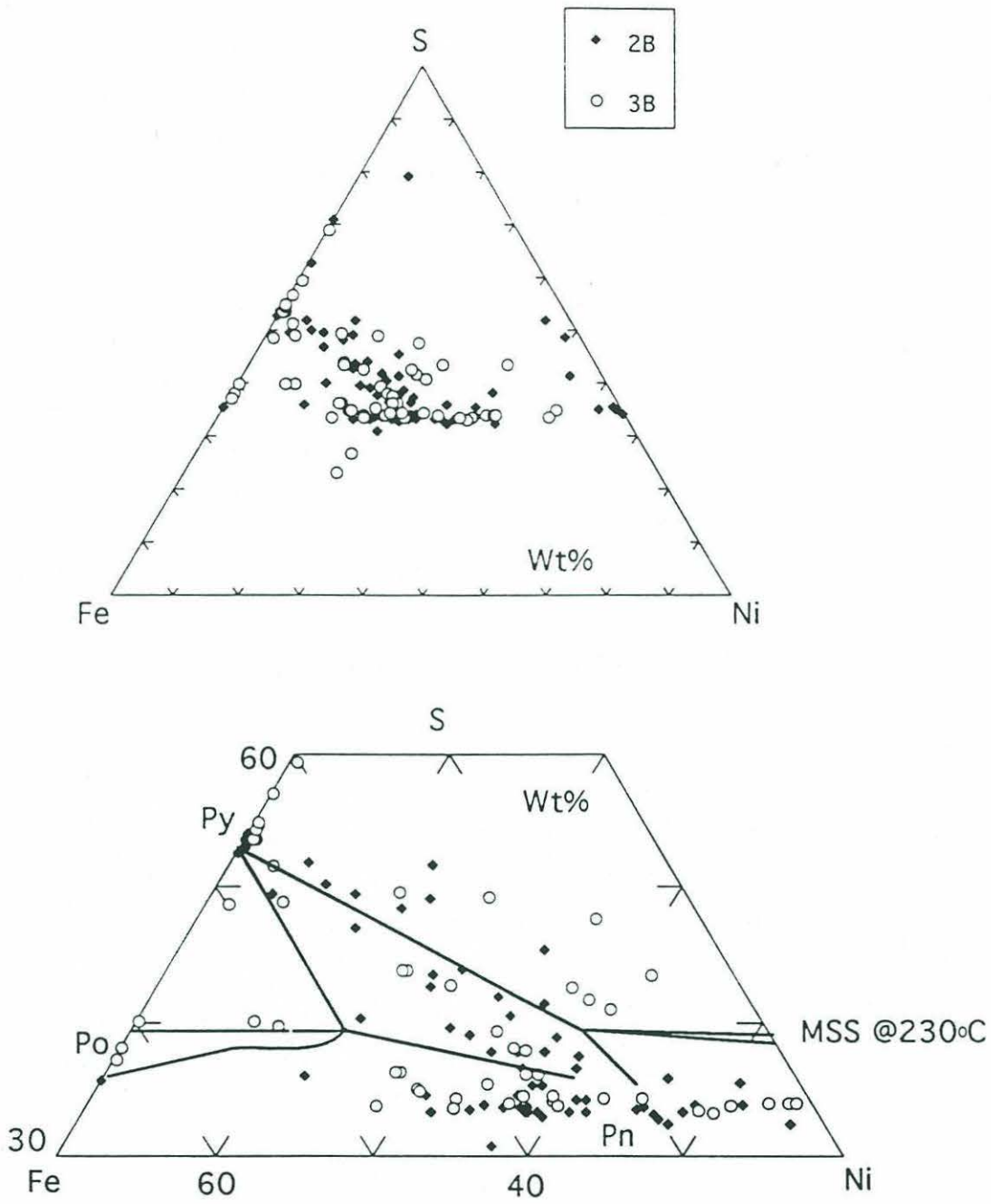

Fig.22: Sulfide compositions from thin sections 2B and 3B of RC 27-9-6-2 plotted in the S-Fe-Ni phase diagram in wt%. A blow-up of the MSS (monosulfide solid solution) field at 230°C is shown in the bottom of the figure. The 230°C S-Fe-Ni system is from Craig (1973) and Misra and Fleet (1973). Common sulfide phases are also shown for comparison. Py: pyrite; Po: pyrrrhotite; Pn: pentlandite.

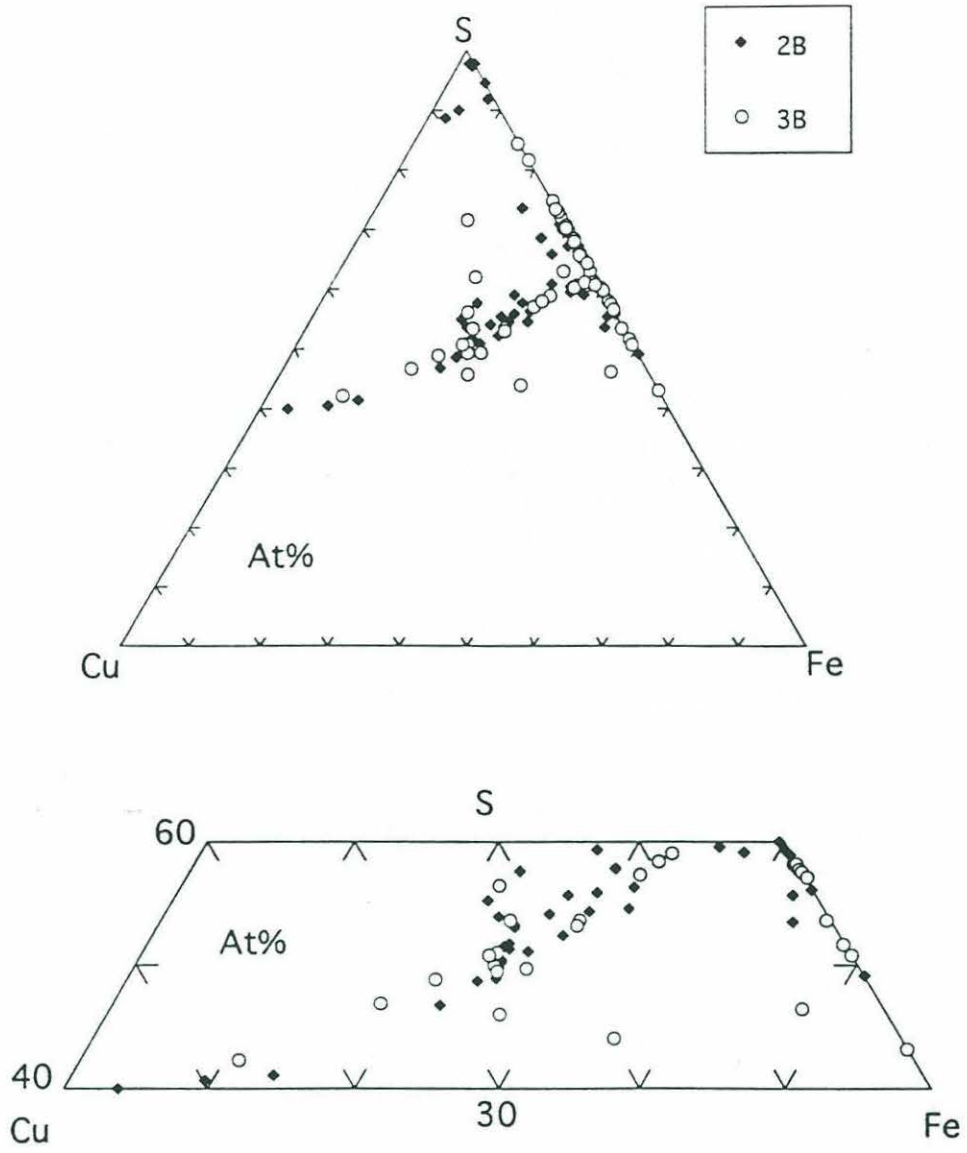

Fig.23: Sulfide compositions from thin sections 2B and 3B of RC 27-9-6-2 plotted in the S-Cu-Fe phase diagrams in atomic percent. An enlarged portion of the central region is shown at the bottom of the figure.

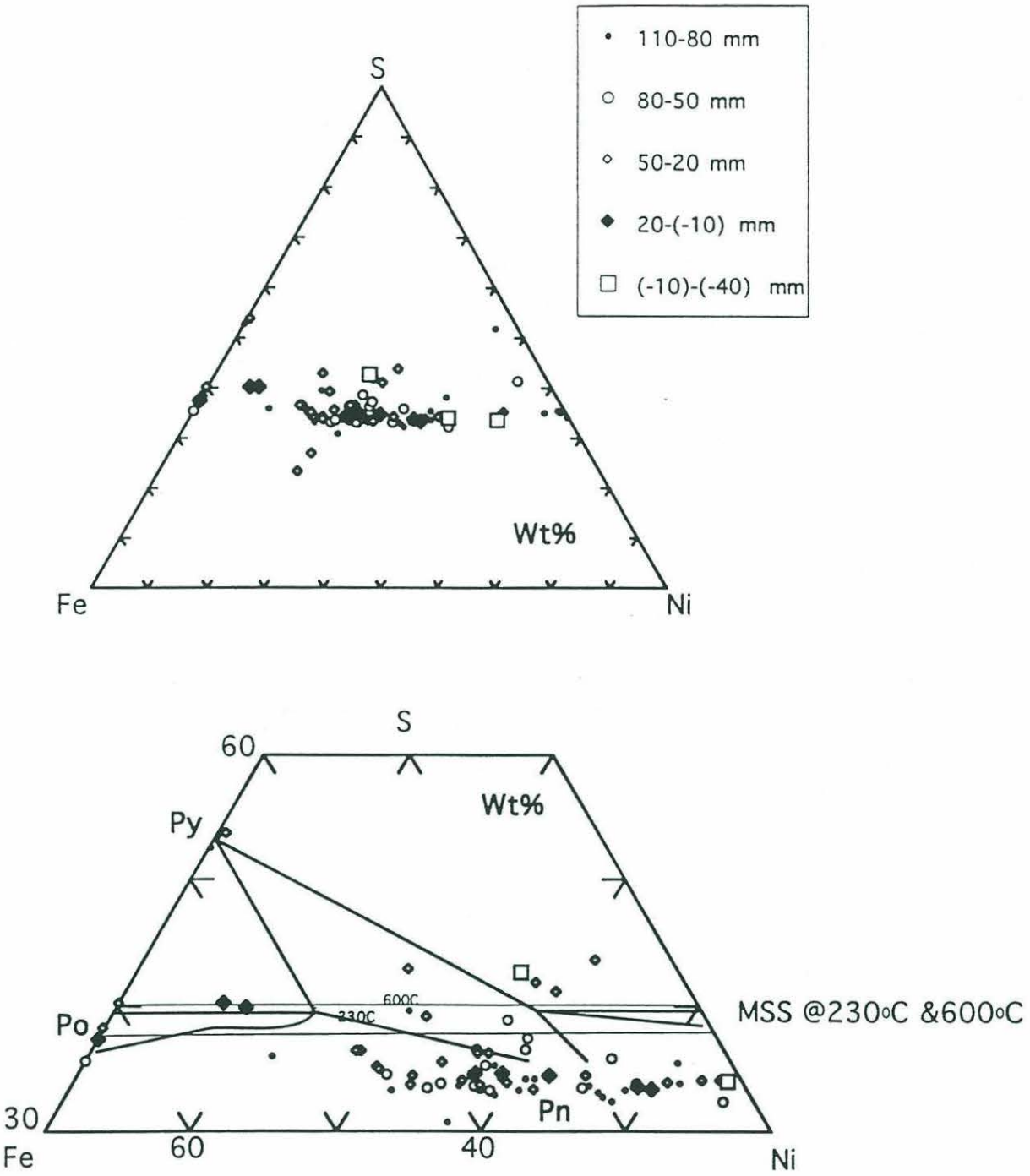

Fig.24: Sulfide compositions from thin sections 2B and 3B of RC 27-9-6-2 plotted in the S-Fe-Ni phase diagrams in wt%. The distance is based on the reference coordinate (see Plate). The compositional limits of MSS at 600°C are from Naldrett et al. (1967). Others as in Fig.21.

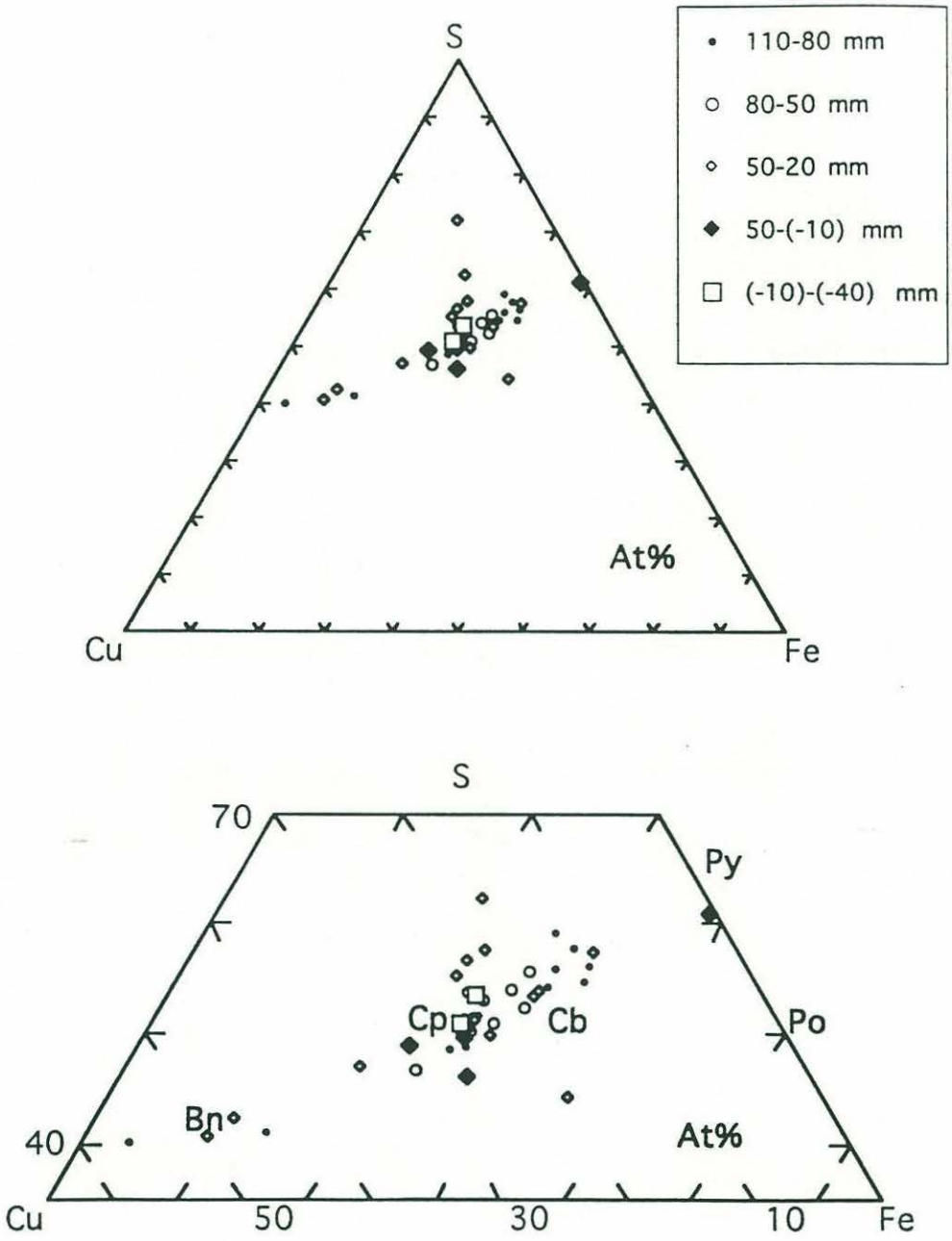

Fig.25: Sulfide compositions from thin sections 2B and 3B of RC 27-9-6-2 plotted in S-Cu-Fe phase diagrams in atomic percent. The distance is the vertical distance relative to the pyroxenite vein. Py: pyrite; Po: pyrrhotite; Cb: cubanite; Cp: chalcopyrite; Bn: bornite.

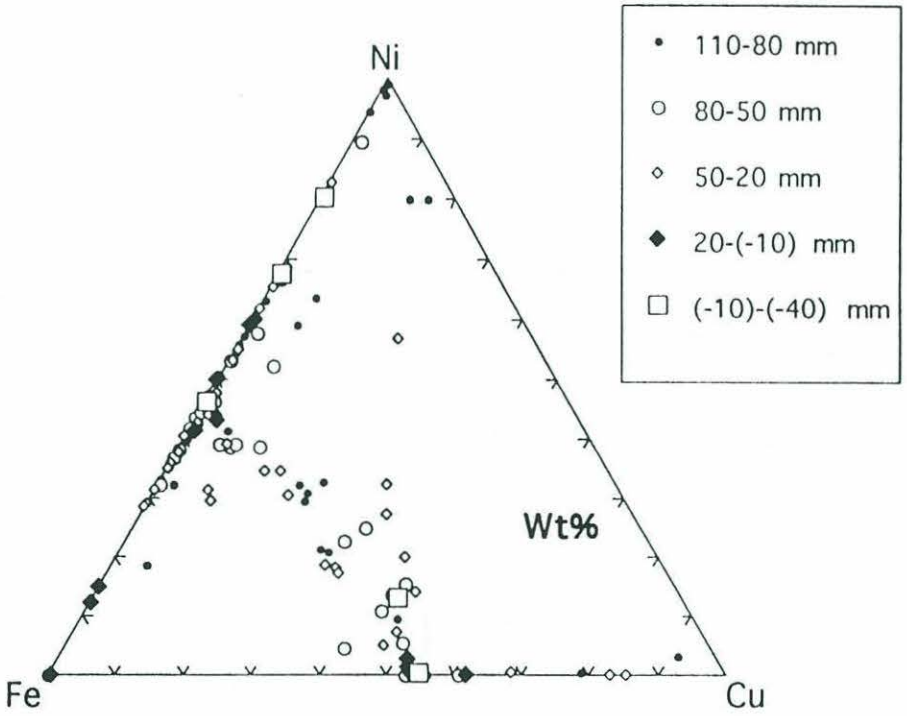

Fig.26: Sulfide compositions from thin sections 2B and 3B ofRC 27-9-6-2 plotted in the Ni-Fe-Cu ternary diagram in weight percent. The distance is the vertical distance relative to the pyroxenite vein.

9. OSMIUM ISOTOPES

9.1 Sulfides as Host for Os in Refractory Peridotites

It has been shown that sulfides may be a major Os reservoir in various kinds of rocks (Roy-Barman et al., 1994; Hart and Ravizza, 1996). One major question which needs to be answered for the Os system is what the bulk earth isotopic value should be. This study presents an empirical way of obtaining the primary Os composition in severely altered abyssal peridotites. Through the studies of the peridotites, we should be able to constrain the upper value of bulk earth Os isotopic ratio. It has been argued that the Os isotopic composition is too high for abyssal peridotites to be a residual mantle reservoir, and that the high value is actually caused by seawater alteration. However, given the relatively simple melting history, abyssal peridotites are good candidate to understand the primary processes in the suboceanic residual mantle (Johnson et al., 1990). The strategy in this study was thus to utilize the high Os concentration of sulfides to avoid the contamination problem and, possibly, the sea water alteration problem in the peridotites. Researchers have studied the history of sulfides and PGEs in orogenic peridotites. If these peridotites share a similar depletion history for sulfides as the abyssal peridotites, it may shed some light on the Os budget in the depleted suboceanic mantle.

9.2 A Summary of the Leaching Results

For a complete discussion of the leaching procedures, please refer to the methodology chapter and Table 3. The hydrogen peroxide leaching has leached a more radiogenic component in the leachate, and the residue has a slightly lower isotopic composition and higher concentration than the bulk rock. The same result also applies to the HCl leaching, indicating that both leachings remove some radiogenic Os and leave behind the more concentrated residues, which are closer to a primary composition. The oxidizing nitric acid leaching result is reversed, in the sense that the leachate has a higher concentration of Os than the bulk rock data. The stronger chrome-oxide acid in the sequential leaching basically shows the same tendency for the leachate to concentrate Os in the oxidized part of the sample. These oxidizing leach experiments strongly suggest that the major Os budget is contained in the acid-attackable, oxidizable part of the rock, which is probably sulfides, and possibly some other reduced phases formed during the serpentinization. The analysis of a leached, magnetic fraction from sub-sample E results in a moderately high Os isotopic composition and very high Os concentration. Considering that the magnetic separation component probably contains magnetite and monoclinic pyrrhotite (Fe_7S_8, which is a low

temperature form of pyrrhotite), this result demonstrates that the leaching mainly releases Os from the sulfide. In addition, the isotopic composition of sample LEM is in the range of normal abyssal peridotites, indicating that either the sea water alteration is not as prevalent as we thought, or that the serpentinization does not shift the isotopic composition very much. It should be noted that for such high Os concentrations in the sulfides, it is unlikely that they are affected to a large degree by sea water alteration. In Os analysis there is the well known 'nugget effect', which states that the reproducibility of Os concentration is poor because the Os concentrates in some rare tiny phases that are difficult to mix well when doing the sampling. I argue that the leaching results are not totally biased by such effects, considering both the nice trend showed in the sequential leaching experiment and the consistent results from the nitric acid leaching. Therefore, this leaching technique offers a meaningful opportunity to study the different aspects of the data.

9.3 Heterogeneous Os Isotopic Composition

The 187/186 Os isotopic compositions found in this study range from 1.034 to 1.148 for the unleached whole rock analyses, with an average at around 1.09. 1.148 is the highest value ever reported for an abyssal peridotite. The heterogeneous isotopic compositions in this 11'' by 81/2'' sample are anomalous, considering all the published data from Snow (1995) and Martin (1991). It has long been suggested that the data from abyssal peridotites are too high to be primary, due to the influence of extensive seawater alteration (seawater $^{187}Os/^{186}Os$ is about 8.5). In addition, studies on chondrites (Luck and Allegre, 1983; Walker and Morgan, 1989) show that the value of the primary mantle should be about 1.07. The residual abyssal peridotites should have an Os isotopic ratios less than this because of the refractory nature of Os and the incompatibility of Re during melting processes. In fact, even taking the present day bulk silicate earth value (Luck and Allegre, 1991; Martin et al., 1992) into account, the abyssal peridotites should have a value no higher than 1.10. Thus, there must be some other processes involved than just partial melting and sea water alteration to explain the distribution of Os isotopic compositions in this sample.

9.3.1 The possible mixing trends---the magmatic origin

Fig. 27 illustrates all the possible mixing trends between sources. The parameters for each source are listed in Table 15. First order observation shows that there might be two ways to explain the data. The first one is by a magmatic process. Three different mixing trends are shown by lines 1, 2 and 3. It should be noted that based on the Nd (≈0.5130)

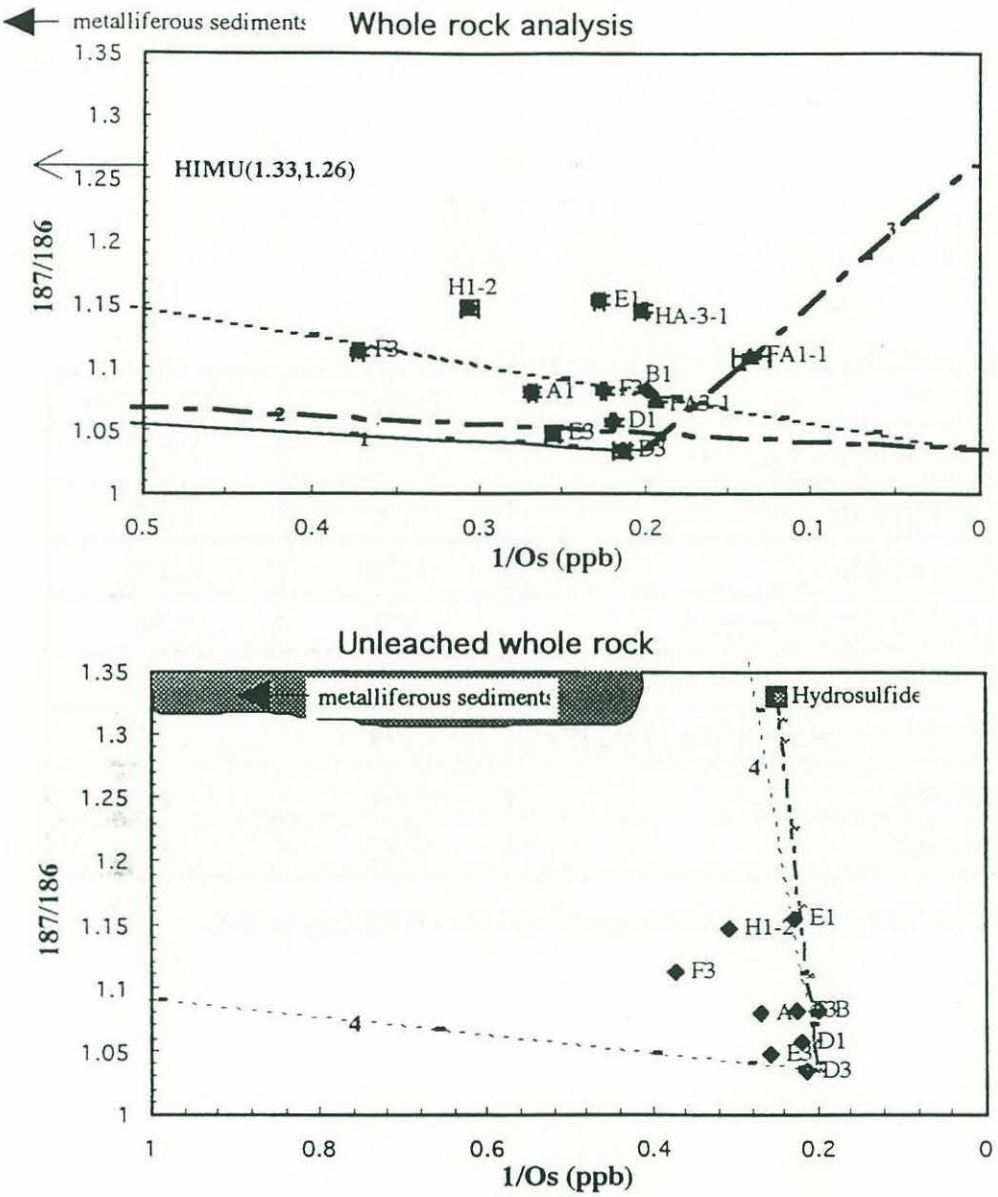

Fig.27: $^{187}Os/^{186}Os$ vs. Os concentrations in whole rock analyses and leachates from RC 27-9-6-2. The field for metalliferous sediments is shown for illustration only. For end member compositions and mixing parameters, see Table 15.

	Os (ppb)	$^{187}Os/^{186}Os$
The peridotite (this study)	5.00	1.034
The melt (HIMU component)	0.30	1.26
Residue sulfide	1500	1.034
The sulfide (HIMU sulfide)	200	1.26
Mixture of the melt and the sulfide	1.00	1.26
hydrosulfide (from Ravizza et al., 1996)	3.99	1.33
Sediment I	0.01	8
Sediment II	0.50	8

Table 15: The parameters of the sources for the Os mixing models.

and the slightly enriched Sr (≈0.7045) isotopic data of the hand-picked, leached clinopyroxene from the clinopyroxenite vein, a mixture of HIMU component and MORB and/or EMII may be responsible for the source composition of the exotic melt. Given the isotopic data of basalts from the Atlantis II Fracture Zone (Snow, 1993; $^{87}Sr/^{86}Sr$=0.702690-0.702893; $^{143}Nd/^{144}Nd$=0.512981-0.513149; $^{206}Pb/^{204}Pb$=17.462-18.114; $^{207}Pb/^{204}Pb$=15.382-15.505; $^{208}Pb/^{204}Pb$=37.089-37.839), it is unlikely that there is an enriched endmember component existing in the suboceanic mantle in this region. The gabbros from the ODP drill site 735b in the northern ridge of the transform fault show similar isotopic ratios to the basalts (Snow, 1993; Kempton et al., 1991). One exceptional gabbroic sample from site 735b contains $^{187}Os/^{186}Os$ at about 1.27 (Blusztajn, unpublished data). Regardless of possible sea water alteration, a hypothetical HIMU component could explain the high Os isotopic composition of this sample. Thus, the first mixing trend (line 1) represents mixing between the enriched component and the abyssal peridotite.

It has long been suggested that primitive melts from the deep mantle are sulfur saturated, and consequently there should be sulfides retained as residual phases during mantle melting (Roy-Barman et al., 1994; Hart and Ravizza, 1996). As the melt reaches shallower mantle, sulfur would be undersaturated in the melt, because the solubility of sulfur is positively dependent on the iron content in the melt (FeO) and temperature, and negatively dependent on pressure (Hart and Ravizza, 1996, and ref. within). Consequently, before the melt ascends into the conductive cooling region, it probably consumes some mantle sulfides on the way up, through some reaction processes. Taking melt-rock interaction into account, the pressure decrease and the slight increase of the FeO content in the melt would cause the sulfur solubility to increase even more. Therefore, as soon as the undersaturated melt infiltrated the subridge mantle, it would quickly dissolve sulfides from the sample, to balance the undersaturation. The first scenario we can envision here is that the residual sulfides in the peridotite were consumed and possibly reequilibrated with the melt. This is shown by the second mixing trend (line 2), which shows that some of the samples away from the clinopyroxenite vein, (samples D1, E2 and H1-1) are probably affected by the above scenario.

After the first stage of modification, the melt has probably been close to the point of sulfur saturation. Some part of this melt has probably been trapped in, and ascended with the host rock into the conductive cooling region. Here the melt became sulfur-saturated, due to the temperature decrease, and started to crystallize sulfides. For simplicity, we assume that the sulfides are precipitated with the same isotopic composition as the melt. This second scenario is represented by the third mixing trend (line 3), in which the bulk

peridotite mixes with the sulfides precipitated from the melt (the HIMU sulfides). This mixing line could also be regarded as an 'apparent' mixing line, in the sense that the bulk peridotite concentration can be varied along with the amount of sulfide contained in the peridotite. Allowing the Os concentration to vary in the peridotite is invoking the 'nugget' effect. In the real mixing, the end members are sulfides from both the residual mantle and the melt, thus the real effect apparently depends on both the amount of sulfide in the residue and the isotopic composition of the melt. Therefore, we could draw a group of 'apparent' mixing lines for a range of concentrations. Taking the concentration range from the bulk rock analysis (a variation from 2 to 5 ppb), the 'apparent' mixing lines bracket most of the data points except H1-1, H1-2 and F1. In addition, as an alternative to the sea water alteration hypothesis, the apparent mixing effect of residual peridotites with basaltic liquid can actually explain most of the existing peridotite data.

The second stage of 'apparently' mixing the bulk abyssal peridotite with the melt seems to be able to explain most the data, though it is always possible to look for an alternative explanation using three-component mixing. By mixing the residual sulfides with a mixture of the HIMU melt and the HIMU sulfides, this combination provides a totally different physical phenomena than the 'apparent' mixing trend. This is illustrated in Fig. 27 as a dotted mixing line. Mixing with about 0.2 to 0.5 wt% of HIMU sulfides coincidentally passes through the data mainly from the clinopyroxenite vein (samples F, A and B), which suggests a scenario whereby a batch of sulfur-saturated melt is quenched in situ while infiltrating into the host rock. The sulfide texture also provides some information about this type of mixing. The dominant occurrence of sulfides in the vein is as inclusions in the clinopyroxene, which may suggest that the sulfides are trapped immiscible melt during the clinopyroxene recrystallization.

9.3.2 The possible mixing trends-alteration processes

In addition to a magmatic model, the second way to describe the data is as a result of alteration processes. Also shown in Fig. 27 are fields for both Mn-nodule and metalliferous sediments (Esser and Turekian, 1988; Ravizza and Turekian, 1992; Ravizza and McMurtry, 1993), and mixing lines (line 4) between the abyssal peridotite and sediments. The sulfide data from the TAG hydrothermal mount (Ravizza et al., 1996) is also plotted for illustration. Sea water alteration is a conventional way to explain the variable and high Os isotopic ratios in abyssal peridotites. As shown by line 4, it seems that mixing with different compositions of sediments or hydrothermal sulfides can cover the entire data group. However, the sample does not appear to be contaminated by these materials on the surface. The highest Os isotopic composition is not from the outer rim (area A and B) or

surface part of the sample. Another possibility to introduce the contaminants is by the mechanism suggested by Snow et al. (1994). An extremely fine grained radiogenic Os component can penetrate into the peridotite at very high water/rock ratio and low temperature. However, since 'orphan Sr' was not identified in this study, and given the facts that most of these sediments have pretty elevated Sr isotopic compositions, it is less likely that the heterogeneity of the isotopic data is caused only by the alteration/contamination. Furthermore, low temperature seawater alteration by a diffusion process does not seem to be satisfied, since this rock is young (less than 1 Ma) and has undergone obvious melt-rock interaction. However, one cannot conclude that seawater alteration did not operate on this sample at all. Some data points, such as H1-1 and E1, could still be best explained by such alteration processes.

To sum up, there are several possibilities to explain the variable Os isotopic compositions in this peridotite:

1, The most obvious possibility is the mixing of a HIMU (or any other enriched source) component with the abyssal peridotite, given the occurrence of the clinopyroxenite vein. However, most of the dredged and drilled basalts from this area are quite uniform and depleted in other isotopic compositions (Snow, 1993). The only other evidence of high $^{187}Os/^{186}Os$ with relatively enriched $^{143}Nd/^{144}Nd$ is one gabbroic sample from Site 735b (Blusztajn, unpublished data), which is believed to be primary data. The details of how this enriched magmatic component is transported or introduced into the transform fault region is unclear thus far.

2, Given the fact that the Nd isotopic system is the least likely to be affected by seawater alteration, the nearly depleted end-member MORB-mantle component (DMM) values of most of the basalts and peridotites from this region indicate that the clinopyroxene vein was originally a MORB melt. Regardless of the elevated Sr isotopes, which may be affected by alteration, this possibility would raise the depleted mantle $^{187}Os/^{186}Os$ up to or higher than 1.10. This is possible, given the $^{187}Os/^{186}Os$ value of 1.09 from the picked sulfide data from the Famous basalts (Roy-Barman et al., 1994). In this case, the source of the clinopyroxenite vein is a normal MORB melt, with an Os isotopic composition around 1.10.

3, If every isotopic system was affected by seawater alteration, which would shift the Nd isotope toward lower values, and the Sr and Os isotope ratios toward higher values, then the different degrees of alteration for these systems could not be explained by a simple mixing mechanism. A diffusion-type of alteration (selective alteration at low temperature) is necessary to explain the much larger shift in the Os isotopic system than in the Nd system. The faster reaction rate of the sulfides would lead to greater change in Os during alteration

than for the silicates, such as clinopyroxene, which is the major reservoir of Nd in the peridotites. However, in this case, it is not possible to separate out the effect of melt-rock reaction from seawater alteration, for both processes have the same direction of influence.

9.4 Conclusion

To conclude, there are no absolute answers to explain the distribution of the Os data. As shown from the above arguments, it remains uncertain that the heterogeneity in isotopic composition is largely primary, or modified by low temperature event(s). Though the lowest value, ≈ 1.034 for $^{187}Os/^{186}Os$, is adopted in this study for modelling abyssal peridotite, we are not saying that it is the real value for the depleted mantle. The influence of melt-rock reaction is quite large in the current case, though it remains uncertain how large the effect of this interaction could be in normal suboceanic upper mantle. Lorand (1989c) studied orogenic lherzolites, and reported that there are systematic changes in sulfide component between pyroxenite dikes and lherzolites away from the dike. However, such a change is not evident for the sulfides compositions in this study. Since the evidence for the melt-rock reaction from trace elements and some of the isotopic systems is obvious, we do not want to pay much attention to the ambiguous sulfide compositions resulting from modification during subsequent events. It should also be borne in mind that this rock is dredged from a transform fault, where the conductive cooling region is much deeper than any other area in the mid-ocean ridge system. This faster cooling rate is probably one of the reasons that the melt-rock interaction signature has been preserved without being modified by other processes.

10. CONCLUSIONS

1. The existence of the clinopyroxene vein in this abyssal peridotite offers an excellent opportunity to study the effects of melt-rock reaction. These effects are evident in the rare earth element concentrations from the clinopyroxenes both inside and outside of the clinopyroxenite vein, as well as in the isotopic compositions. However, the origin of the exotic melt is uncertain at this point. It could be either a mixture of MORB and HIMU components, or a normal MORB melt modified by the melt-rock reaction process.

2. Sulfides are shown to be the major reservoir for Os in abyssal peridotites, through a series of leaching experiments. The leaching experiments also show that the degree of alteration in the peridotite is probably not as severe as anticipated, in terms of Os geochemistry. The mechanism of sea water alteration for silicates and sulfides is probably also very different. Besides, no anomalously high $^{87}Sr/^{86}Sr$ (higher than the sea water value) is found in different size fractions of the magnetic separations, indicating that sea water alteration by infiltration of fine particles from the sea floor is quite unlikely in this area. Simple mass balance calculations also show that the sample suffered very little loss or gain of elements during the alteration. Combined with the sulfide mineralogy, this suggests that most of the modification from the sea water in this sample happened during the serpentinization.

3. The exotic clinopyroxenite vein is shown to have a profound influence on the rest of the sample in both the REEs and the isotopic systems. One of the major impacts of this complexity is probably the introduction of a heterogeneity in the Os isotopes. Given the uncertainty in the origin of the vein, and in the bulk earth Os value, it cannot be concluded so far whether the whole spectrum of Os isotopic variations in the abyssal peridotite is caused by a melt-rock reaction process, nor how seriously the sea water alteration processes can affect the Os isotopic system. However, this sample provides a good opportunity for further studies on both processes.

ACKNOWLEDGMENTS

I would like to thank my thesis advisor, Stan Hart, for his patient guidance, encouragement and valuable discussions on this work, for the generously sharing of his time and ideas for me and for careful readings of the preliminary versions of this thesis.

My thanks also go to Henry Dick, for his encouragement and many helpful suggestions, and for his generously providing the sample and the ion probe data. Thanks especially to Jurek Blusztajn, Greg Ravizza and Bernhard Peucker-Ehrenbrink, for many valuable suggestions concerning various aspects of the thesis, and geochemistry in general. I would like to specifically acknowledge their efforts in teaching me to run the mass spectrometer and the clean laboratory.

Last but not the least I would like to thank my family and friends for their support throughout my stay in the Joint Program. Their continual encouragement has kept me on going during difficult times.

REFERENCES

Abrajano, T.A., N.C. Sturchio, J.K. Bohlke, G.L. Lyon, R.J. Poreda and C.M. Stevens, Methane-dyfrogen gas seeps, Zambales Ophiolite, Phillippines: deep or shallow origin? *Chem. Geol.*, 71, 211-222, 1988.

Allan, J.F., and H.J.B. Dick, Cr-rich spinel as a tracer for melt migration and melt-wall rock interaction in the mantle: Hess Deep, Leg 147, In Gillis, K., Mevel, C., Allan, J., et al., *Proc. ODP, Sci. Results, 147*: College Station, TX (Ocean Drilling Program), 157-172, 1996.

Anders, E., and M. Ebihara, Solar-system abundances of the elements, *Geochim. Cosmochim. Acta.*, 46, 2363-2380, 1982.

Barton, P.B. JR., Sulfide petrology, *Mineral. Soc. Amer. Spec. Pap.*, 3, 187-198, 1970.

Berndt, M.E., D.E. Allen and W.E. Seyfried, JR., Reduction of CO2 during serpentinization of olivine at 300{C and 500 bar, *Geology*, 24, 351-354, 1996.

Boudier, F., and A. Nicolas, Structural controls on partial melting in the Lanzo peridotites, in Magma Genesis, edited by H.J.B. Dick, *Oreg. Dep. Geol. Miner. Ind. Bull.*, 96, 63-78, 1977.

Carlson, R.W., and A.J. Irving, Depletion and enrichment history of subcontinental lithospheric mantle: An Os, Sr, Nd and Pb isotopic study of ultramafic xenoliths from the northwestern Wyoming Craton, *Earth Planet. Sci. Lett.*, 126, 457-472, 1994.

Charlou, J.L., and J.P. Donval, Hydrothermal methane venting between 12°N and 26°N along the Mid-Atlantic Ridge, *J. Geophys. Res.*, 98, 9625-9642, 1993.

Craig, J.R., Pyrite-pentlandite assemblages in the Fe-Ni-S system, *Am. J. Sci.* 273A, 496-510, 1973.

Craig, J.R., and S.D. Scott, Sulfide phase equilibria, in P.H. Ribbe (Ed.), Sulfide Mineralogy, Reviews in Mineralogy, v.1, *Mineral. Soc. Amer.*, 1976.

DePaolo, D.J., Trace element and isotopic effects of combined wallrock assimilation and fractional crystallization, *Earth Planet. Sci. Lett.*, 53, 189-202, 1981.

Dick, H.J.B., Evidence of partial melting in the Josephine peridotite, in Magma Genesis, edited by H.J.B. Dick, *Oreg. Dep. Geol. Miner. Ind. Bull.*, 96, 63-78, 1977.

Dick, H.J.B., Abyssal peridotites, very slow spreading ridges and ocean ridge magmatism, in Magmatism in the Ocean Basins, edited by Saunders, A.D. and Norry, M.J., *Geological Soc. Spec. Publication*, 42, 71-105, 1989.

Dick, H.J.B., and T. Bullen, Chromian spinel as a petrogenetic indicator in abyssal and alpine-type peridotites and spatially associated lavas. *Contrib. Mineral. Petrol.*, 86, 54-76, 1984.

Dick, H.J.B., and R.L. Fisher, Mineralogical studies of the residues of mantle melting: abyssal and alpine-type peridotites. in Kornprobst, J. (Ed.), *Kimberlites II: The Mantle and Crust-Mantle Relationships*, Elsevier, Amsterdam, 295-308, 1984.

Dick, H.J.B., H. Schouten, P. Meyer, D. Gallo, H. Bergh, R. Tyce et al., Tectonic evolution of the Atlantic II Fracture Zone, *Proc. ODP, Sci. Results, 118*: College Station, TX (Ocean Drilling Program), part B, 1991.

Dick, H.J.B., and J.H. Natland, Late-stage melt evolution and transport in the shallow mantle beneath the East Pacific Rise, In Gillis, K., Mevel, C., Allan, J., et al., Proc. ODP, *Sci. Results, 147*: College Station, TX (Ocean Drilling Program), 103-134, 1996.

Eckstrand, O.R., The Dumont serpentinite: A model for control of nickeliferous opaque mineral assemblages by alteration reactions in ultramafic rocks, *Econ. Geol.*, 70, 183-201, 1975.

Elthon, D., Chemical trends in abyssal peridotites: refertilization of depleted suboceanic mantle, *J. Geophys. Res.*, 97, 9015-9025, 1992.

Esser, B.K., and K.K. Turenkian, Accretion rate of extraterrestrial particles determined from osmium isotope systematics of Pacific pelagic clay and manganese nodules, *Geochim. Cosmochim. Acta.*, 52, 1383-1388, 1988.

Frank, F.C., Two-component flow model for convection in the earthUs upper mantle, *Nature*, 220, 350-352, 1968.

Frost, B.R., On the stability of sulfides, oxides, and native metals in serpentinite, *J. Petrol.*, 26, 31-63, 1985.

Garuti, G., C. Gorgoni and G.P. Sighinolfi, Sulfide mineralogy and chalcophile and siderophile element abundances in the Ivrea-Verbano mantle peridotites (Western Italian Apls), *Earth Planet. Sci. Lett.*, 70, 69-87, 1984.

Hart. S.R., and G.E. Ravizza, Os Partitioning Between Phases in Lherzolite and Basalt, in *Earth Processes: Reading the Isotopic Code*, edited by A.Basu and S.R. Hart, Geophys. Monograph 95, pp. 123-134, 1996.

Hauri, E.H., and S.R. Hart, Re-Os isotope systematics of HIMU and EMII oceanic island basalts from the south Pacific Ocean, *Earth Planet. Sci. Lett.*, 114, 353-371, 1993.

Hoffman, E.L., A.J. Naldrett, J.C. Van Loon, R.G.V. Hancock and A. Mason, The determination of all the platium group elements and gold in rocks and ore by neutron activation analysis after preconcentration by a nickel sulfide fire-assay technique for large samples, *Anal. Chim. Acta.*, 102, 157-166, 1978.

Irving, A.J., A review of experimental studies of crystal/liquid trace element partitioning, *Geochim. Cosmochim. Acta.*, 42, 743-770, 1978.

Janecky, D.R., and W.E. Seyfried, JR., Hydrothermal serpentinization of peridotite within the oceanic crust: Experimental investigations of mineralogy and major element chemistry, *Geochim. Cosmochim. Acta.*, 50, 1357-1378, 1986.

Johnson, G.K., and J.E. Bauman, JR., Equilibrium constants for the aquated iron (II) cation, *Inorg. Chem.*, 17, 2774-2779, 1978.

Johnson, K.T.M., H.J.B. Dick and N. Shimizu, Melting in the oceanic upper mantle: an ion-microprobe study of diopsides in abyssal peridotites, *J. Geophys. Res.*, 95, 2661-2678, 1990.

Kelemen, P.B., Reaction between ultramafic wall rock and fractionating basaltic magma, I, Phase relations, the origin of calc-alkaline magma series, and the formation of discordant dunite, *J. Petrol.*, 31, 51-98, 1990.

Kelemen, P.B., H.J.B. Dick, and J.E. Quick, Production of harzburgite by pervasive melt-rock reaction in the upper mantle, *Nature*, 358, 635-641, 1992.

Kelemen, P.B., J.A. Whitehead, E. Aharonov, and K.A. Jordahl, Experiments on flow focusing in soluble porous media with applications to melt extraction from the mantle, *J. Geophys. Res.*, 100, 475-496, 1995.

Kelemen, P.B., N. Shimizu and T. Donn, Relative depletion of niobium in some arc magmas and the continental crust: partitioning of K, Nb, La and Ce during melt/rock reaction in the upper mantle, *Earth Planet. Sci. Lett,* 120, 111-134, 1993.

Kempton, P.D., C.J. Hawkesworth and M. Fowler, Geochemistry and isotopic composition of gabbros from layer 3 of the Indian Ocean crust, Hole 735b, in von Herzen, R.P., P.T. Robinson, et al. (Eds.) *Proc. ODP, Sci. Results 118*: College Station, TX (Ocean Drilling Program), 127-142, 1991.

Kimball, K.L., F.S. Spear and H.J.B. Dick, High temperature alteration of abyssal ultramafics from the Islas Orcadas Fracture Zone, South Atlantic, *Contrib. Mineral. Petrol.*, 91, 307-320, 1985.

Lorand, J.P., Cu-Fe-Ni-S mineral assemblages in mantle peridotites from the Table Mountain and Blow-Me-Down Mountain ophiolite massifs (Bay-of-Islands area, Newfoundland); relationships with silicate melts and fluids, *Lithos*, 20, 59-77, 1987.

Lorand, J.P., Mineralogy and chemistry of Cu-Fe-Ni sulfides in orogenic-type spinel peridotit bodies from Ariege (Northeastern Pyrenees, France), *Contrib. Mineral. Petrol.*, 103, 335-345, 1989a.

Lorand, J.P., Sulfide petrology of spinel and garnet pyroxenite layers from mantle-derived spinel lherzolite massifs of Ariege, Northeastern Pyrenees, France, *J. Petrol.*, 30, 987-1015, 1989b.

Lorand, J.P., The Cu-Fe-Ni sulfide component of the amphibole-rich veins from the Lherz and Freychinede spinel peridotite massifs (Northeastern Pyrenees, France): A comparison with mantle-derived megacrysts from alkali basalts, *Lithos*, 23, 281-298, 1989c.

Luck, J.M., Geochimie du Rhenium-Osmium: Methode et Applications, Univ. Paris VII, 1982.

Luck, J.M., and C.J. Allegre, 187Re-186Os systematics in meteorites and cosmochemical consequences, *Nature*, 302, 130-132, 1983.

Luck, J.M., and C.J. Allegre, Osmium isotopes in ophiolites, *Earth Planet. Sci. Lett.*, 107, 406-415, 1991.

Martin, C.E., Os isotopic characteristics of mantle derived rocks. *Geochim. Cosmochim. Acta.*, 55, 1421-1434, 1991.

Martin, C.E., B.K. Esser and K.K. Turekian, Re-Os isotopic constraints on the formation of mantle and crustal reservoirs, *Austral. J. Earth Sci.*, 38, 1992.

Martin. C.E., R.W. Carlson, S.B. Shirey, F.A. Frey and C.Y. Chen, Os isotopic variation in basalts from Haleakala Volcano, Maui, Hawaii: A record of magmatic processes in oceanic mantle and crust, *Earth Planet. Sci. Lett.*, 128, 287-301, 1994.

Misra, K., and M.E. Fleet, The chemical composition of synthetic and natural pentlandite assemblages, *Econ. Geol.*, 68, 518-539, 1973.

Moody, J.B., An experimental study on the serpentinization of iron-bearing olivines. *Can. Mineral.*, 14, 462-478, 1976.

Naldrett, A.J., J.R. Craig, and G. Kullerud, The central portion of the Fe-Ni-S system and its bearing on pentlandite exsolution in iron-nickel sulfides ores, *Econ. Geol.*, 62, 826-847, 1967.

O'Hanley, D.S., and M.D. Dyar, The composition of lizardite 1T and the formation of magnetite in serpentinites, *Am. Mineral.*, 78, 391-404, 1993.

Palmer, M.R., K.K. Falkner, K.K. Turekian and S.E. Calvert, Sources of osmium isotopes in manganese nodules, *Geochim. Cosmochim. Acta.*, 52, 1197-1202, 1988.

Pearson, D.G., S.B. Shirey, R.W. Carlson, F.R. Boyd, P.H. Nixon et al., Re-Os and Sm-Nd isotopic constraints on the chronology of lithospheric mantle formation and enrichment events (abst.), *EOS*, 73, 527, 1991.

Pegram, W.J., and C.J. Allegre, Osmium isotopic compositions from oceanic basalts, Earth Planet. Sci. Lett., 111, 59-68, 1992.

Ravizza G. and K.K. Turenkian, The osmium isotopic compositions of organic-rich marine sediments, *Earth Planet. Sci. Lett.*, 110, 1-6, 1992.

Ravizza, G. and G.M. McMurtry, Osmium isotopic variations in metalliferous sediments from the East Pacific Rise and the Bauer Basin, *Geochim. Cosmochim. Acta.*, 57, 4301-4310, 1993.

Ravizza, G., C.E. Martin, C.R. German and G. Thompson, Os isotopes as tracers in seafloor hydrothermal systems: metalliferous deposits from the TAG hydrothermal area, 26{N Mid-Atlantic Ridge, *Earth Planet. Sci. Lett.*, 138, 105-119, 1996.

Reisberg, L.C., C.J. Allegre and J.M. Luck, The Re-Os systematics of the Rhonda Ultramafic Complex of southern Spain, *Earth Planet. Sci. Lett.*, 105, 196-213, 1991.

Roy-Barman. M., and C.J. Allegre, 187Os/186Os ratios of mid-ocean ridge basalts and abyssal peridotites, *Geochim. Cosmochim. Acta.*, 58, 5043-5054, 1994.

Roy-Barman, M., G.J. Waswerburg, and D.A. Pananastassiou, Osmium Isotopic Composition of Sulfides from Basaltic Glasses, in *Abstracts of the Eighth International Conference on Geochronology, Cosmochronology and Isotope Geology*, edited by M.A. Lanphere, G.B. Dalrymple and B.D. Turrin, U. S. Geol. Survey Circular 1107, p.272, 1994.

Sanford, R.F., Mineralogical and chemical effects of hydration reactions and applications to serpentinization, *Am. Mineral.*, 66, 290-297, 1981.

Shiga, Y., Behavior of iron, nickel, cobalt and sulfur during serpentinization, with reference to the Hayachine ultramafic rocks of the Kamaishi mining district, Northeastern *Japan, Can. Mineral.*, 25, 611-624, 1987.

Shimizu, N., M.P. Semet and C.J. Allegre, Geochemical applications of quantitative ion-microprobe analysis, *Geochim. Cosmochim. Acta.*, 42, 1321-1334, 1978.

Sleep, N.H., Segregation of magma from a mostly crystalline much, *Geol. Soc. Am. Bull.*, 85, 1223-1232, 1974.

Smith, G.M., D.R. Janecky, S.K. Banerjee and W.E. Seyfried, Magnetic characteristics of experimental natural serpentinites, *EOS*, 63, 1982.

Snow, J.E., The Isotope Geochemistry of Abyssal Peridotites and Related Rocks, Ph.D. diss., MIT/WHOI, pp. 346, 1993.

Snow, J.E., and L. Reisberg, Os isotopic systematics of the MORB mantle: results from altered abyssal peridotites, *Earth Planet. Sci. Lett.*, 133, 411-421, 1995.

Snow, J.E., S.R. Hart and H.J.B. Dick, Nd and Sr isotope evidence linking mid-ocean-ridge basalts and abyssal peridotites, *Nature*, 371, 57-60, 1994.

Streckeisen, A., To each plutonic rock its proper name, *Earth Sci. Reviews*, 12, 1-33, 1976.

Tamura, H., K. Goto and J. Nagayama, Effect of anions on the oxygenation of ferrous ion in neutral solutions, *J. Inorg. Nucl. Chem.*, 38, 113-117, 1976.

Turcotte, D.L., and J.L. Ahern, A porous flow model for magma migration in the asthenosphere, *J. Geophys. Res.*, 767-772, 1978.

von Herzen, P.R., P.T. Robinson et al., *Proc. ODP, Sci. Results, 118*: College Station, TX (Ocean Drilling Program), 1991.

Walker, R.J., and J.W. Morgan, Rhenium-osmium isotope systematics of carbonaceous chondrites, *Science*, 243, 519-522, 1989.

Walker, R.J., R.W. Carlson, S.B. Shirey and F.R. Boyd, Os, Sr, Nd and Pb isotope of subcontinental mantle. systematics of southern African peridotite xenoliths: Implications for the chemical evolution, *Geochim. Cosmochim. Acta.*, 53, 1583-1595, 1989.

Zindler, A., S.R. Hart, F.A. Frey and S.B. Jacobsen, Nd and Sr isotope ratios and rare-earth element abundances in Teykjanes Peninsula basalts: evidence for mantle heterogeneity beneath Iceland, *Earth Planet. Sci. Lett.*, 45, 249-262, 1979.